

Control of Gantry and Tower Cranes

Hanafy M. Omar

Dissertation submitted to the Faculty of the
Virginia Polytechnic Institute and State University
in partial fulfillment of the requirements for the degree of

Doctor of Philosophy
in
Engineering Mechanics

Ali Nayfeh, Chairman
Pushkin Kachroo
Saad Ragab
Scott Hendricks
Slimane Adjerid

January, 2003
Blacksburg, Virginia

Keywords: Gantry Crane, Tower Crane, Anti-Swing Control, Gain-Scheduling Feedback,
Time-Delayed Feedback, Fuzzy Control

Copyright 2003, Hanafy M. Omar

Control of Gantry and Tower Cranes

Hanafy M. Omar

(ABSTRACT)

The main objective of this work is to design robust, fast, and practical controllers for gantry and tower cranes. The controllers are designed to transfer the load from point to point as fast as possible and, at the same time, the load swing is kept small during the transfer process and completely vanishes at the load destination. Moreover, variations of the system parameters, such as the cable length and the load weight, are also included. Practical considerations, such as the control action power, and the maximum acceleration and velocity, are taken into account. In addition, friction effects are included in the design using a friction-compensation technique.

The designed controllers are based on two approaches. In the first approach, a gain-scheduling feedback controller is designed to move the load from point to point within one oscillation cycle without inducing large swings. The settling time of the system is taken to be equal to the period of oscillation of the load. This criterion enables calculation of the controller feedback gains for varying load weight and cable length. The position references for this controller are step functions. Moreover, the position and swing controllers are treated in a unified way. In the second approach, the transfer process and the swing control are separated in the controller design. This approach requires designing two controllers independently: an anti-swing controller and a tracking controller. The objective of the anti-swing controller is to reduce the load swing. The tracking controller is responsible for making the trolley follow a reference position trajectory. We use a PD-controller for tracking, while the anti-swing controller is designed using three different methods: (a) a classical PD controller, (b) two controllers based on a delayed-feedback technique, and (c) a fuzzy logic controller

that maps the delayed-feedback controller performance.

To validate the designed controllers, an experimental setup was built. Although the designed controllers work perfectly in the computer simulations, the experimental results are unacceptable due to the high friction in the system. This friction deteriorates the system response by introducing time delay, high steady-state error in the trolley and tower positions, and high residual load swings. To overcome friction in the tower-crane model, we estimate the friction, then we apply an opposite control action to cancel it. To estimate the friction force, we assume a mathematical model and estimate the model coefficients using an off-line identification technique using the method of least squares.

With friction compensation, the experimental results are in good agreement with the computer simulations. The gain-scheduling controllers transfer the load smoothly without inducing an overshoot in the trolley position. Moreover, the load can be transferred in a time near to the optimal time with small swing angles during the transfer process. With full-state feedback, the crane can reach any position in the working environment without exceeding the system power capability by controlling the forward gain in the feedback loop. For large distances, we have to decrease this gain, which in turn slows the transfer process. Therefore, this approach is more suitable for short distances. The tracking-anti-swing control approach is usually associated with overshoots in the translational and rotational motions. These overshoots increase with an increase in the maximum acceleration of the trajectories. The transfer time is longer than that obtained with the first approach. However, the crane can follow any trajectory, which makes the controller cope with obstacles in the working environment. Also, we do not need to recalculate the feedback gains for each transfer distance as in the gain-scheduling feedback controller.

Dedication

To:

My parents,

My wife, and

My daughters: Salma and Omnia

Acknowledgments

First of all, all thanks is due to Allah.

I would like to thank Prof. Ali Nayfeh for his extraordinary patience and his enduring optimism. I admire his knowledge, intelligence, and patience. I am blessed and honored to be his student. I would also like to thank Professors Pushkin Kachroo, Saad Ragab, Scott Hendricks, and Slimane Adjerid for their helpful suggestions and for making time in their busy schedules to serve on my committee.

I owe special thanks to Dr. Moumen Idres for his many enlightening discussions and his patience in reviewing this manuscript.

Special thanks are due to my wife for her extreme patience. She has been and continues to be a constant source of inspiration, motivation, and strength.

Finally, I would like to thank my parents for their endless encouragement and support over the years. They are responsible for there being anything positive in me.

Contents

- 1 Introduction** **1**
- 1.1 Crane Control Approaches 4
- 1.2 Friction Compensation 8
- 1.3 Motivations and Objectives 9
- 1.4 Dissertation Organization 10

- 2 Modeling** **12**
- 2.1 Gantry Cranes 12
- 2.2 Tower Cranes 14

- 3 Design of Control Algorithms** **18**
- 3.1 Friction Estimation and Compensation 19
- 3.2 Gain-Scheduling Adaptive Feedback Controller 28
- 3.2.1 Tower Cranes 30

3.2.2	Simulations	31
3.3	Anti-Swing Tracking Controller	36
3.3.1	Trajectory Design	40
3.3.2	Anti-Swing Controller	41
3.3.3	Simulation	49
4	Experimental Results	54
4.1	Experimental Setup	54
4.2	Calculation of the Motor Gains and Mass Properties of the System	57
4.3	Differentiation and Filtering	59
4.4	Friction Coefficients Estimation	61
4.4.1	Translational Motion	61
4.4.2	Rotational Motion	64
4.5	Gain-Scheduling Feedback Controller	65
4.5.1	Partial-State Feedback Controller	67
4.5.2	Full-State Feedback Controller	70
4.6	The Anti-Swing-Tracking Controllers	76
4.6.1	Delayed-feedback controller	76
4.6.2	Fuzzy controller	82

5	Conclusions and Future Work	91
5.1	Future Work	94
	Bibliography	95

List of Figures

1.1	Gantry crane	2
1.2	Rotary cranes.	3
1.3	Friction compensation diagram.	4
2.1	Gantry-crane model.	13
2.2	Tower-crane model.	14
3.1	Friction model.	19
3.2	Simulation response with friction using $K_p = 4.4$ and $K_d = 1.33$	24
3.3	The simulated response and FFT of the output with and without friction.	26
3.4	The simulated response with friction using the tracking gains $K_p = 100$ and $K_d = 0.2$	27
3.5	Variation of the gains with the cable length using the partial-state feedback controller when $m_t = 0$	32
3.6	Variation of the feedback gains with the cable length using the partial-state feedback controller when $L = 1m$	32

3.7	Effect of changing the load mass.	34
3.8	Effect of changing the cable length.	34
3.9	Effect of changing K	35
3.10	Variation of the feedback gains with the trolley position using partial-state feedback for $M_r = m_r = 0.5$	35
3.11	Time histories of the trolley and tower positions and the load swing angles for a tower crane using partial-state feedback when $L = 1m$ and $m_t = 0.5$	36
3.12	Time histories of the system response for a tower crane with $L = 5m$ using partial-state feedback with the gains calculated for $L = 1m$ and not for $L = 5m$	37
3.13	Time histories of the system response for a tower crane using full-state feedback when $L = 1m$ and $K = 0.4$	37
3.14	A schematic diagram for the anti-swing tracking controller.	39
3.15	Typical optimal-time trajectory.	41
3.16	The damping map of the anti-swing PD controller.	43
3.17	The damping map of the first anti-swing delayed-feedback controller.	44
3.18	A schematic diagram for the second anti-swing delayed-feedback controller	45
3.19	The damping map of the second delayed-feedback controller.	45
3.20	Typical membership functions for the fuzzy controller.	47
3.21	Fuzzy logic control (FLC) configuration.	47
3.22	Time histories of the anti-swing controllers for the translational motion only.	51

3.23	Time histories of the anti-swing controllers for the rotational motion only. . .	52
3.24	Time histories of the anti-swing controllers for the combined motion.	53
4.1	Tower-crane configuration.	55
4.2	Experimental setup diagram.	56
4.3	Motor brake circuit.	56
4.4	DC motor diagram.	58
4.5	Comparison among three differentiators.	60
4.6	The translational motion response for $x_{ref} = 0.6 [0.3 \sin(\frac{2\pi}{4}t) - 0.4 \sin(\frac{2\pi}{3}t)]$	63
4.7	The translational motion response to a step input with friction compensation.	64
4.8	The rotational motion response for $\gamma_{ref} = 2 [-0.4 \sin(\frac{2\pi}{3}t) + 0.3 \sin(\frac{2\pi}{4}t)]$	66
4.9	The rotational motion response to a step input with friction compensation.	67
4.10	Time histories of the translational motion when the trolley moves 0.75 m with and without friction compensation.	69
4.11	Time histories of the translational motion when the crane rotates 90 deg and the trolley is positioned at $x = 0.9$ m with and without friction compensation.	71
4.12	Time histories of the rotational motion when the crane rotates 90 deg and the trolley positioned at $x = 0.9$ m with and without friction compensation.	72
4.13	Time histories of the translational motion when the crane rotates 90 deg and the trolley is moved $x = 0.75$ m with and without friction compensation.	73

4.14	Time histories of the rotational motion when the crane rotates $90\ deg$ and the trolley is moved $x = 0.75\ m$ with and without friction compensation.	74
4.15	Time histories of the combined motion with different values of the gain K	76
4.16	Time histories of the translational motion when the trolley is subjected to a disturbance with and without friction compensation.	77
4.17	Time histories of the anti-swing delayed-feedback controller for the combined motion with and without friction compensation.	79
4.18	Time histories of the anti-swing delayed-feedback controller for the rotational motion for final times trajectory.	80
4.19	Time histories of the translational motion using the delay controller with and without friction compensation.	81
4.20	Time histories of the rotational motion using delayed-feedback controller with and without friction compensation.	83
4.21	Time histories of the rotational motion using delay controller with and without friction compensation.	84
4.22	Time histories of the combined motion using delayed-feedback controller with and without friction compensation.	85
4.23	Time histories due to external disturbance using delay controller with and without friction compensation.	86
4.24	Time histories of the anti-swing controllers for the translational motion only.	87
4.25	Time histories of the anti-swing controllers for the rotational motion only.	88
4.26	Time histories of the anti-swing controllers for the combined motion.	89

4.27 Time histories of the anti-swing controllers due to disturbance. 90

List of Tables

3.1	Effect of the zero-band length on the estimation using $K_p = 4.4$ and $K_d = 1.33$.	23
3.2	Effect of the filter cut-off frequency on the estimation which includes Coulomb friction using $K_p = 4.4$ and $K_d = 1.33$.	25
3.3	Effect of the filter cut-off frequency on the estimation without Coulomb friction using $K_p = 4.4$ and $K_d = 1.33$.	25
3.4	Effect of the zero-band value on the estimation with Coulomb friction using the tracking gains $K_p = 100$ and $K_d = 0.2$.	27
3.5	Effect of the filter cut-off frequency on the estimation with Coulomb friction using the tracking gains $K_p = 100$ and $K_d = 0.2$.	28
3.6	Illustration of the generation of the fuzzy rules from given data.	48
3.7	The generated fuzzy rules.	48
3.8	The degrees of the generated fuzzy rules.	49
4.1	Estimated friction coefficients for the translational motion.	62
4.2	Estimated friction coefficients for the rotational motion.	65
4.3	The feedback gains of the rotational motion using full-state feedback	75

Chapter 1

Introduction

Cranes are widely used to transport heavy loads and hazardous materials in shipyards, factories, nuclear installations, and high-building construction. They can be classified into two categories based on their configurations: gantry cranes and rotary cranes.

Gantry cranes are commonly used in factories, Figure 1.1. This type of cranes incorporates a trolley, which translates in a horizontal plane. The payload is attached to the trolley by a cable, whose length can be varied by a hoisting mechanism. The load with the cable is treated as a one-dimensional pendulum with one-degree-of-freedom sway. There is another version of these cranes, which can move also horizontally but in two perpendicular directions. The analysis is almost the same for all of them because the two-direction motions could be divided into two uncoupled one-direction motions.

Rotary cranes can be divided into two types: boom cranes which are commonly used in shipyards, and tower cranes which are used in construction, Figure 1.2. In these cranes, the load-line attachment point undergoes rotation. Another degree of freedom may exist for this point. For boom cranes, this point moves vertically, whereas it moves horizontally in tower cranes. Beside these motions, the cable can be lowered or raised. The cable and the load are treated as a spherical pendulum with two-degree-of-freedom sway.



Figure 1.1: Gantry crane

In this work, we design our controllers based on a linearized model of tower cranes. Hence, the nonlinearities, such as Coulomb friction, are not included. Unfortunately, when the designed controllers were validated on a tower-crane model, we found that the friction is very high. This friction results in high steady-state error for position control even without swing control. If the swing control is included, the response is completely unacceptable. Therefore, controllers designed based on linear models are not applicable to real systems unless the friction is compensated for. This can be done by estimating the friction, and then applying an opposite control action to cancel it, which is known as friction compensation, Figure 1.3. To estimate the friction force, we assume a mathematical model, and then we estimate the model coefficients using an off-line identification technique, such as the method of least squares (LS). First, the process of identification is applied to a theoretical model of a DC motor with known friction coefficients. From this example, some guidelines and rules are deduced for the choice of the LS parameters. Then, the friction coefficients of the



(a) Boom crane.



(b) Tower crane.

Figure 1.2: Rotary cranes.

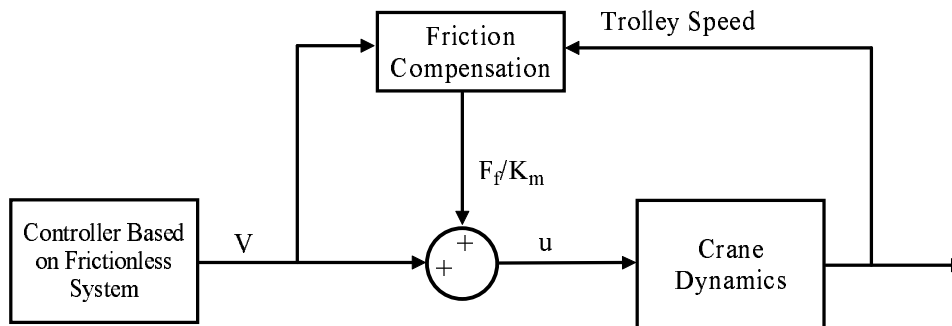


Figure 1.3: Friction compensation diagram.

tower-crane model are estimated and validated.

1.1 Crane Control Approaches

Cranes are used to move a load from point to point in the minimum time such that the load reaches its destination without swinging. Usually a skilful operator is responsible for this task. During the operation, the load is free to swing in a pendulum-like motion. If the swing exceeds a proper limit, it must be damped or the operation must be stopped until the swing dies out. Either option consumes time, which reduces the facility availability. These problems have motivated many researchers to develop control algorithms to automate crane operations. However, most of the existing schemes are not suitable for practical implementation. Therefore, most industrial cranes are not automated and still depend on operators, who sometimes fail to compensate for the swing. This failure may subject the load and the environment to danger. Another difficulty of crane automation is the nature of the crane environment, which is often unstructured in shipyards and factory floors. The control algorithm should be able to cope with these conditions. Abdel-Rahman et al. (2002) presented a detailed survey of crane control. In the following, we concentrate on reviewing the general approaches used in this field.

The operation of cranes can be divided into five steps: gripping, lifting, moving the load from point to point, lowering, and ungridding. A full automation of these processes is possible, and some research has been directed towards that task (Vaha et al., 1988). Moving the load from point to point is the most time consuming task in the process and requires a skillful operator to accomplish it. Suitable methods to facilitate moving loads without inducing large swings are the focus of much current research. We can divide crane automation into two approaches. In the first approach, the operator is kept in the loop and the dynamics of the load are modified to make his job easier. One way is to add damping by feeding back the load swing angle and its rate or by feeding back a delayed version of the swing angle (Henry et al., 2001; Masoud et al., 2002). This feedback adds an extra trajectory to that generated by the operator. A second way is to avoid exciting the load near its natural frequency by adding a filter to remove this frequency from the input (Robinett et al., 1999). This introduces time delay between the operator action and the input to the crane. This delay may confuse the operator. A third way is to add a mechanical absorber to the structure of the crane (Balachandran et al., 1999). Implementing this method requires a considerable amount of power, which makes it impractical.

In the second approach, the operator is removed from the loop and the operation is completely automated. This can be done using various techniques. The first technique is based on generating trajectories to transfer the load to its destination with minimum swing. These trajectories are obtained by either input shaping or optimal control techniques. The second technique is based on the feedback of the position and the swing angle. The third technique is based on dividing the controller design problem into two parts: an anti-swing controller and a tracking controller. Each one is designed separately and then combined to ensure the performance and stability of the overall system.

Since the load swing is affected by the acceleration of the motion, many researchers have concentrated on generating trajectories, which deliver the load in the shortest possible time and at the same time minimize the swing. These trajectories are obtained generally

by using optimization techniques. The objective function can be either the transfer time (Manson, 1982), or the control action (Karihaloo and Parbery, 1982), or the swing angle (Sakaw and Shindo, 1981). Another important method of generating trajectories is input shaping, which consists of a sequence of acceleration and deceleration pulses. These sequences are generated such that there is no residual swing at the end of the transfer operation (Karnopp et al., 1992; Teo et al., 1998; Singhose et al., 1997). The resulting controller is open-loop, which makes it sensitive to external disturbances and to parameter variations. In addition, the required control action is bang-bang, which is discontinuous. Moreover, it usually requires a zero-swing angle at the beginning of the process, which can not be realized practically. To avoid the open-loop disadvantages, many researches (Beeston, 1983; Ohnishi et al., 1981) have investigated optimal control through feedback. They found out that the optimal control performs poorly when implemented in a closed-loop form. The poor performance is attributed to limit cycles resulting from the oscillation of the control action around the switching surfaces. Zinober (1979) avoided the limit cycles by rotating the switching surfaces. This approach can be considered as sub-optimal time control. However, the stability of the system has not been proven. Moreover, the control algorithm is too complex to be implemented practically.

Feedback control is well-known to be less sensitive to disturbances and parameter variations. Hence, it is an attractive method for crane control design. Ridout (1989a) developed a controller, which feeds back the trolley position and speed and the load swing angle. The feedback gains are calculated by trial and error based on the root-locus technique. Later, he improved his controller by changing the trolley velocity gain according to the error signal (Ridout, 1989b). Through this approach, the system damping can be changed during transfer of the load. Initially, damping is reduced to increase the velocity, and then it is increased gradually. Consequently, a faster transfer time is achieved. However, the nominal feedback gains are obtained by trial and error. This makes the process cumbersome for a wide range of operating conditions. Salminen et al. (1990) employed feedback control with adaptive gains, which are calculated based on the pole-placement technique. Since the

gains are fixed during the transfer operation, his control algorithm can be best described as gain scheduling rather than adaptation. Hazlerigg (1972) developed a compensator with its zeros designed to cancel the dynamics of the pendulum. This controller was tested on a physical crane model. It produced good results except that the system was underdamped. Therefore, the system response was oscillatory, which implies a longer transfer time. Hurteau and Desantis (1983) developed a linear feedback controller using full-state feedback. The controller gains are tuned according to the cable length. However, if the cable length changes in an unqualified way, degradation of the system performance occurs. In addition, the tuning algorithm was not tested experimentally.

As mentioned before, the objective of the crane control is to move the load from point to point and at the same time minimize the load swing. Usually, the controller is designed to achieve these two tasks simultaneously, as in the aforementioned controllers. However, in another approach used extensively, the two tasks are treated separately by designing two feedback controllers. The first task is an anti-swing controller. It controls the swing damping by a proper feedback of the swing angle and its rate. The second task is a tracking controller designed to make the trolley follow a reference trajectory. The trolley position and velocity are used for tracking feedback. The position trajectory is generally based on the classical velocity pattern, which is obtained from open-loop optimal control or input shaping techniques. The tracking controller can be either a classical Proportional-Derivative (PD) controller (Henry, 1999; Masoud 2000) or a Fuzzy Logic Controller (FLC) (Yang et al., 1996; Nalley and Trabia, 1994; Lee et al., 1997; Itho et al., 1994; Al-Moussa, 2000). Similarly, the anti-swing controller is designed by different methods. Henry (1999) and Masoud (2002) used delayed-position feedback, whereas Nalley and Trabia (1994), Yang et al. (1996), and Al-Moussa (2000) used FLC. Separation of the control tasks, anti-swing and tracking, enables the designer to handle different trajectories according to the work environment. Generally, the cable length is considered in the design of the anti-swing controller. However, the effect of the load mass is neglected in the design of the tracking controller. The system response is slow compared with that of optimal control or feedback control.

Raising the load (hoisting) during the transfer is needed only to avoid obstacles. This motion is slow, and hence variations in the cable length can be considered as a disturbance to the system. Then, the effect of variations in the cable length is investigated through simulation to make sure that the performance does not deteriorate. However, there are few studies that include hoisting in the design of controllers (e.g., Auernig and Troger, 1987).

The effect of the load weight on the dynamics is usually ignored. However, Lee (1998) and Omar and Nayfeh (2001) consider it in the design of controllers for gantry and tower cranes. From these studies, we find that, for very heavy loads compared to the trolley weight, the system performance deteriorates if the load weight is not included in the controller design.

1.2 Friction Compensation

Friction in mechanical systems has nonsymmetric characteristics. It depends on the direction of the motion as well as the position (Canudas, 1988). There are several methods to overcome friction effects. The first uses high-feedback-gain controllers, which may reduce the effect of the friction nonlinearities. However, this approach has severe limitations because the nonlinearities dominate any compensation for small errors. Limit cycles may appear as a consequence of the dynamic interaction between the friction forces and the controller, especially when the controller contains integral terms. The second uses high-frequency bias signal injection. Although it may alleviate friction effects, it may also excite high-frequency harmonics in the system. The third uses friction compensation, which aims to remove the effect of friction completely.

The third method has an advantage over the other methods because the system becomes linear after compensation. So, control algorithms based on the linear model can be applied directly. The compensation is done by estimating the friction of the system, and then applying an opposite control action to cancel it. The compensation can be done on-line

to track the friction variations, which may occur due to changes in the environment and mechanical wear. Many researchers developed adaptive friction compensation for various applications using different adaptation techniques and models (Canudas et al., 1986; Li and Cheng, 1994). However, to obtain a good estimate of friction using the adaptive approach, one needs to persistently excite the system (Astrom and Wittenmark, 1994). In our system, the input signals do not have this characteristic. Moreover, friction can be assumed to be constant during the operation without affecting the system performance. This enables us to estimate the friction off-line using an appropriate persistent excitation.

The estimation process requires a model of friction. Friction models have been extensively discussed in the literature (Armstrong et al., 1994; Canudas, 1995). It is well established that friction is a function of the velocity; however, there is disagreement about the relationship between them. Among these models, we choose the one proposed by Canudas et al. (1986) because of its simplicity and because it represents most of the friction phenomena observed in our experiment, Figure 3.1. This model consists of constant viscous and Coulomb terms. These constants change with the motion direction.

1.3 Motivations and Objectives

Most of the controllers are designed for gantry cranes and a few are designed for tower cranes. Furthermore, a considerable proportion of tower-crane controllers are based on open-loop methods (Golashani and Aplevich, 1995), which are not suitable for practical applications. Those who considered feedback control (e.g., Robinett et al., 1999) ignored the effect of parameter variations. The developed controllers are slow and the coupling between the rotational and translational motions of the tower crane are not well handled. Most of the previous work is based on the assumption of a frictionless system. In real systems, friction has a strong impact on the system performance, and it should be included in the controller design.

The main objective of this work is to design robust, fast, and practical controllers for gantry and tower cranes to transfer loads from point to point in a short time as fast as possible and, at the same time, keep the load swing small during the transfer process and completely eliminate it at the load destination. Moreover, variations of the system parameters, such as the cable length and the load weight, are taken into account. Practical considerations, such as the control action power, maximum acceleration, and velocity, are also taken into account. In addition, friction effects are included in the design using a friction compensation technique.

1.4 Dissertation Organization

This work is organized as follows:

Chapter 1 is an introduction to crane systems with a literature review of crane automation, followed by motivations and objectives.

In Chapter 2, we develop full nonlinear mathematical models of gantry and tower cranes. Then, these nonlinear models are simplified in different ways to make them suitable for controller design.

In Chapter 3, a friction compensation algorithm is introduced followed by a procedure for estimating the friction coefficients. This chapter also contains the design, analysis, and simulation of the control algorithms. First, we design a gain scheduling PD controller for the linear model of gantry cranes. Next, this controller is modified to handle tower cranes by considering the coupling between the rotational and translational motions. The gains of the PD controller are obtained as a function of the cable length and the load weight. Then, we use another approach in which the transfer process and the swing control are separated in the controller design. This approach requires designing two controllers independently: an anti-swing controller and a tracking controller. The objective of the anti-swing controller is

to reduce the load swing. The tracking controller aims to track the trajectory generated by the anti-swing controller and the reference trajectory. According to this approach, we design a classical PD controller and a fuzzy controller for anti-swinging. Two anti-swing controllers based on a delayed feedback technique are also introduced.

In Chapter 4, a tower crane model is used to test the proposed control algorithms. The layout of the experimental setup is described. The system parameters are calculated and then used to estimate the friction coefficients. The results are discussed and the merits and pitfalls of different control approaches are identified.

Chapter 5 contains the conclusions and suggestions for future work.

Chapter 2

Modeling

2.1 Gantry Cranes

We use the Lagrangian approach to derive the equations of motion. It follows from Figure 2.1 that the load and trolley position vectors are given by

$$\vec{r}_L = \{x + L \sin(\phi), -L \cos(\phi)\} \quad \text{and} \quad \vec{r}_T = \{x, 0\} \quad (2.1)$$

Then, the kinetic and potential energies of the whole system are given by

$$T = \frac{1}{2}m \vec{r}_L \cdot \vec{r}_L + \frac{1}{2}M \vec{r}_T \cdot \vec{r}_T \quad (2.2)$$

$$V = -mgL \cos(\phi) \quad (2.3)$$

Let the generalized forces corresponding to the generalized displacements $\vec{q} = \{x, \phi\}$ be $\vec{F} = \{F_x, 0\}$. Constructing the Lagrangian $\mathcal{L} = T - V$ and using Lagrange's equations

$$\frac{d}{dt} \left(\frac{\partial \mathcal{L}}{\partial \dot{q}_j} \right) - \frac{\partial \mathcal{L}}{\partial q_j} = F_j, \quad j = 1, 2 \quad (2.4)$$

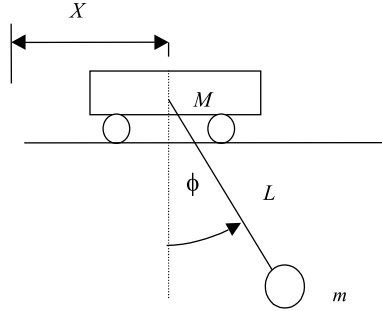


Figure 2.1: Gantry-crane model.

we obtain the following equations of motion:

$$(m + M) \ddot{x} + mL\ddot{\phi} \cos(\phi) + m\ddot{L} \sin(\phi) + 2m\dot{L}\dot{\phi} \cos(\phi) - mL\dot{\phi}^2 \sin(\phi) = F_x \quad (2.5)$$

$$L\ddot{\phi} + g \sin(\phi) + 2\dot{L}\dot{\phi} + \ddot{x} \cos(\phi) = 0 \quad (2.6)$$

For safe operation, the swing angle should be kept small. In this study, we assume that changing the cable length is needed only to avoid obstacles in the path of the load. This change can be considered small also. Using these two assumptions and dividing equation (2.5) by M , we reduce the equations of motion to

$$\ddot{x} - m_t g \phi = \bar{F}_x \quad (2.7)$$

$$L\ddot{\phi} + g\phi + \ddot{x} = 0 \quad (2.8)$$

where

$$m_t = \frac{m}{M}, \quad \bar{F}_x = \frac{F_x}{M} \quad (2.9)$$

Because the motor has a small time constant relative to the mechanical system, the force exerted by it can be considered as a constant gain and expressed as

$$\bar{F}_x = K_{mx} V_x \quad (2.10)$$

where V_x is the input voltage to the motor.

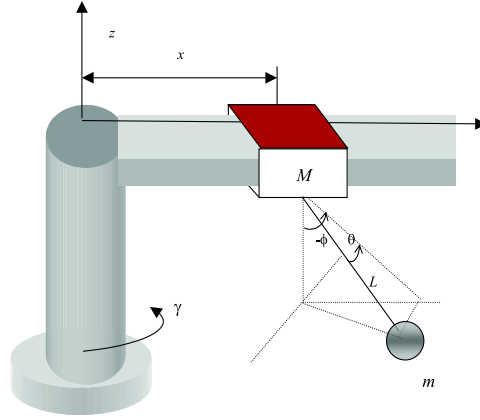


Figure 2.2: Tower-crane model.

2.2 Tower Cranes

We use the Lagrangian approach to derive the equations of motion of tower cranes. It follows from Figure 2.2 that the load and trolley position vectors can be written as

$$\vec{r}_L = \{x - L \cos(\theta) \sin(\phi), L \sin(\theta), -L \cos(\theta) \cos(\phi)\}$$

$$\vec{r}_T = \{x, 0, 0\} \quad (2.11)$$

The velocities of the trolley and the load can be calculated using

$$\dot{\vec{r}} = \frac{d\vec{r}}{dt} + \vec{\omega} \times \vec{r} \quad (2.12)$$

where $\vec{\omega} = \{0, 0, \dot{\gamma}\}$ is the angular velocity of the tower. The kinetic and potential energies are given by

$$T = \frac{1}{2} m \dot{\vec{r}}_L \cdot \dot{\vec{r}}_L + \frac{1}{2} M \dot{\vec{r}}_T \cdot \dot{\vec{r}}_T + \frac{1}{2} J_o \dot{\gamma}^2 \quad (2.13)$$

$$V = -mgL \cos(\theta) \cos(\phi) \quad (2.14)$$

where J_o is the moment of inertia of the tower and the jib about the z -axis. The generalized forces corresponding to the generalized displacement vector $\vec{q} = \{x, \phi, \gamma, \theta\}$ are

$$\vec{F} = \{F_x, 0, T_\gamma, 0\} \quad (2.15)$$

Constructing the Lagrangian $\mathcal{L} = T - V$ and using Lagrange's equations

$$\frac{d}{dt} \left(\frac{\partial \mathcal{L}}{\partial \dot{q}_j} \right) - \frac{\partial \mathcal{L}}{\partial q_j} = F_j, \quad j = 1, 2, 3, 4 \quad (2.16)$$

we obtain the equations of motion

$$\begin{aligned} & (m + M)\ddot{x} + mL \cos(\theta) \sin(\phi) \dot{\gamma}^2 - (m + M)x\dot{\gamma}^2 - 2mL \cos(\theta) \dot{\gamma} \dot{\theta} + mL \cos(\theta) \sin(\phi) \dot{\theta}^2 \\ & + 2mL \cos(\phi) \sin(\theta) \dot{\theta} \dot{\phi} - 2m\dot{L}(\sin(\theta) \dot{\gamma} + mL \cos(\theta) \sin(\phi) \dot{\phi}^2 - \sin(\theta) \sin(\phi) \dot{\theta} \\ & + \cos(\theta) \cos(\phi) \dot{\phi}) - m \cos(\theta) \sin(\phi) \ddot{L} - mL \sin(\theta) \ddot{\gamma} + mL \sin(\theta) \sin(\phi) \ddot{\theta} \\ & - mL \cos(\theta) \cos(\phi) \ddot{\phi} = F_x \end{aligned} \quad (2.17)$$

$$\begin{aligned} & L \cos(\theta)^2 \ddot{\phi} + \cos(\theta)(g \sin(\phi) - L \cos(\theta) \cos(\phi) \sin(\phi) \dot{\gamma}^2 + \cos(\phi) x \dot{\gamma}^2 - \cos(\theta) \cos(\phi) \ddot{x} \\ & + 2L \cos(\theta) \cos(\phi) \dot{\gamma} \dot{\theta} - 2L \sin(\theta) \dot{\theta} \dot{\phi} + 2\dot{L}(\cos(\phi) \sin(\theta) \dot{\gamma} + \cos(\theta) \dot{\phi})) \\ & + L \cos(\theta) \cos(\phi) \sin(\theta) \ddot{\gamma} = 0 \end{aligned} \quad (2.18)$$

$$\begin{aligned} & (J_o + mL^2 \sin(\theta)^2 + m \cos(\theta)^2 L^2 \sin(\phi)^2 - 2m \cos(\theta) L \sin(\phi) x + mx^2 + Mx^2) \ddot{\gamma} \\ & + 2m \cos(\theta) x \dot{L} \dot{\theta} - mL \sin(\theta) x \dot{\theta}^2 - 2m \cos(\phi) L^2 \sin(\theta)^2 \dot{\theta} \dot{\phi} - m \cos(\theta) L^2 \sin(\theta) \sin(\phi) \dot{\phi}^2 \\ & - mL \dot{L}(2 \sin(\phi) \dot{\theta} - \cos(\phi) \sin(2\theta) \dot{\phi}) + x(-2m \cos(\theta) \sin(\phi) \dot{L} + 2(m + M) \dot{x}) \\ & + mL^2(\cos(\phi)^2 \sin(2\theta) \dot{\theta} + \cos(\theta)^2 \sin(2\phi) \dot{\phi}) + 2mL((\sin(\theta)^2 + \cos(\theta)^2 \sin(\phi)^2) \dot{L} \\ & - \cos(\theta) \sin(\phi) \dot{x} + \sin(\theta) \sin(\phi) x \dot{\theta} - \cos(\theta) \cos(\phi) x \dot{\phi})) + m \sin(\theta) x \ddot{L} - mL \sin(\theta) \ddot{x} \\ & + (-m \cos(\theta)^2 L^2 \sin(\phi)) - mL^2 \sin(\theta)^2 \sin(\phi) + m \cos(\theta) L x \ddot{\theta} \\ & + m \cos(\theta) \cos(\phi) L^2 \sin(\theta) \ddot{\phi} = T_\gamma \end{aligned} \quad (2.19)$$

$$\begin{aligned} & L \ddot{\theta} + g \cos(\phi) \sin(\theta) + 2 \cos(\theta) \dot{x} \dot{\gamma} - \frac{1}{4} L \sin(2\theta) \dot{\gamma}^2 - \frac{1}{4} L \cos(\phi)^2 \sin(2\theta) \dot{\gamma}^2 - x \sin(\theta) \sin(\phi) \dot{\gamma}^2 \\ & + \frac{1}{4} L \sin(2\theta) \sin(\phi)^2 \dot{\gamma}^2 + \dot{L}(-2 \sin(\phi) \dot{\gamma} + 2\dot{\theta}) - L \cos(\phi) \dot{\gamma} \dot{\phi} + L \cos(\theta)^2 \cos(\phi) \dot{\gamma} \dot{\phi} \\ & + L \cos(\phi) \sin(\theta)^2 \dot{\gamma} \dot{\phi} + L \cos(\theta) \sin(\theta) \dot{\phi}^2 + \sin(\theta) \sin(\phi) \ddot{x} + (-L \sin(\phi) + x \cos(\theta)) \ddot{\gamma} = 0 \end{aligned} \quad (2.20)$$

Equations (2.17)-(2.20) are nonlinear and complex; they are used in the simulations. However, for analysis and control design, we need to simplify them. We assume small swing angles, neglect the cable length variations, and assume that the rates of change of x and γ are the same order of magnitude as the swing angles and their rates. Dividing equations (2.17) and (2.18) by M and J_o , respectively, we obtain

$$\ddot{x} + m_t g \phi = \bar{F}_x \quad (2.21)$$

$$L\ddot{\phi} + g\phi - \ddot{x} + L\dot{\gamma}\theta = 0 \quad (2.22)$$

$$(1 + M_r x^2)\dot{\gamma} - m_r g x \theta = \bar{T}_\gamma \quad (2.23)$$

$$L\ddot{\theta} + g\theta + x\dot{\gamma} - L\dot{\gamma}\phi = 0 \quad (2.24)$$

where

$$m_t = \frac{m}{M}, \quad M_r = \frac{M}{J_o}, \quad m_r = \frac{m}{J_o}, \quad \bar{F}_x = \frac{F_x}{M}, \quad \bar{T}_\gamma = \frac{T_\gamma}{J_o} \quad (2.25)$$

The two motors are modeled as constant gains; that is,

$$\bar{F}_x = K_{m_x} V_x \quad (2.26)$$

$$\bar{T}_\gamma = K_{m_\gamma} V_\gamma \quad (2.27)$$

For controller design, we need to simplify these equations further. We neglect the nonlinear

terms and reduce equations (2.21)-(2.24) to

$$\ddot{x} + m_t g \phi = K_{mx} V_x \quad (2.28)$$

$$L\ddot{\phi} + g\phi - \ddot{x} = 0 \quad (2.29)$$

$$(1 + M_r x^2)\ddot{\gamma} - m_r g x \theta = K_{m\gamma} V_\gamma \quad (2.30)$$

$$L\ddot{\theta} + g\theta + x\ddot{\gamma} = 0 \quad (2.31)$$

Equations (2.28) and (2.30) represent the translational motion, and equations (2.30) and (2.31) represent the rotational motion.

Chapter 3

Design of Control Algorithms

In this chapter, we design control algorithms using two approaches. In the first approach, a gain-scheduling feedback controller is designed to move loads from point to point within one oscillation cycle without inducing large swings. The settling time of the system is taken to be equal to the period of oscillation of the load. This criterion enables the calculation of the controller feedback gains for varying load weights and cable lengths. The position references for this controller are step functions. Moreover, the position and swing control are treated in a unified way.

In the second approach, the transfer process and the swing control are separated in the controller design. This approach requires designing two controllers independently: an anti-swing controller and a tracking controller. The objective of the anti-swing controller is to reduce the load swing. The tracking controller aims to follow a reference trajectory. We use a PD-controller for tracking, while the anti-swing controller is designed using three different methods: (a) a classical PD controller, (b) two controllers based on a delayed-feedback technique, and (c) a fuzzy logic controller that maps the delayed-feedback controller performance.

Throughout this work, we design the controllers based on the linear model of the

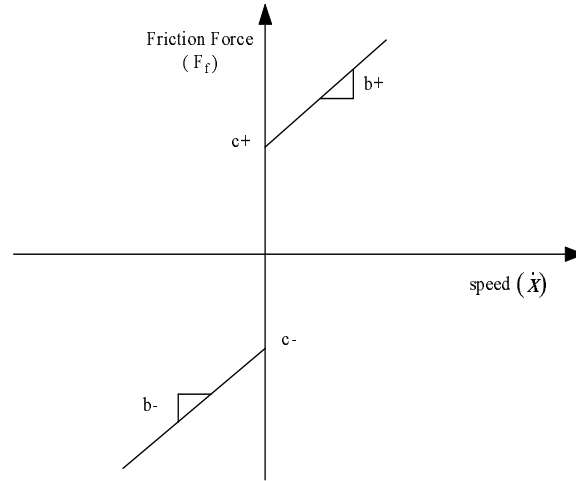


Figure 3.1: Friction model.

gantry crane. Next, these controllers are modified to handle tower cranes by considering the coupling between the rotational and translational motions.

3.1 Friction Estimation and Compensation

The friction model in Figure 3.1 can be expressed in the form

$$F_f = (c_+ - b_+ \dot{x})\eta + (-c_- - b_- \dot{x})\xi + F_{fs}(1 - \eta)(1 - \xi) \quad (3.1)$$

where c and b are the Coulomb and viscous friction coefficients, respectively, the positive and minus signs refer to the positive and negative directions of the velocity, and F_{fs} is the stiction friction at zero-velocity. The stiction friction theoretically appears at zero velocity. It opposes the motion until the control action exceeds it. It also depends on the direction of the motion. To cancel it, we need to reverse the control action after it passes zero velocity, which generates limit cycles. Consequently, the system response becomes oscillatory and the response is unacceptable. To avoid this problem, we assume the stiction to be a continuous

function of the control action with a sharp slope in the form

$$F_{fs} = f_{sh} + f_s \tanh(AV) \quad (3.2)$$

where f_s and A are the magnitude and slope of the friction. A shift f_{sh} is introduced to account for asymmetric characteristics of the friction. Due to the error resulting from the numerical computation and differentiation, the zero velocity should be defined as a region instead of a crisp value. Therefore, we introduce the parameters ξ and η defined as

$$\begin{aligned} \xi = 0, \eta = 0 & \quad |\dot{x}| < d_s \\ \xi = 0, \eta = 1 & \quad \dot{x} > d_s \\ \xi = 1, \eta = 0 & \quad \dot{x} < -d_s \end{aligned} \quad (3.3)$$

where d_s is the upper limit of the zero-velocity region.

The Coulomb and viscous friction coefficients are determined using the method of least squares, while the stiction friction parameters are determined experimentally to be equal to the control action at which the motor starts to move. Then, the estimated friction force F_f is added to the control action to linearize the model as follows:

$$\ddot{x} = K_m(u - F_f/K_m) \rightarrow \ddot{x} = K_m V \quad (3.4)$$

where V is the control action determined from the linear model. The actual control action is

$$u = V + F_f/K_m \quad (3.5)$$

where K_m is the motor constant, which is a known parameter.

The translational and rotational motions outside the zero-velocity region, without stiction friction, can be represented by

$$\ddot{x} + b\dot{x} = K_m u - c_+ \eta + c_- \xi \quad (3.6)$$

Without affecting the friction model, we denote the viscous friction coefficient by b for both directions. Using this notation, we write the linear model of equation (3.6) as

$$\ddot{x} + b\dot{x} = K_m u \quad (3.7)$$

The discrete form of this linear system with a sampling period T_s and a zero-order hold is

$$\frac{X(z)}{V(z)} = \frac{a_1 z + a_2}{(z-1)(z-a)} \quad (3.8)$$

where

$$\begin{aligned} a_1 &= \frac{K_m}{b^2}(bT_s - 1 + e^{-bT_s}) \\ a_2 &= \frac{K_m}{b^2}(1 - e^{-bT_s} - bT_s e^{-bT_s}) \\ a &= e^{-bT_s} \end{aligned} \quad (3.9)$$

It is difficult to obtain a linear regression form using the above parameters. Assuming bT_s to be small and approximating e^{-bT_s} with $1 - bT_s$, we obtain $a_1 = 0$, $a_2 = K_m T^2$, and $a = 1 - bT_s$. Then, the simplified discrete form of equation (3.7) can be written as

$$[x(k) - 2x(k-1) + x(k-2)]/T_s^2 = -b[x(k-2) - x(k-1)]/T_s + K_m u(k-2) \quad (3.10)$$

We can put this discrete model in another form by defining the discrete acceleration and velocity as

$$\begin{aligned} \ddot{x}_d(k) &= [x(k) - 2x(k-1) + x(k-2)]/T_s^2 \\ \dot{x}_d(k) &= [x(k-2) - x(k-1)]/T_s \end{aligned} \quad (3.11)$$

Then, the discrete form in equation (3.10) becomes

$$\ddot{x}_d(k) = -b\dot{x}_d(k) + K_m u(k-2) \quad (3.12)$$

Adding the Coulomb friction to the model and considering the viscous friction in both directions, we write the discrete model as

$$\ddot{x}_d(k) = -b_+ \dot{x}_d(k) \eta - b_- \dot{x}_d(k) \xi + K_m u(k-2) - c_+ \eta + c_- \xi \quad (3.13)$$

The regression form in matrix notation is

$$y(k) = \phi(k)\Theta \quad (3.14)$$

where

$$\begin{aligned} y(k) &= \frac{\ddot{x}_d(k)}{K_m} - u(k-2) \\ \phi(k) &= \begin{bmatrix} \dot{x}_d(k)\eta & \dot{x}_d(k)\xi & -\eta & \xi \end{bmatrix} \\ \Theta &= \begin{bmatrix} \frac{b_+}{K_m} & \frac{b_-}{K_m} & \frac{c_+}{K_m} & \frac{c_-}{K_m} \end{bmatrix}^T \end{aligned}$$

Using the method of least squares, we calculate the unknown parameters vector Θ from

$$\Theta = (Y^T Y)^{-1} Y^T \Phi \quad (3.15)$$

where $Y = [y(1) \ y(2) \ \dots \ y(n)]$, $\Phi = [\phi(1) \ \phi(2) \ \dots \ \phi(n)]$, and n is the number of samples.

To apply the estimation technique, we stabilize the system using a PD controller. Then, a *PE* reference is applied. The output is filtered and then used to estimate the unknown parameters using equation (3.15). First, the procedure is applied to a theoretical model with known parameter values to understand the effect of friction on the estimation. From this study, we obtain some guidelines for the real-system estimation. The model used in this theoretical study is

$$\ddot{x} = K_m V + (c_+ - b_+ \dot{x})\eta + (-c_- - b_- \dot{x})\xi \quad (3.16)$$

where η and ξ are as described before but with $d_s = 0$. We choose the parameter values to be $K_m = 1.7$, $b_+ = 1.8$, $b_- = 5.5$, $c_+ = 1.1$, and $c_- = 1.2$. The output of the PD controller is determined from

$$V = K(X_{ref} - x - K_d \dot{x}) \quad (3.17)$$

The reference velocity is not used because we found that it overestimates the parameter values. In this study, we use two sets of gains. The first is based on the feedback gains determined from the gain-scheduling feedback controller: $K_p = 4.4$ and $K_d = 1.33$. The other is based on the tracking controller: $K = 100$ and $K_d = 0.2$. For the signal to be *PE*, it should contain n sinusoidal components for estimating $2n$ parameters (Astrom and Wittenmark, 1994). The reference signal is chosen to be

$$X_{ref} = 0.3 \sin\left(\frac{2\pi}{4}t\right) - 0.4 \sin\left(\frac{2\pi}{3}t\right) \quad (3.18)$$

Table 3.1: Effect of the zero-band length on the estimation using $K_p = 4.4$ and $K_d = 1.33$.

d_s	b_+/K_m	b_-/K_m	c_+/K_m	c_-/K_m
exact	2.8	5.5	1	1.2
0	5.341387	8.694841	0.669620	0.855119
0.005	3.640265	6.285023	0.893631	1.119057
0.01	2.899597	5.625552	0.991304	1.189285
0.05	2.832908	5.519729	1.000881	1.201942
0.1	2.823311	5.517687	1.002365	1.202331

For the first set of gains, the response is shown in Figure 3.2. It contains a large band of zero velocity due to friction. The acceleration in this band is very high and oscillatory due to the discontinuity in friction. The data in this band should be excluded from the estimation to obtain good results. Table 3.1 shows the estimated parameters with different values for the zero-velocity band d_s . Including the zero-band in the estimation gives incorrect results. The zero-band should be increased to include all oscillatory accelerations, and it should not pass this limit to have enough data for good estimation. We should mention that the zero-band is nearly 0.01 m/sec .

The data used in this theoretical study do not contain noise except for that generated from the numerical differentiation. So, we do not need to filter the data before the estimation process. However, for the real system there is noise, which should be removed by a low-pass filter. The critical parameter in the filter choice is the cut-off frequency ω_c . It should be chosen so that the system frequencies are kept, and the unwanted high frequencies are removed. In systems without Coulomb friction, the maximum frequency in the output can be estimated from the input signal to the system. However, in the presence of Coulomb friction, high frequencies are generated in the output. These frequencies should not be removed because they are due to friction. So, we have to find out the maximum frequency, which

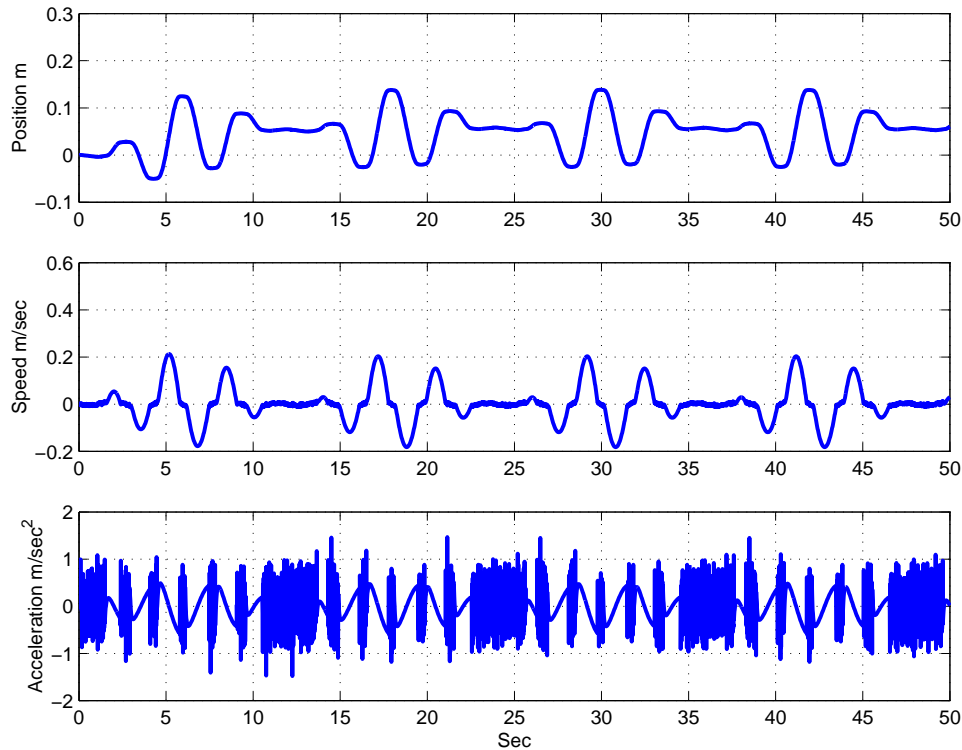


Figure 3.2: Simulation response with friction using $K_p = 4.4$ and $K_d = 1.33$.

should be kept to obtain a good representation of friction in the output signal. Figure 3.3 shows the Fast Fourier Transform FFT of the output in the presence and absence of Coulomb friction. We note that Coulomb friction introduces high frequencies in the system. Table 3.1 shows the estimated parameters with different cut-off frequencies. The high frequency in the reference signal is 0.25Hz. The zero-band velocity is chosen to be $d_s = 0.05$. We note that the filter used for the off-line estimation is a Butterworth filter of order 5 with zero-phase response (Oppenheim et al., 1989). However, we have to keep in mind that this zero-phase filter can not be implemented in real-time control.

To reduce the effect of the zero-band velocity on the estimation, we use the second set of high PD gains. Figure 3.4 shows the response of the same system when the PD gains changed to $K_p = 100$ and $K_d = 0.2$. We note that the zero-band velocity is very small

Table 3.2: Effect of the filter cut-off frequency on the estimation which includes Coulomb friction using $K_p = 4.4$ and $K_d = 1.33$.

ω_c	b_+/K_m	b_-/K_m	c_+/K_m	c_-/K_m
exact	2.8	5.5	1	1.2
0.5	5.823359	9.735506	0.725377	0.727089
1.0	3.101434	5.687506	0.995972	1.216083
2.0	2.643425	5.408402	1.031581	1.216711
5.0	2.817789	5.524590	1.003190	1.201192
10.0	2.836635	5.520508	1.000291	1.201844

Table 3.3: Effect of the filter cut-off frequency on the estimation without Coulomb friction using $K_p = 4.4$ and $K_d = 1.33$.

ω_c	b_+/K_m	b_-/K_m	c_+/K_m	c_-/K_m
exact	2.8	5.5	0.0	0.0
0.5	3.281546	4.786741	-0.052189	.090821
1.0	2.545240	5.607126	0.062907	-0.01946
2.0	2.715645	5.537910	0.025070	-0.003621
5.0	2.819954	5.524590	0.000689	0.000550
10.0	2.819037	5.517529	0.001074	0.000335

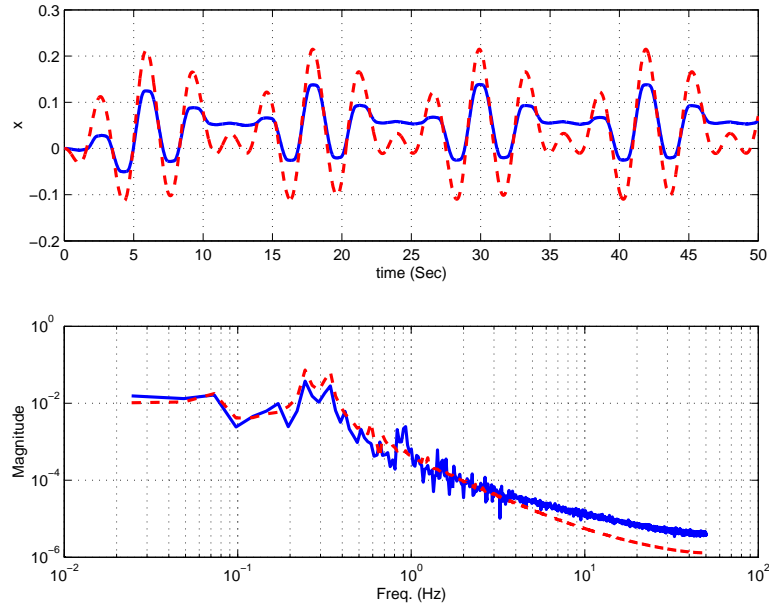


Figure 3.3: The simulated response and FFT of the output: — with friction and - - - without friction.

compared to that of the first set of gains. Table 3.4 shows the values of the estimated parameters for different values of d_s , whereas Table 3.5 shows the effect of ω_c with $d_s = 0.02$.

From this study, we obtain some guidelines, which can be beneficial in real-system estimation. These guidelines are summarized as follows:

- Coulomb friction adds high frequencies to the system output. These frequencies should not be removed by filtering, otherwise the estimated parameters will not be correct, especially the viscous friction coefficients. Therefore, the filter cut-off frequency should be chosen properly. It should be increased with Coulomb friction. At the same time, high frequencies resulting from the measurement and numerical differentiation should be removed. It was found that a cut-off frequency of $0.1 f_s$ is a reasonable choice, where f_s is the sampling frequency.

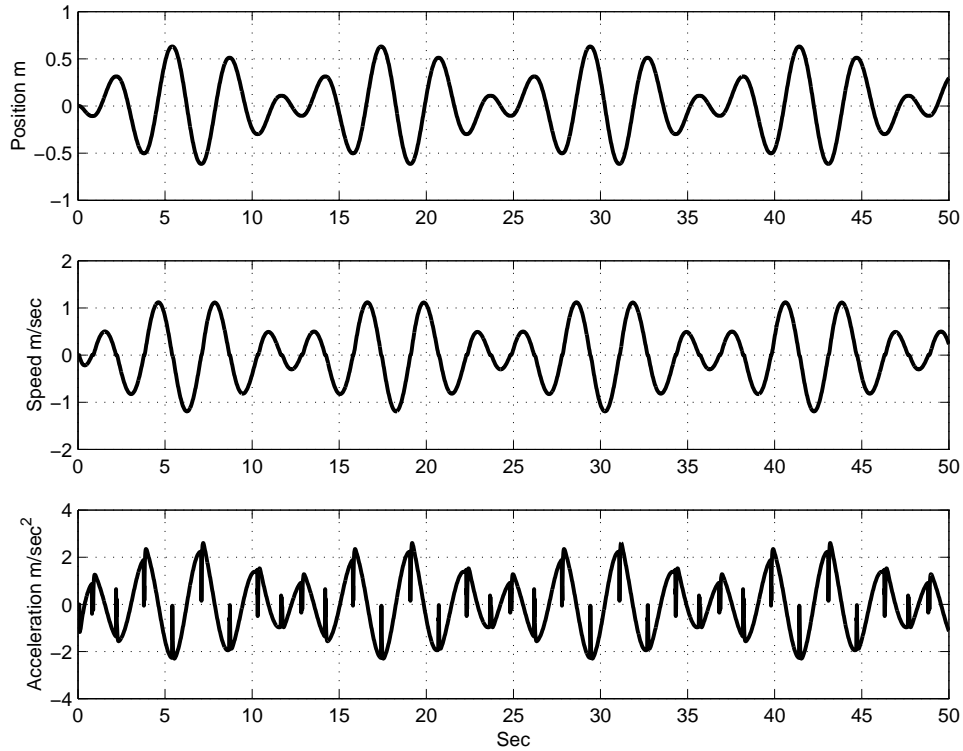


Figure 3.4: The simulated response with friction using the tracking gains $K_p = 100$ and $K_d = 0.2$.

Table 3.4: Effect of the zero-band value on the estimation with Coulomb friction using the tracking gains $K_p = 100$ and $K_d = 0.2$.

d_s	b_+/K_m	b_-/K_m	c_+/K_m	c_-/K_m
exact	2.8	5.5	1	1.2
0	2.979380	5.642228	0.885693	1.112756
0.01	2.849118	5.542317	0.981689	1.185655
0.02	2.832579	5.530738	0.993986	1.194183
0.05	2.823444	5.521993	1.000868	1.200712

Table 3.5: Effect of the filter cut-off frequency on the estimation with Coulomb friction using the tracking gains $K_p = 100$ and $K_d = 0.2$.

ω_c	b_+/K_m	b_-/K_m	c_+/K_m	c_-/K_m
exact	2.8	5.5	1	1.2
0.5	4.213892	5.877469	0.121192	0.776435
1.0	3.253598	6.169105	0.708620	0.722327
5.0	2.842247	5.576426	0.987037	1.160845
10.0	2.830800	5.536750	0.995481	1.189793

- The acceleration and velocity are obtained by numerical differentiation, which introduces some errors, especially around zero velocity. Also, due to the discontinuity in the friction at zero velocity, the acceleration is very high and oscillatory. This results in bad estimates of the friction coefficients. Therefore, the data in the zero-velocity region should be excluded to obtain a realistic estimation.
- The estimated friction coefficients are not greatly affected by the change in the motor constant K_m . A small error in determining K_m does not affect the estimation process.

3.2 Gain-Scheduling Adaptive Feedback Controller

We use state feedback to control the position of the trolley and at the same time reduce the load swing. We first propose a controller having the form

$$V_x = K(x_r - K_x x - K_{\dot{x}} \dot{x} + K_{\phi} \phi) \quad (3.19)$$

Now, the question arises on how to adjust the gains in this controller to obtain the best performance for a wide range of cable lengths and loads. The main objective is to make the swing angle as small as possible. The minimum number of load oscillations during which this

can be achieved is one cycle. We note that, when the trolley response is critically damped, the load completes one cycle, which indicates that the settling time for the trolley should be equal to the period of the load. We use this criterion to choose the location of the closed-loop poles and hence the feedback gains (Hurteau and Desantis, 1983). The design procedure is described next.

To make the trolley response critically damped, we choose its poles to be repeated and equal to $-a$. Because the load performance should be oscillatory, we choose its poles to be $-\zeta \omega_n \pm \omega_n \sqrt{1 - \zeta^2} j$. The final closed-loop characteristic equation is

$$(s + a)^2 (s^2 + 2\zeta \omega_n s + \omega_n^2) = 0 \quad (3.20)$$

From simulations, the best damping ratio that can be chosen is $\zeta = \frac{1}{\sqrt{2}}$. Using the above mentioned settling time criterion, we have

$$\frac{4}{a} = \frac{2\pi}{\sqrt{g/L}} \rightarrow a = \frac{4\sqrt{g/L}}{2\pi} \quad (3.21)$$

Comparing the required closed-loop characteristic equation (3.20) with that of the system, we obtain the following four nonlinear algebraic equations:

$$\pi K K_{\dot{x}} K_{m_x} - 8\sqrt{\frac{g}{L}} - 4\pi \xi \omega_n = 0 \quad (3.22)$$

$$2L\pi\omega_n \left(8\sqrt{\frac{g}{L}}\xi + \pi\omega_n \right) - \pi^2 K K_{m_x} (L K_x + K_\phi) + 8g - g\pi^2 (2 + m_t) = 0 \quad (3.23)$$

$$8\pi \sqrt{\frac{g}{L}} L \omega_n^2 - g\pi^2 K K_{\dot{x}} K_{m_x} + 16g\xi\omega_n = 0 \quad (3.24)$$

$$8\omega_n^2 - \pi^2 K K_x K_{m_x} = 0 \quad (3.25)$$

The steady-state error is given by $A \left(1 - \frac{1}{K_x} \right)$, where A is the value of the step input to the system. For zero steady-state error, we let $K_x = 1$. Because K_{m_x} is known and fixed, we

end up with four equations in the four unknowns $(K, K_{\dot{x}}, K_{\phi}, \omega_n)$, which can be calculated symbolically as functions of (m_t, L) . At this stage, there is no control over K , which is the dominant factor in determining the maximum acceleration of the trolley, especially at the beginning of the motion.

Because the acceleration increases as the error increases, for long travel distances, the motor acceleration required at the beginning will be very high, which is not realistic. Also, this acceleration increases as L decreases because it will be required to move the load to its target in a short time; this requires a high speed and consequently a large acceleration at the beginning of the process. To overcome this problem, we predetermine K not to exceed the maximum acceleration of the motor. Now, we end up with four equations in the four unknowns $(K_x, K_{\dot{x}}, K_{\phi}, \omega_n)$, which can be calculated as before as functions of (m_t, L, K) . However, the steady-state error will not be zero. To make it zero, we add another gain. This leads to the full-state feedback controller

$$v = K \left(x_{rm} - K_x x - K_{\dot{x}} \dot{x} + K_{\phi} \phi + K_{\dot{\phi}} \dot{\phi} \right) \quad (3.26)$$

Applying the characteristic equation (3.20) and comparing it with that of the system, we obtain four nonlinear equations, which are the same as equations (3.22)-(3.25) except that there is an additional term $\pi K K_{\tau} K_{\dot{\phi}}$ in equation (3.22). By choosing $K_x = 1$ to obtain a zero steady-state error and choosing K not to exceed the maximum available control action, we determine $(K_{\dot{x}}, K_{\phi}, K_{\dot{\phi}}, \omega_n)$ as functions of the remaining parameters (m_t, L) .

The stability of the system is governed by ω_n . For asymptotic stability, it should be positive, which is guaranteed when the gains are calculated.

3.2.1 Tower Cranes

The translational equations of motion are similar to the equations of motion of gantry cranes. The same controller can be used for controlling this motion. The rotational equations of

motion are coupled with the translational equations by the trolley position x . This coupling can be relaxed by assuming x to be constant at any instant. This enables the use of the same control techniques used for gantry cranes. Moreover, the feedback gains are varied with the trolley position.

3.2.2 Simulations

The full nonlinear equations of motion are used in the simulations with the following numerical values in SI units in meters and kilograms:

$$K_{mx} = K_{m\gamma} = 1.34, \quad M_r = 0.5$$

The time is scaled by the oscillation period of the load; that is, $\bar{t} = \frac{t}{2\pi/\sqrt{g/L}} = \frac{t}{T}$. This scaling makes the responses similar for all values of L .

Gantry Cranes

Variation of the feedback gains with the cable length for $m_t = 0$ using the partial state-feedback controller is shown in Figure 3.5. We note that K is inversely proportional to the cable length because the load natural frequency increases with the cable length, which decreases the system settling time and consequently increases K . So, it is better to raise the load as much as possible to transfer it in a short time. However, the speed of the trolley should not exceed the motor maximum speed. The swing-angle gain is linearly proportional to L . If the swing distance $L\phi$ was used in the feedback instead of ϕ , K_ϕ would be independent of L .

It follows from Figure 3.6 that the swing-angle gain decreases linearly with m_t , whereas the other gains do not change. Examining equation (2.21), we note that $m_t g \phi$ can be considered as an extra force in the trolley equation, which affects the trolley accel-

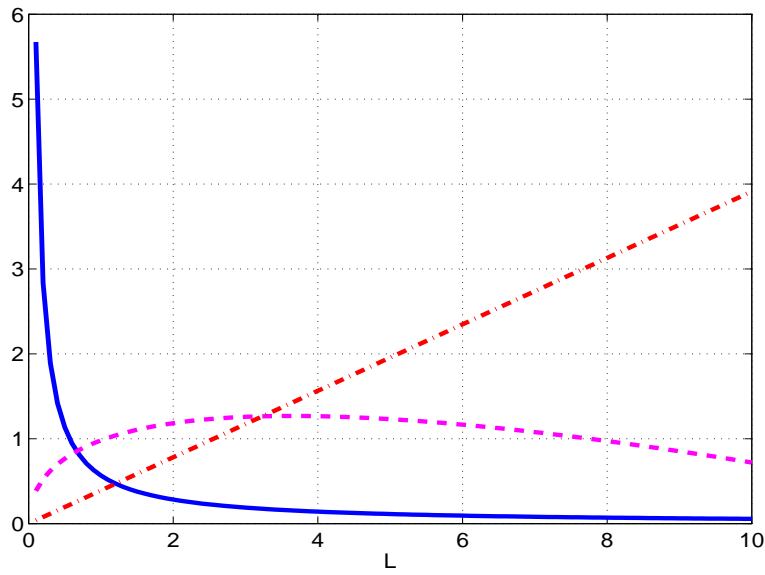


Figure 3.5: Variation of the gains with the cable length using the partial-state feedback controller when $m_t = 0$: — $K/10$, - - - K_x , and -.-.- $K_\phi/10$.

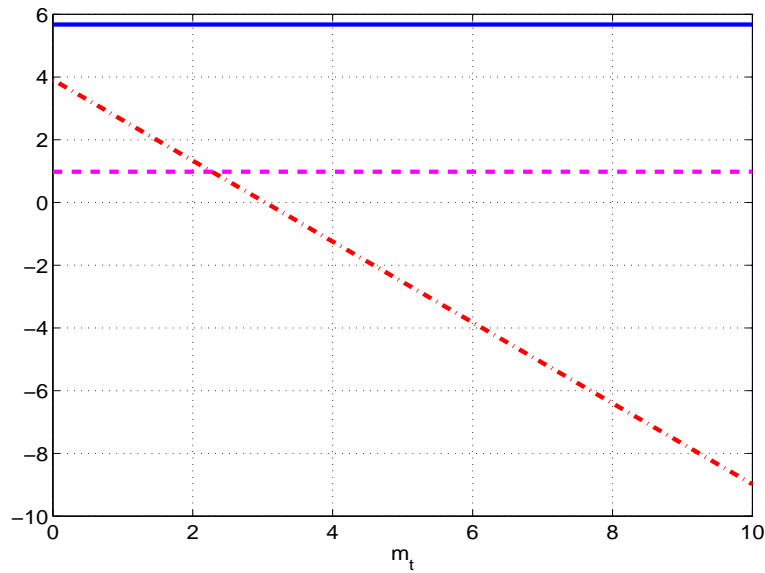


Figure 3.6: Variation of the feedback gains with the cable length using the partial-state feedback controller when $L = 1m$: — K , - - - K_x , -.-.- K_ϕ .

eration and consequently the swing angle. Variation of K_ϕ with m_t can be considered a compensation for this force.

The effect of changing the load mass on the performance of the system is shown in Figure 3.7. From inspection of the time histories, it is seen that the system response deteriorates if the gains are not adapted for the change in the load mass. An overshoot and hence an increase in the number of load oscillations occurs if the gains calculated for $m_t = 0$ were used when $m_t = 5$ because K_ϕ is larger than that required. We note a similar deterioration in the performance when the cable length is changed without adapting the gains, as shown in Figure 3.8. The deterioration increases with increasing cable length and load weight. However, the performance is more sensitive to variations in the cable length than to variations in the load mass. We note that, if the gains corresponding to a long cable were used to control the system with a shorter cable, there would not be an overshoot or an increase in the load oscillations. This is so because the used gain slow down the system more than required. Variations of the feedback gains with cable length for $m_t = 0$ and the load mass for $L = 1m$ using the full-state feedback controller are the same as those obtained in the case of partial-state feedback controller. The results of implementing the full-state feedback controller for different values of K are shown in Figure 3.9. The control action and the maximum swing angle decrease with decreasing K , while the response is slightly slower.

Tower Cranes

In these simulations, we choose $m_t = 1$, and hence $m_r = M_r * m_t = 0.5$. Variation of the feedback gains with the trolley position for the rotational motion controller is shown in Figure 3.10. The swing-angle gain K_θ is inversely proportional to the trolley position x , while the gain K increases with increasing x . The derivative gain $K_{\dot{\gamma}}$ is nearly independent of the trolley position. The response for $L = 1m$ is shown in Figure 3.11. It shows the similarity between tower and gantry cranes, the load is transferred such that it completes

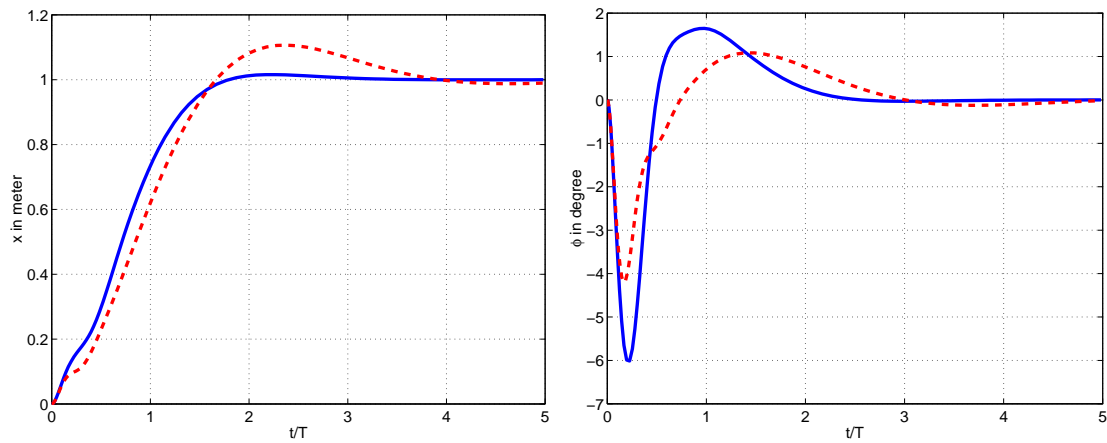
(a) Trolley position x (b) Load swing ϕ

Figure 3.7: Effect of changing the load mass on (a) the trolley position x and (b) the load swing angle ϕ when $m_t = 5$ and $L = 1m$: — using the gains corresponding to $m_t = 5$ and - - - using the gains corresponding to $m_t = 0$.

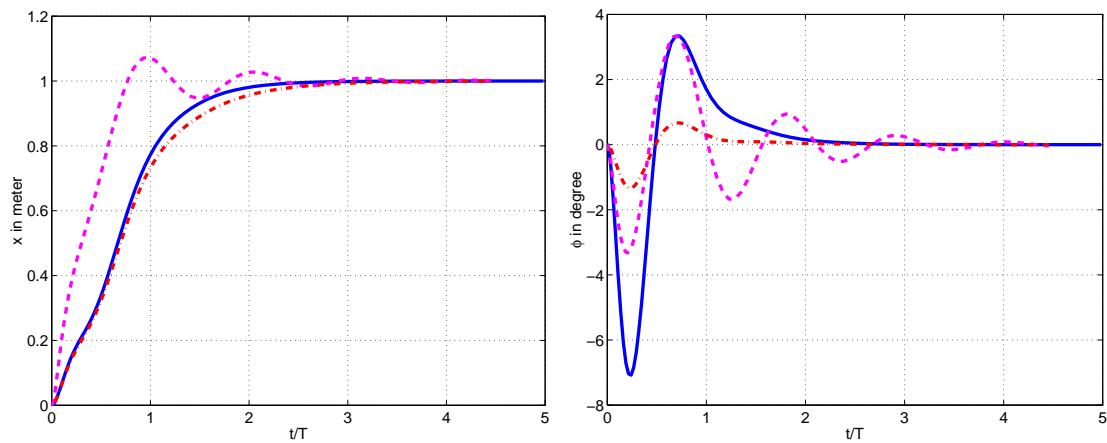
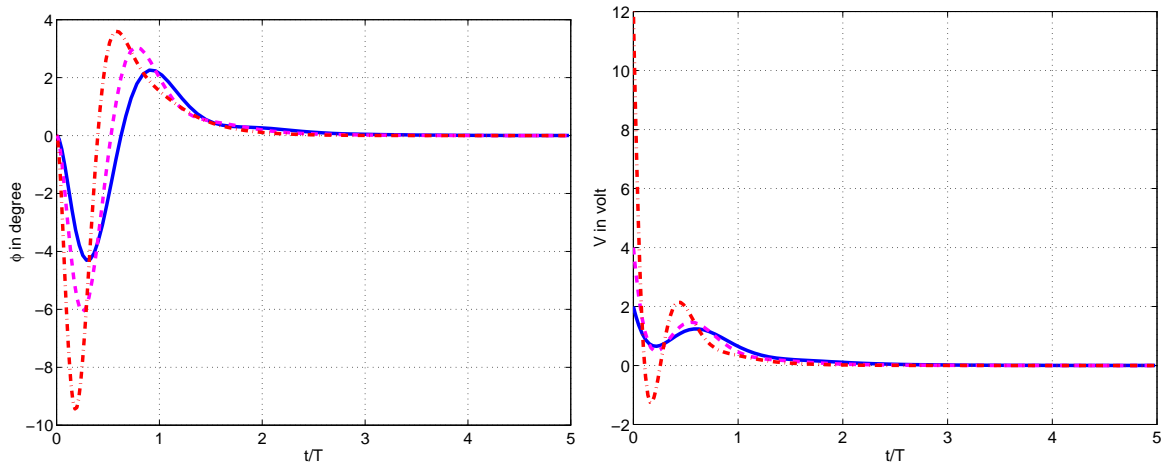
(a) Trolley position x (b) Load swing ϕ

Figure 3.8: Effect of changing the cable length on (a) the trolley position x and (b) the load swing angle using full-state feedback: — $L = 1m$ using the adapted gains, - - - $L = 5m$ using the gains corresponding to $L = 1m$, and -.-.- $L = 5m$ using the adapted gains.



(a) Load swing angle ϕ

(b) Control action

Figure 3.9: Effect of changing K on the (a) load swing angle ϕ and (b) the control action using full-state feedback when $L = 1m$ and $m_t = 0$: — $K = 2$, - - - $K = 4$, and -.-.- $K = 12$.

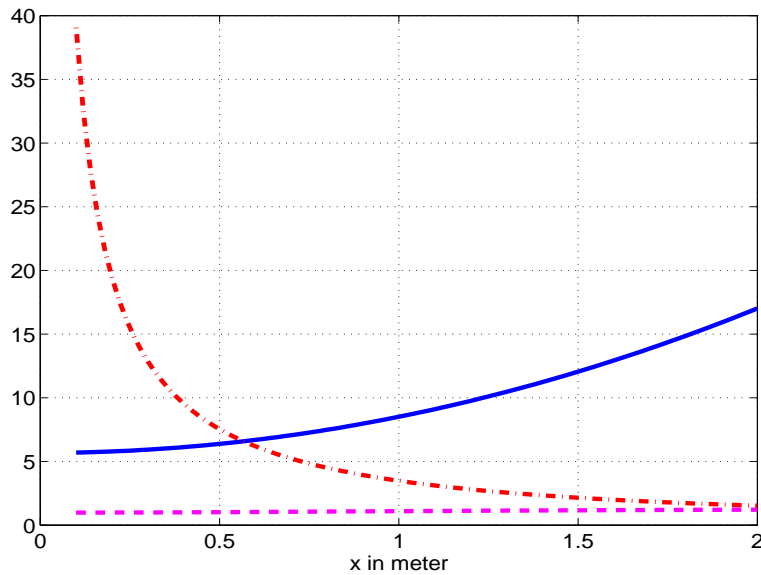


Figure 3.10: Variation of the feedback gains with the trolley position using partial-state feedback for $M_r = m_r = 0.5$: — K , - - - K_γ , and -.-.- K_θ .

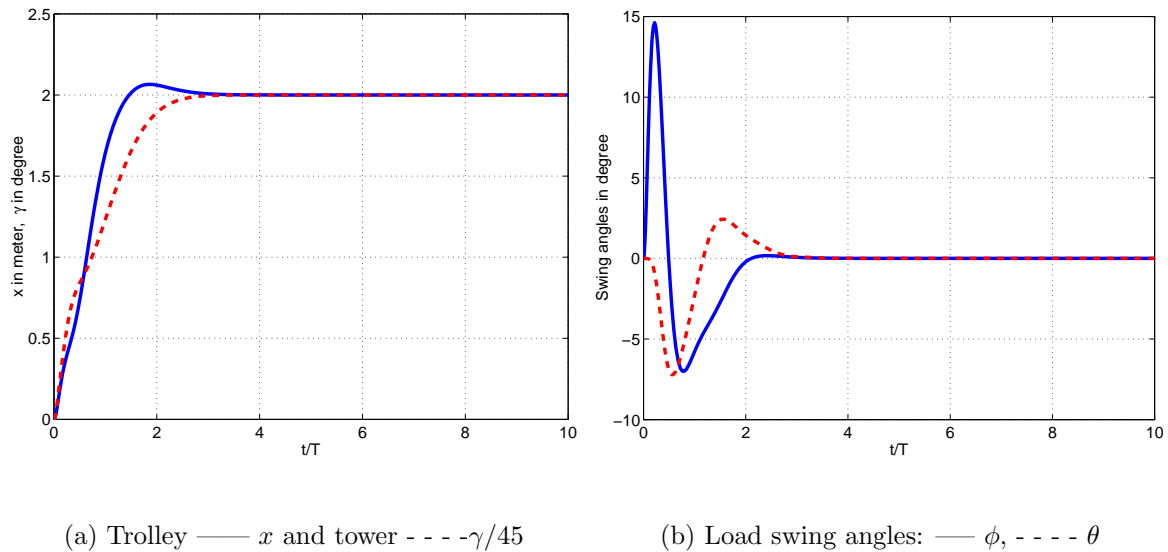


Figure 3.11: Time histories of (a) the trolley and tower positions and (b) the load swing angles for a tower crane using partial-state feedback when $L = 1m$ and $m_t = 0.5$.

only one oscillation cycle at the end of the motion. In Figure 3.12, the cable length is changed to $L = 5m$ while the gains are calculated for $L = 1m$. It is obvious that the response deteriorates if the gains are not adapted to account for the variation in the cable length L .

The response using full-state feedback with $K = 0.4$ and $L = 1m$ is shown in Figure 3.13. Comparing Figures 3.11 and 3.13, we note that the swing and the control action decrease with decreasing K . At the same time, the response becomes slower because of the decrease in the control authority.

3.3 Anti-Swing Tracking Controller

In order to make the designed controller valid for all cable lengths and load weights, we start by normalizing the equations of motion (2.28)-(2.31) using the cable length L and the load

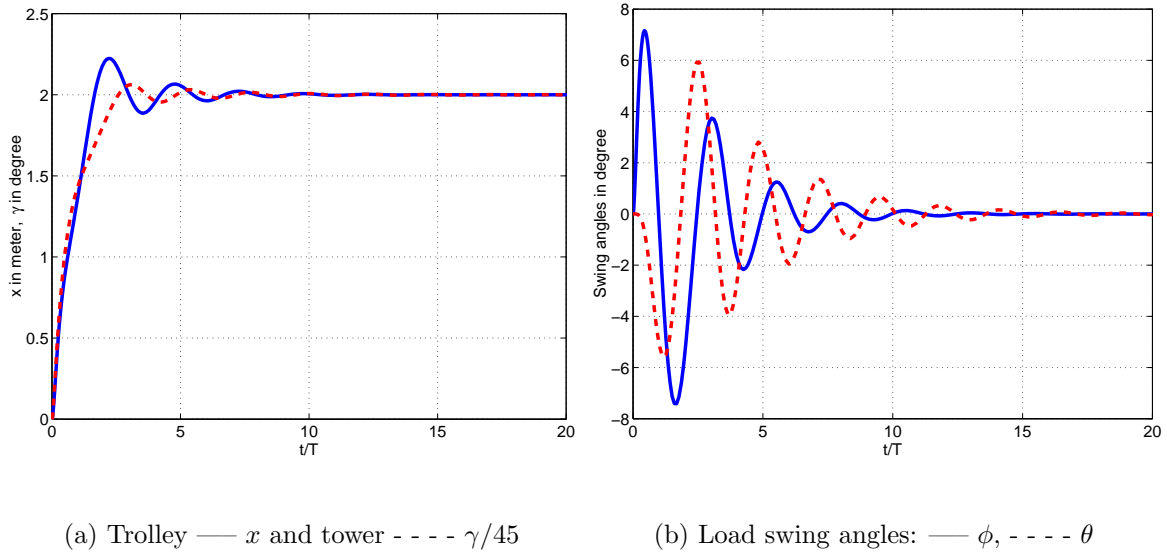


Figure 3.12: Time histories of the system response for a tower crane with $L = 5m$ using partial-state feedback with the gains calculated for $L = 1m$ and not for $L = 5m$.

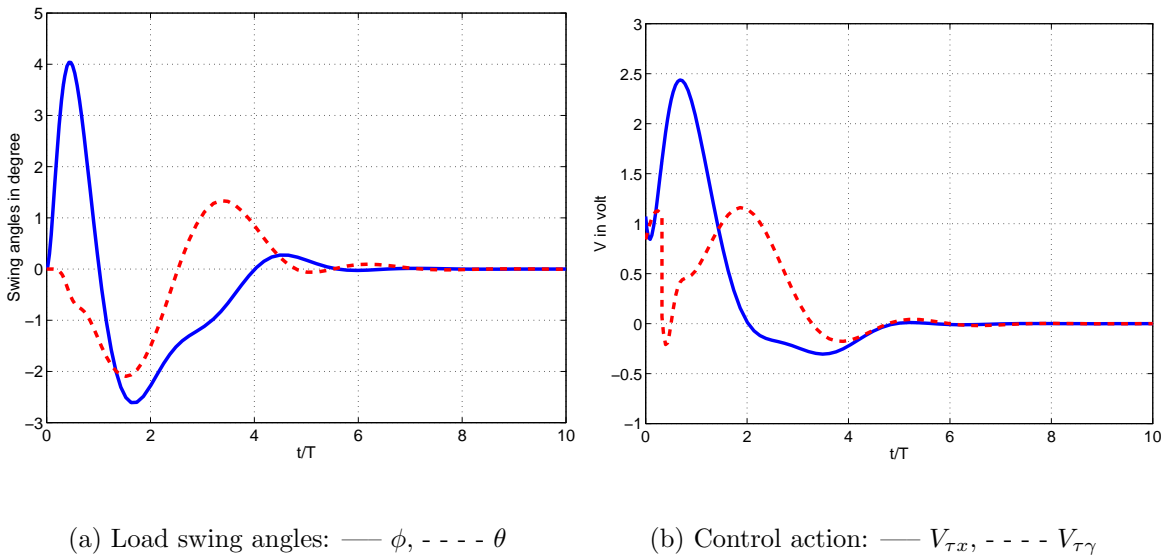


Figure 3.13: Time histories of the system response for a tower crane using full-state feedback when $L = 1m$ and $K = 0.4$

oscillation period T . In the following, we denote the derivative with respect to τ by a prime (i.e., $\frac{dx}{d\tau} = x'$). The normalized equations become

$$\bar{x}'' = \bar{V}_x \quad (3.27)$$

$$\phi'' + a\phi = \bar{x}'' \quad (3.28)$$

$$\gamma'' = \bar{V}_\gamma \quad (3.29)$$

$$\theta'' + a\theta = -\bar{x}\gamma'' \quad (3.30)$$

where

$$\bar{V}_x = \frac{T^2}{L} (K_{mx}V_x - m_t g \phi) \quad (3.31)$$

$$\bar{V}_\gamma = \frac{T^2}{(1 + M_r x^2)} (K_{m\gamma}V_\gamma + m_r g x \theta) \quad (3.32)$$

$$a = \frac{4\pi^2}{T^2} \quad (3.33)$$

To make the rotational equations similar to the translational equations, we replace the rotation angle γ by a new variable y where

$$y = -\bar{x}\gamma \quad (3.34)$$

In order to simplify the analysis, we assume \bar{x} to be constant. With this assumption, the

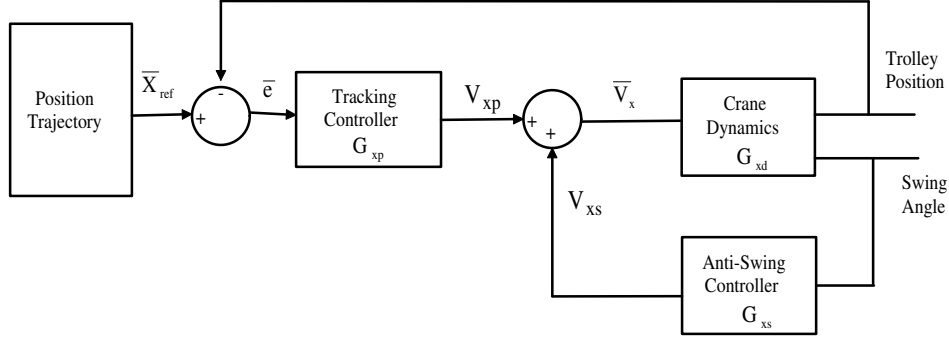


Figure 3.14: A schematic diagram for the anti-swing tracking controller.

rotational equations become

$$y'' = \bar{V}_y \quad (3.35)$$

$$\theta'' + a\theta = y'' \quad (3.36)$$

where $\bar{V}_y = -\bar{x}\bar{V}_\gamma$. These equations are similar to the translational equations. Therefore, we design the controllers for only the translational motion. After determining the control actions \bar{V}_x and \bar{V}_y , we determine the actual voltages to be sent to the motors from

$$V_x = \frac{1}{K_{mx}} \left[\frac{L}{T^2} \bar{V}_x + m_t g \phi \right] \quad (3.37)$$

$$V_\gamma = \frac{1}{K_{m\gamma}} \left[\frac{-L(1 + M_r x^2)}{xT^2} \bar{V}_y - m_r g \bar{x} \theta \right] \quad (3.38)$$

The block diagram of the anti-swing controller for the translational motion is shown in Figure 3.14. The controller consists of two parts: a tracking controller and an anti-swing controller. The function of the tracking controller is to make the trolley follow a prescribed trajectory, while the function of the anti-swing controller is to damp the load swing. The tracking controller gains are first chosen to obtain good tracking, then the anti-swing controller gains are determined to obtain good load-swing damping, which will

ensure the stability of the system. The system stability is determined from the characteristic equation

$$(s^2 + a)(s^2 + G_p(s)) + s^2 G_s(s) = 0 \quad (3.39)$$

The design of the tracking controller is based on the position equation (3.27). We chose a PD controller for simplicity. The control action determined by this controller is

$$V_{xp} = K_{px}\bar{e} + K_{dx}\bar{e}' = \frac{1}{L}(K_{px}e + T K_{dx}\dot{e}) \quad (3.40)$$

where e represents the position error, which is determined from $\bar{e} = \bar{x}_{ref} - \bar{x}$. The corresponding transfer function in the normalized time domain is given by

$$G_{xp}(s) = \frac{V_{xp}(s)}{\bar{e}(s)} = K_{px} + K_{dx}s \quad (3.41)$$

The controller gains K_{px} and K_{dx} are chosen to achieve good tracking of the trajectory without inducing overshoot (i.e., critically damped system). The tracking accuracy increases as K_{px} increases. In order to achieve a critically damping system, we relate the derivative gain to the proportional gain by

$$K_{dx} = 2\sqrt{K_{px}} \quad (3.42)$$

In the following analysis and simulations, we use $K_{px} = 100$ and $K_{dx} = 20$.

3.3.1 Trajectory Design

The trajectory can be designed using an input shaping technique, which takes into account load-swing suppression. However, the resulting trajectory requires longer time (Teo et al., 1998). We can depend on the anti-swing controller for suppressing the load oscillations and design the trajectory to achieve optimal time. The optimal-time solution of a rigid-body motion subjected to acceleration and velocity constraints is a rectangular "bang-bang" input. For sufficiently long motion, such that the maximum velocity can be reached, the acceleration input and velocity profiles are shown in Figure 3.15. The final time to travel a distance Z is

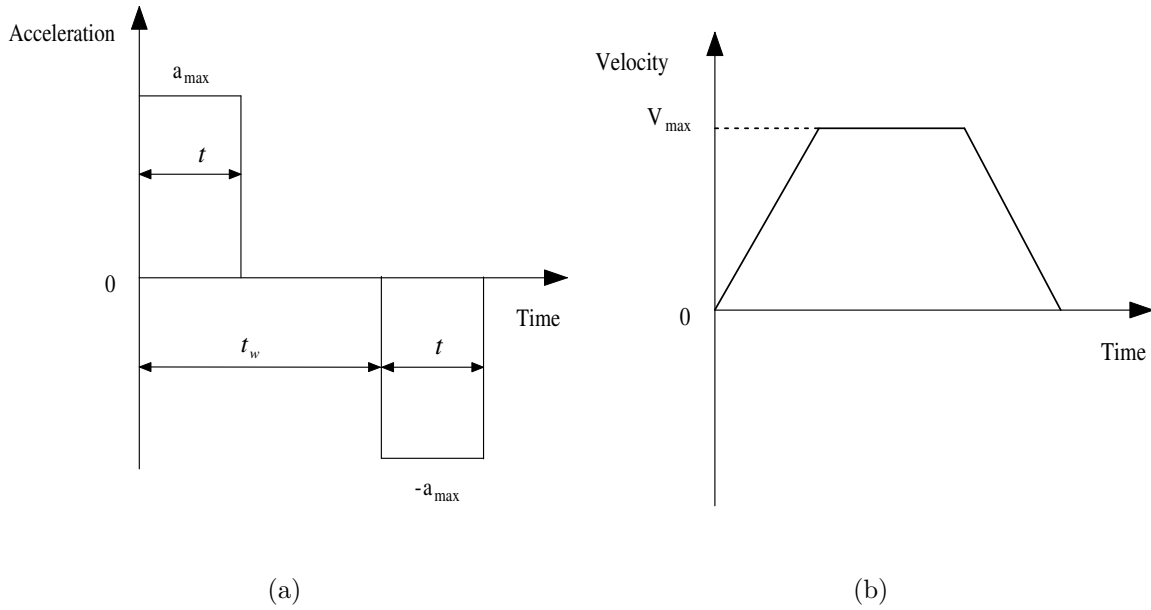


Figure 3.15: Typical optimal-time trajectory: (a) acceleration profile and (b) velocity profile.

computed as

$$t_f = t_w + \Delta t = \frac{Z}{V_{max}} + \frac{V_{max}}{a_{max}} \quad (3.43)$$

3.3.2 Anti-Swing Controller

The objective of the anti-swing controller is to damp the load oscillations described by the swing equation

$$\phi'' + a\phi = x'' = V_{xs} \quad (3.44)$$

This equation has zero damping. A damping term can be added by a proper feedback from the swing angle and its rate using many techniques, such as classical, fuzzy, and delay control.

PD Controller

For the classical PD controller, the contribution of the anti-swing controller to the control action is given by

$$V_{xs} = K_{ps}\phi + K_{ds}\phi' = K_{ps}\phi + K_{ds}T\dot{\phi} \quad (3.45)$$

The corresponding transfer function of this anti-swing controller in the normalized time domain is given by

$$G_{xs}(s) = \frac{V_{xs}}{\phi(s)} = K_{ps} + K_{ds}s \quad (3.46)$$

The controller gains K_{ps} and K_{ds} are chosen to obtain high damping, fast response, and global stability. We determine the stability of the system by solving the characteristic equation (3.39). Figure 3.16 shows the stability map as a function of the PD anti-swing controller gains. The damping ratio shown is determined from the dominating poles. The maximum damping obtained from this controller is nearly 0.45, which occurs at $K_{ps} = 30$ and $K_{ds} = -8$.

Delayed-Feedback Controller

Instead of using the swing angle and its rate in the feedback, a delayed swing angle alone can do the same task. In this case, the anti-swing controller is given by

$$V_{xs} = K_{del}\phi(t - \tau_{del}) \quad \Rightarrow \quad G_{xs}(s) = \frac{V_{xs}}{\phi(s)} = K_{del}e^{-\tau_{del}s} \quad (3.47)$$

In this case, the characteristic equation of the system can be written as

$$(s^2 + a)(s^2 + K_{dx}s + K_{px}) + K_{del}s^2e^{-\tau_{del}s} = 0 \quad (3.48)$$

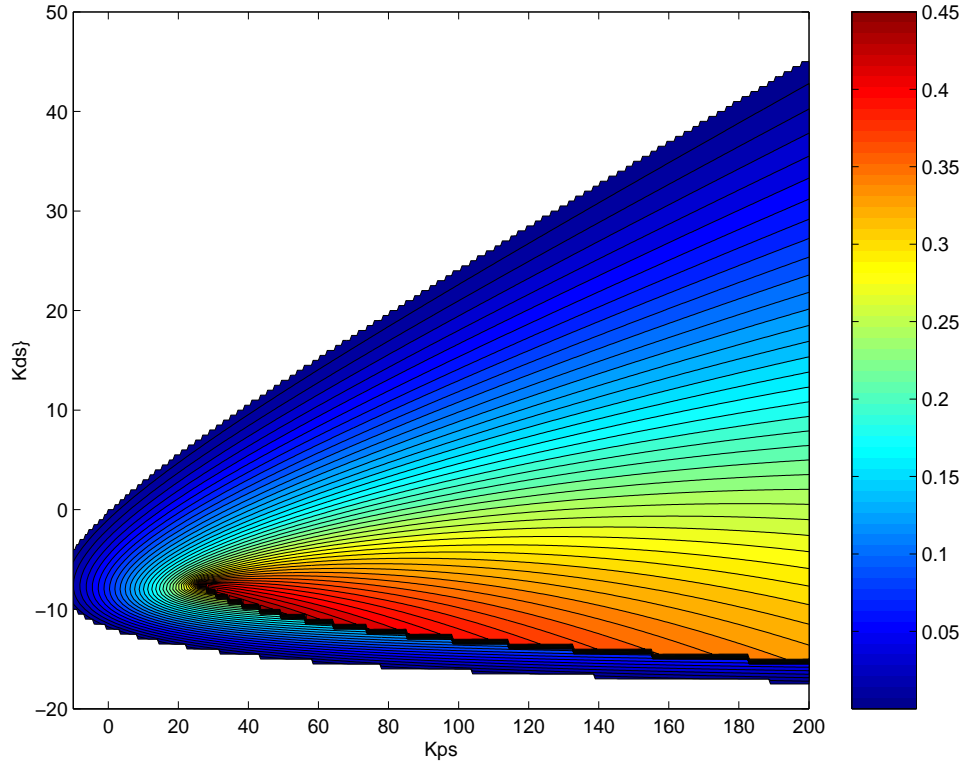


Figure 3.16: The damping map of the anti-swing PD controller.

To calculate the damping in the stability region as a function of the controller parameters K_{del} and τ_{del} , we use the Pade' approximation to approximate the delay term; that is,

$$e^{-\tau_{del}s} = \left(\frac{1 - \frac{\tau}{2l}s}{1 + \frac{\tau}{2l}s} \right)^l \quad l = 1, 2, \dots \quad (3.49)$$

The approximation improves as l increases; $l = 20$ was found to be adequate. The damping ratio is determined from the dominant complex poles. Figure 3.17 shows the damping ratio as a function of the delay controller parameters. It is found that the maximum damping ratio obtained from this controller is nearly 0.45, which occurs at $K_{del} = -90$ and $\tau_{del} = 0.1$.

The delayed-feedback controller can be applied in another configuration as shown in Figure 3.18 (Masoud, 2000). The output from the anti-swing controller in this case represents

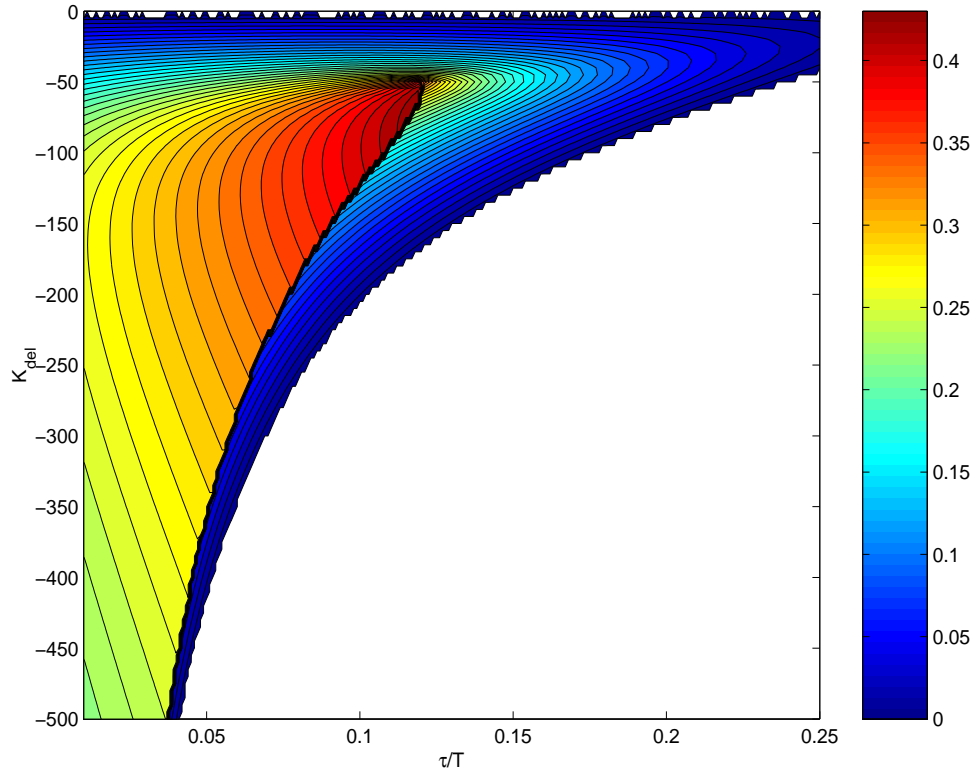


Figure 3.17: The damping map of the first anti-swing delayed-feedback controller.

a correction to the trajectory. The characteristic equation of this system is given by

$$(s^2 + a)(s^2 + K_{dx}s + K_{px}) - K_{del}s^2(K_{dx}s + k_{px})e^{-\tau_{del}s} = 0 \quad (3.50)$$

Following the same procedure, the damping ratio map for this controller is shown in Figure 3.19. The maximum damping ratio obtained from this controller is nearly 0.3, which occurs at $K_{del} = 0.33$ and $\tau_{del} = 0.31$.

We note that the PD controller and the first delay controller produce nearly the same damping ratio, which is higher than that of the second delay controller. We choose the first delay controller rather than the PD controller because we do not need the swing rate to implement the controller. The swing rate is usually determined by differentiating the swing angle, which results in a noisy signal.

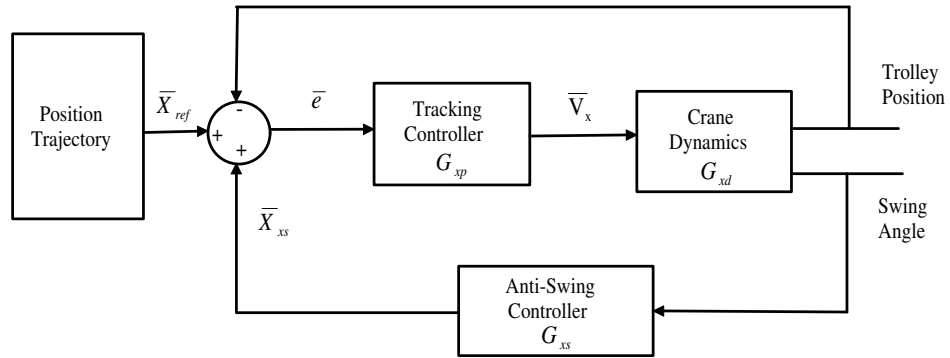


Figure 3.18: A schematic diagram for the second anti-swing delayed-feedback controller

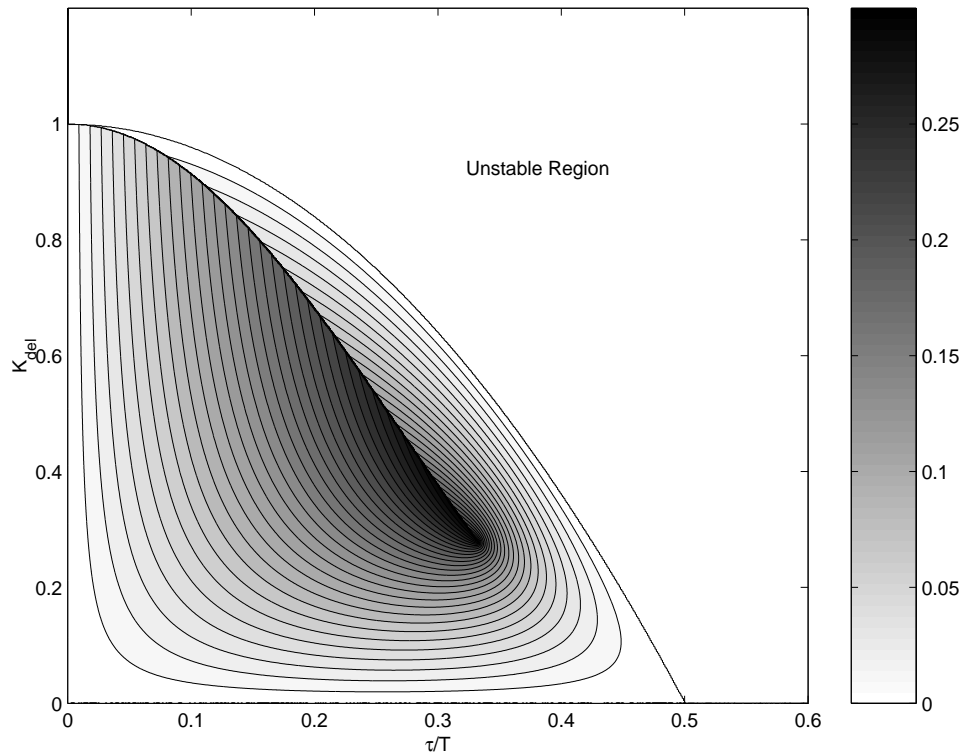


Figure 3.19: The damping map of the second delayed-feedback controller.

Fuzzy Controller

Fuzzy control can also be used to design the anti-swing controller. The fuzzy controller consists of a set of linguistic rules (Jamshidi et al., 1998). To implement these rules, we

fuzzify the control inputs $(\phi, \dot{\phi})$ according to fuzzy membership functions, Figure 3.20. Then, the output of this process is used by an inference system to determine the control output according to the fuzzy rules. This process gives a control action in a fuzzy form, which is then converted to a crisp value suitable for operating the actuator by a process called defuzzification. Figure 3.21 shows the configuration of the fuzzy controller. Usually, the fuzzy variables $(\phi, \dot{\phi}, V_s)$ are normalized using the scaling factors $(K_\phi, K_{\dot{\phi}}, K_V)$, respectively.

The question arises now is how to construct the rule set. The rules can be obtained from an expert operator or by using engineering sense (Wang et. al., 1992). In this work, we use an alternate approach to determine the rules. We map the performance of the anti-swing controllers mentioned in the previous sections. We choose to map the first delay controller response, however the same procedure can be used for the PD and second delay controllers. First, we choose the scaling factors. If we consider $\phi_{max} = 10^\circ = 0.174 \text{ rad}$ is the maximum swing angle, the scaling factors determined from the delay controller are

$$K_\phi = \frac{1}{\phi_{max}}, \quad K_{\dot{\phi}} = \frac{1}{1.5}, \quad K_v = -90 \phi_{max} \quad (3.51)$$

We run the system using the delay controller with the initial swing, say $\phi_o = 10^\circ$, and obtain the input and output from the anti-swing controller. These data are normalized using the scaling factors by multiplying the inputs by K_ϕ and $K_{\dot{\phi}}$ and dividing the output by K_v . The normalized data are denoted by x_1 , x_2 , and y respectively.

During this mapping process, we use the membership functions shown in Figure 3.20 with $a = 1/3, b = 2/3$ for all variables. For each data sample $x_1(i)$, $x_2(i)$, and $y(i)$, we determine the degrees of membership in different regions. For example, $x_1 = 0.2$ has 0.4 degree in ZO , 0.6 degree in PS , and zero degree in all other regions. Similarly, $x_2 = -0.6$ has 0.8 degree in NM , 0.2 degree in NS , and $y = 0.9$ has 0.3 degree in PM and 0.7 degree in PB . For each data pair, we can construct a maximum of four rules as shown in Table 3.6.

Since there are many data pairs and each pair may generate four rules, it is highly

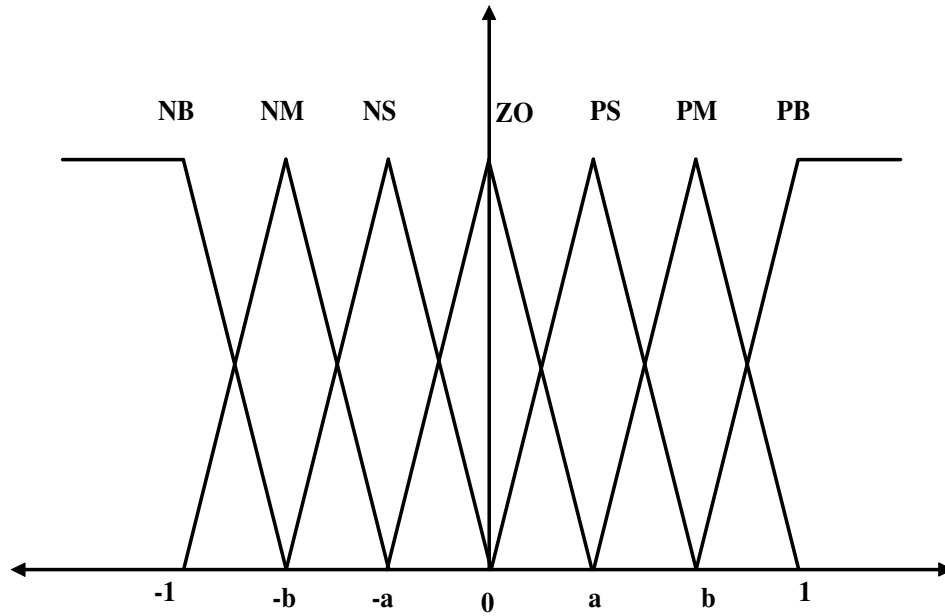


Figure 3.20: Typical membership functions for the fuzzy controller.

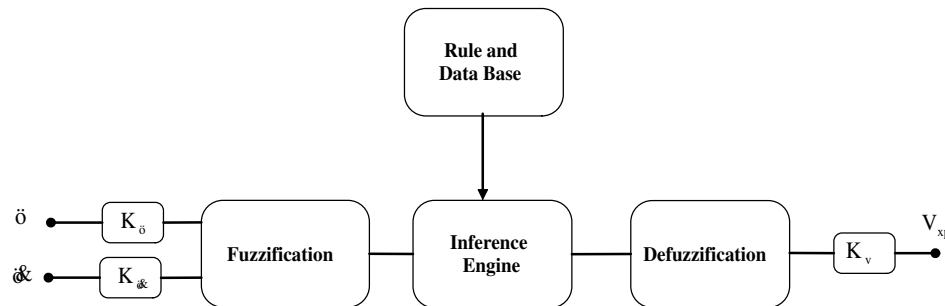


Figure 3.21: Fuzzy logic control (FLC) configuration.

probable that there will be some conflicting rules; that is, rules that have the same 'if part' but a different 'then part'. One way to resolve this conflict is to assign a degree to every rule generated from data pairs and accept only the rule from the conflicting group that has maximum degree. The degree $D(Rule)$ of each rule can be determined from the product of the degrees of membership. For example, the degree of the first rule in Table 3.6 is

$$D(Rule1) = 0.8 * 0.4 * 0.7 = 0.224 \tag{3.52}$$

Table 3.6: Illustration of the generation of the fuzzy rules from given data.

		$\dot{\phi}$						
		NB	NM	NS	ZO	PS	PM	PB
ϕ	NB							
	NM							
	NS							
	ZO		PB (0.224)	PB (0.056)				
	PS		PB (0.336)	PB(0.084)				
	PM							
	PB							

The above steps are repeated for different initial swing angles and transfer distances, Z_x , to completely fill the fuzzy rule table. The generated fuzzy rules and the corresponding degree of membership of each rule are shown in Tables 3.7 and 3.8, respectively.

Table 3.7: The generated fuzzy rules.

		$\dot{\phi}$						
		NB	NM	NS	ZO	PS	PM	PB
ϕ	NB	NS	NB	NB	NB	NB	NB	NB
	NM	PB	PS	NS	NM	NM	NB	NB
	NS	PB	ZO	ZO	NS	NM	NB	NB
	ZO	PB	PM	PS	ZO	NS	NM	NB
	PS	PB	PB	PM	PS	ZO	ZO	NB
	PM	PB	PB	PM	PM	PS	NS	NB
	PB	PB	PB	PB	PB	PM	PB	PS

Table 3.8: The degrees of the generated fuzzy rules.

		$\dot{\phi}$						
V_s		NB	NM	NS	ZO	PS	PM	PB
	NB	0.9902	0.9536	0.9613	0.9505	0.9937	0.9834	1.0000
	NM	0.9034	0.5655	0.9199	0.5608	0.7117	0.9290	0.9822
	NS	0.9802	0.9437	0.7393	0.7657	0.5910	0.6448	0.9608
ϕ	ZO	0.9894	0.8615	0.8664	1.0000	0.8664	0.8615	0.9894
	PS	0.9608	0.6448	0.5910	0.7657	0.7393	0.9437	0.9802
	PM	0.9822	0.9290	0.7117	0.5608	0.9199	0.5655	0.9034
	PB	1.0000	0.9834	0.9937	0.9505	0.9613	0.9536	0.9902

3.3.3 Simulation

The designed anti-swing controllers are independent of the load cable length and weight due to the normalization and feedback linearization. To demonstrate the performance of the controllers, we use the following data in the simulations:

$$L = 1.0 \text{ m}, \quad m_t = 0.09, \quad m_r = 0.28, \quad M_r = 0.27, \quad K_{mx} = 2.0, \quad K_{m\gamma} = 1.14 \quad (3.53)$$

Three maneuvers are used to examine the anti-swing delay and fuzzy controllers. First, a gantry crane is considered, where the trolley is commanded to transfer a load to a certain position without rotating the jib. In the second maneuver, the trolley is placed at a certain position, while the crane is commanded to rotate to a certain angle. The third maneuver combines both of the translational and rotational motions. In order to compare the responses of the anti-swing controllers with that of the gain-scheduling controller, we choose the final times of the trajectories to be equal to one time period of the load swing (i.e., $t_f = T$).

In the first maneuver, the trolley is placed at $x = 0.25 \text{ m}$, and then it is commanded to move to $x = 1.0 \text{ m}$ without rotating the jib; that is, γ is set equal to zero. The data used to generate this trajectory are

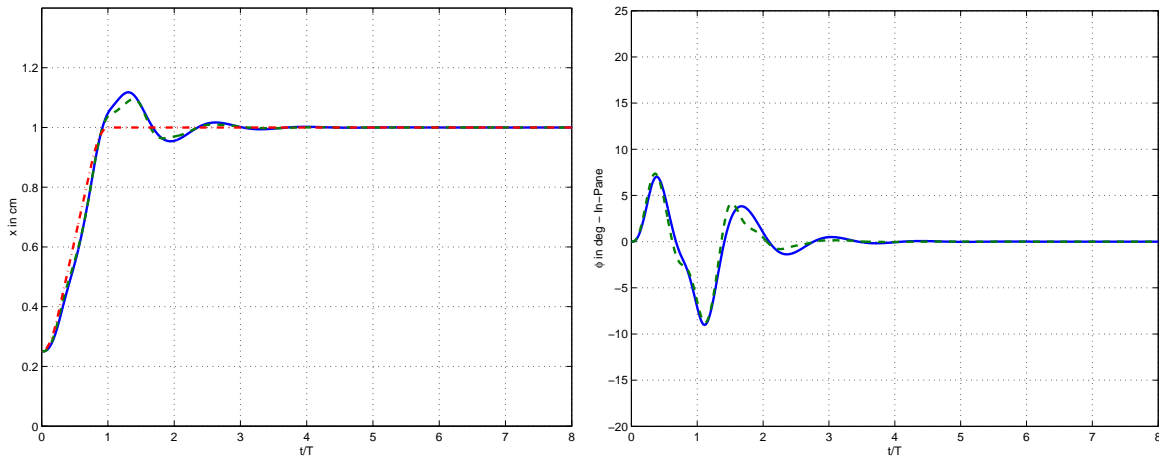
$$Z_x = 0.75 \text{ m}, \quad \Delta t_x = \frac{T}{4}, \quad t_{fx} = T \quad \Rightarrow \quad V_{maxx} = 0.4982, \quad a_{maxx} = 0.9929 \quad (3.54)$$

Figure 3.22 shows the response using the anti-swing delay and fuzzy controllers. The responses of the two controllers are nearly similar. This similarity is expected because the fuzzy controller is a mapping of the delay controller. In contrast with the delay controller, the fuzzy controller does not have any delay. Both controllers successfully transfer the load to its final destination without residual oscillations. Although we designed the final time of the trajectory to be equal to only one swing period, the real final time approaches three periods due to the effect of the anti-swing control. For the same reason, the system response exhibits an overshoot. This overshoot increases with an increase in the trajectory acceleration. We recall that the gain-scheduling controller makes the system reach its destination in a shorter time without overshoot. On the other hand, the anti-swing controller can handle any smooth trajectory other than a step input.

In the second maneuver, the crane is rotated by an angle $\gamma = 90 \text{ deg}$, while the trolley is located at $x = 0.9 \text{ m}$. The data used to generate the rotational motion trajectory are

$$Z_\gamma = 90 \text{ deg}, \quad \Delta t_\gamma = \frac{T}{4}, \quad t_{f\gamma} = T \quad \Rightarrow \quad V_{max\gamma} = 1.0435, \quad a_{max\gamma} = 2.0796 \quad (3.55)$$

In the third maneuver, we start with the trolley at $x = 0.25 \text{ m}$ and command it to move along the jib to $x = 1.0 \text{ m}$. At the same time, the crane is rotated by $\gamma = 90 \text{ deg}$. The trajectories used in this maneuver are obtained from equations (3.54) and (3.55). The responses of the second and third maneuvers are shown in Figures 3.23 and 3.24, respectively. The position overshoot is slightly smaller in the case of the fuzzy controller. However, the load swing angles are smaller in the case of the delay controller. Both controllers take nearly three swing periods to transfer the load to its destination without residual oscillations. In the second maneuver, although we planned to move the system in a rotational motion only, the

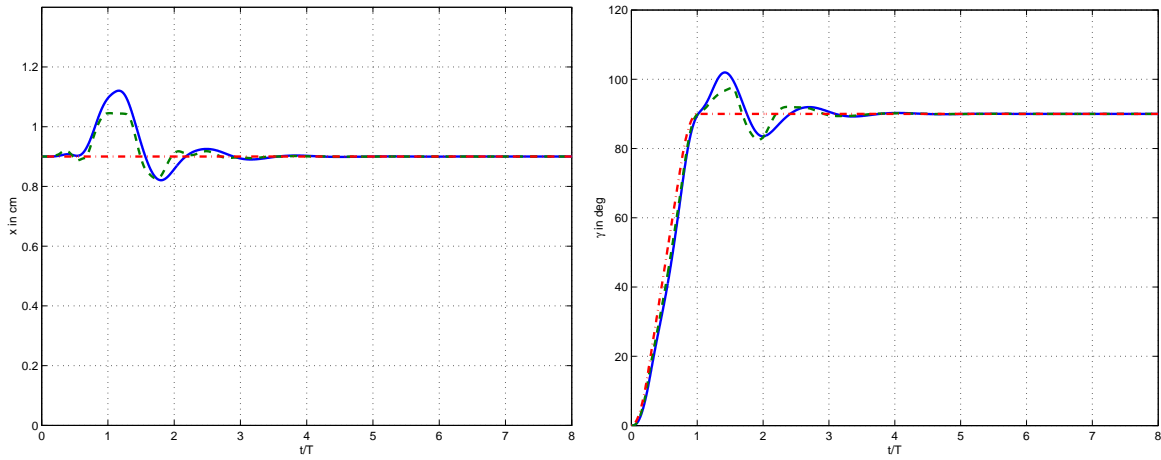


(a) Trolley position

(b) In-plane load-swing angle

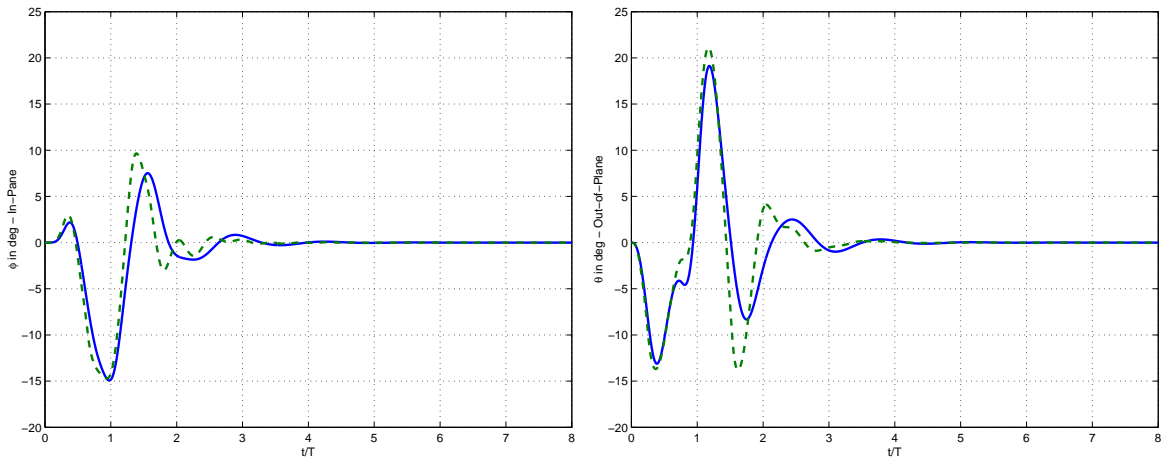
Figure 3.22: Time histories of the anti-swing controllers for translational motion only: — delay, - - - fuzzy, and -.-.- reference trajectory.

translational motion is excited due to the coupling between the translational and rotational motions. The anti-swing controller, working with the tracking controller, successfully damps the in-plane swing and brings the trolley back to its initial position on the jib.



(a) Trolley position

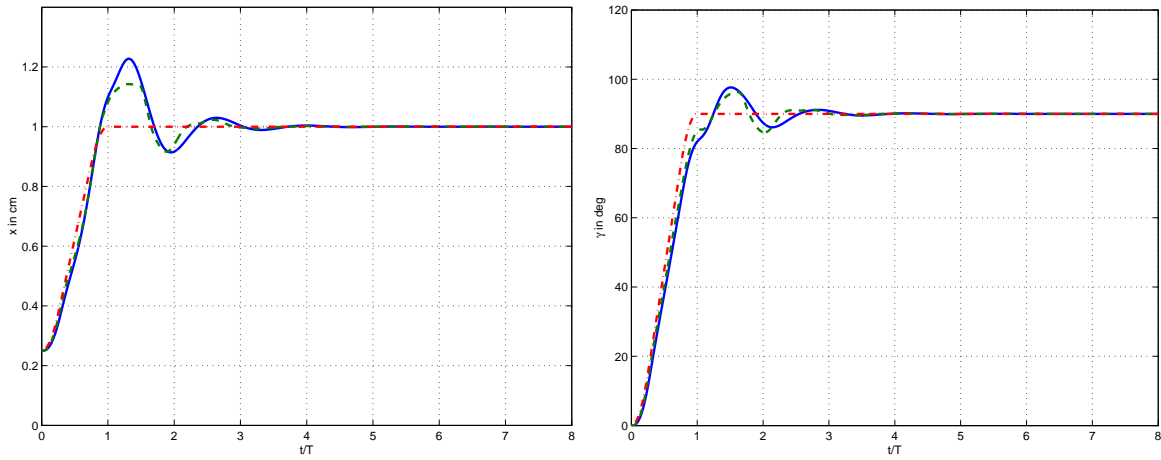
(b) Rotation angle



(c) In-plane load-swing angle

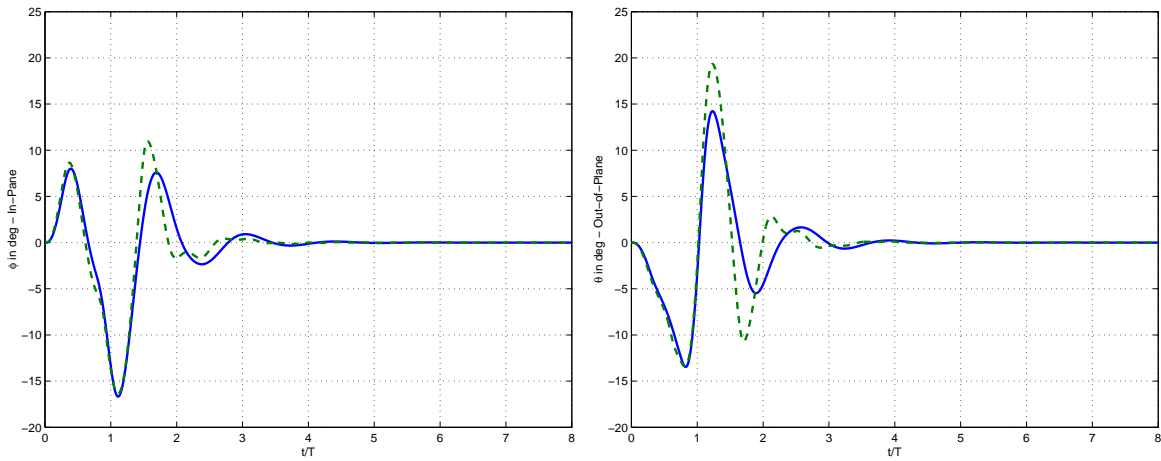
(d) Out-of-plane load-swing angle

Figure 3.23: Time histories of the anti-swing controllers for the rotational motion only: — delay, — fuzzy, and -.-.- reference trajectory.



(a) Trolley position

(b) Rotation angle



(c) In-plane load-swing angle

(d) Out-of-plane load-swing angle

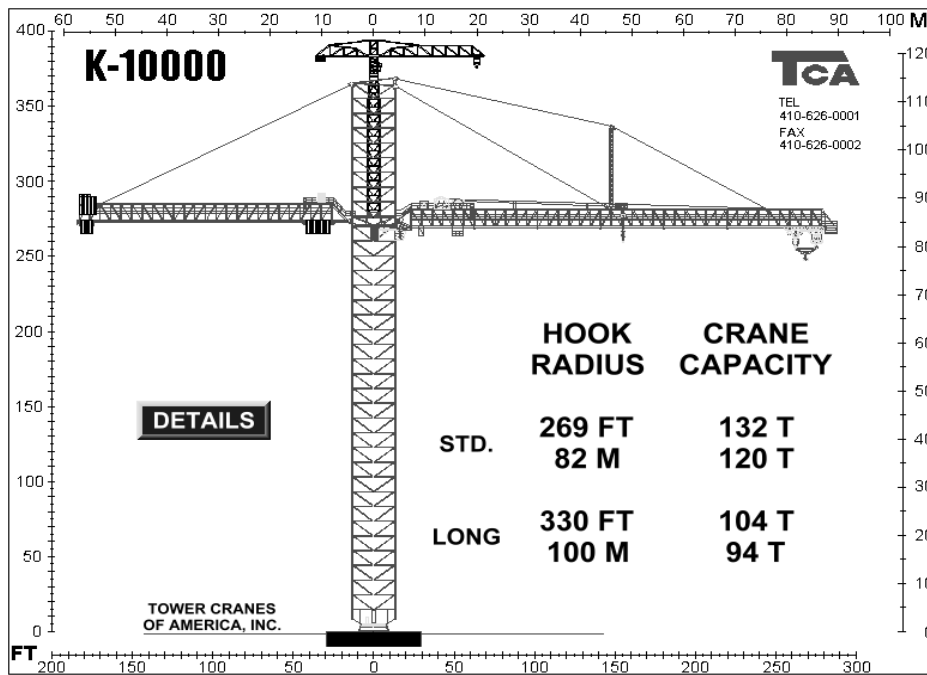
Figure 3.24: Time histories of the anti-swing controllers for the combined motion: — delay, - - - fuzzy, and -.-.- reference trajectory.

Chapter 4

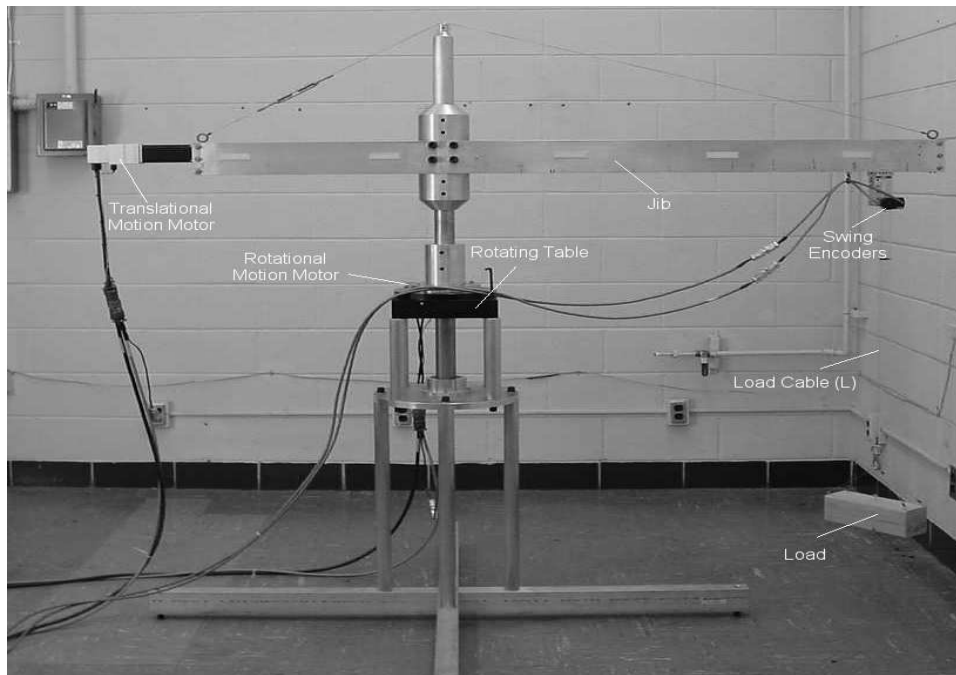
Experimental Results

4.1 Experimental Setup

To validate the designed controllers, a tower-crane model as shown in Figure 4.1 of an actual one was built at Virginia Tech. The control algorithms are implemented on a PC using C++. An interfacing board (IB) is used to link the computer with the tower-crane system, as shown in the experimental setup diagram in Figure 4.2. The tower crane is composed of a trolley assembly moving horizontally on a leadscrew, which is driven by a brushless servomotor. The leadscrew has a pitch $p = 0.5 \text{ in/rev}$. The jib assembly rotates on a rotating table with gear ratio $n = 45$. A servomotor drives the rotating table. Each motor has an optical encoder with a resolution of 2000 lines/rev . These encoders measure the positions of the motors, which in turn are sent to the IB. The motors are equipped with internal brakes, which are engaged when the power is disabled. These brakes require a 24 voltage for opening. The load-swing angles are measured by two optical encoders with a resolution of 6000 lines/rev . Five-volt signals are used to feed the swing encoders. These encoders are connected to digital counters built in the IB; the result is sent to the PC. The output signals of the encoders are the feedback signals of the system. According to these



(a) Actual crane



(b) Crane model used in the experiment

Figure 4.1: Tower-crane configuration.

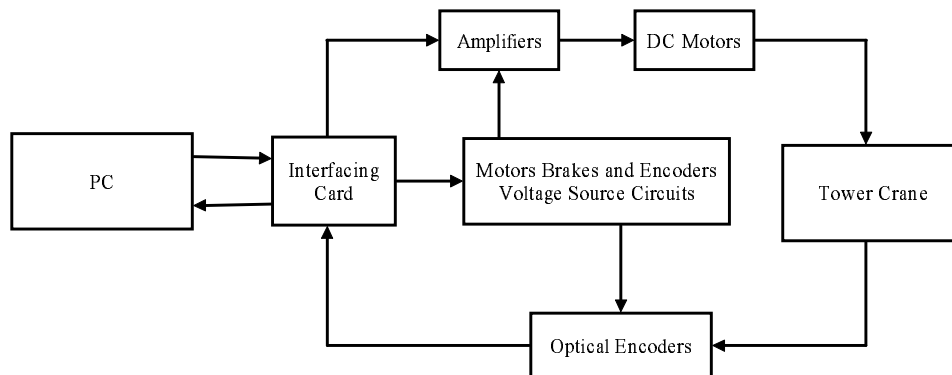


Figure 4.2: Experimental setup diagram.

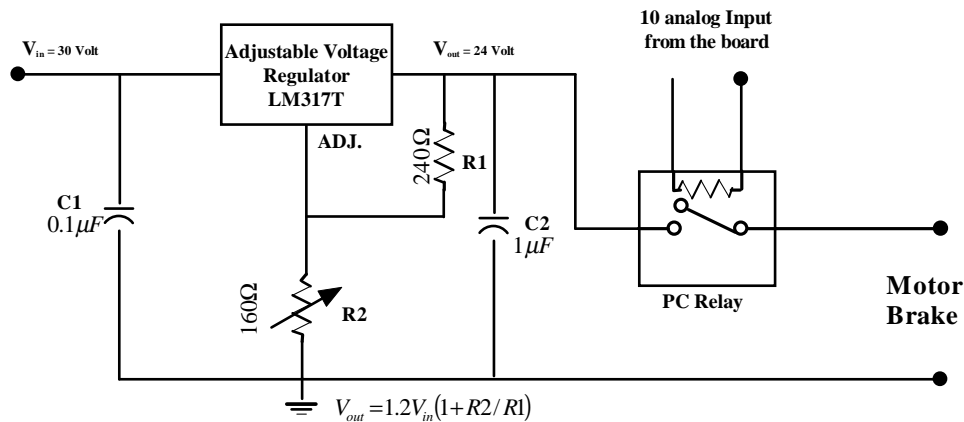


Figure 4.3: Motor brake circuit.

signals, the control algorithm calculates the proper control actions. These actions are sent to the motors. Because the motors require high power for operating, each motor is connected to an amplifier. Each amplifier serves as a communication unit between its motor and the IB. The 24-volt circuit used to open the motor brake is shown in Figure 4.3. It consists of a voltage regulator with a switch, which is opened using a 10-volt control signal generated from the PC. The 5-volt circuit, which feeds the swing encoders, is also a voltage-regulating circuit similar to that used with the brakes.

The interfacing board has 8 channels of encoder input with a 24-bit counter and 8

channels of analog output with a 13-bit resolution and range between -10 volts to 10 volts. It also contains 32 bits, which are configurable in various input and output combinations, and an interval timer capable of interrupting the PC. The timer interval is programmed to 10 minutes in 25 microsecond increments (Servo-to-Go, 1999).

The amplifier can operate the motor in either the velocity mode or the torque mode. We choose the torque mode to be consistent with the crane model and the designed controllers.

4.2 Calculation of the Motor Gains and Mass Properties of the System

We determine the system parameters from the crane configuration and the motor characteristics. In the following analysis, we use SI units unless otherwise mentioned. From Figure 4.4, the equation of motion of a motor rotating with an angle ψ , neglecting friction, is

$$J_{eq}\ddot{\psi} = \frac{K_{torque}}{R}V - \frac{K_{bemf}K_{torque}}{R}\dot{\psi} \quad (4.1)$$

where J_{eq} , K_{torque} , K_{bemf} , and R are the equivalent moment of inertia projected on to the motor axis, the torque constant of the motor, its back emf constant, and the motor resistance, respectively. Here, J_{eq} is the summation of the motor moment of inertia and the equivalent moments of inertia of the mechanical components attached to the motor. The motors for the rotational and translational motions are similar. The motor properties are $J_{motor} = 1.3 \times 10^{-5}$, $K_{torque} = 0.2$, and $R = 1.1$.

For the translational motion, the motor rotates a leadscrew, which drives the trolley. The trolley assembly mass is $M_{trolley} \approx 1.97$. The equivalent moment of inertia of the leadscrew and the trolley are $J_{screw} \approx 1.54 \times 10^{-4}$ and $J_{trolley} \approx 8 \times 10^{-6}$, respectively. Therefore, the equivalent moment of inertia is $J_{eq} = J_{screw} + J_{trolley}/e + J_{motor} \approx 1.83 \times 10^{-4}$,

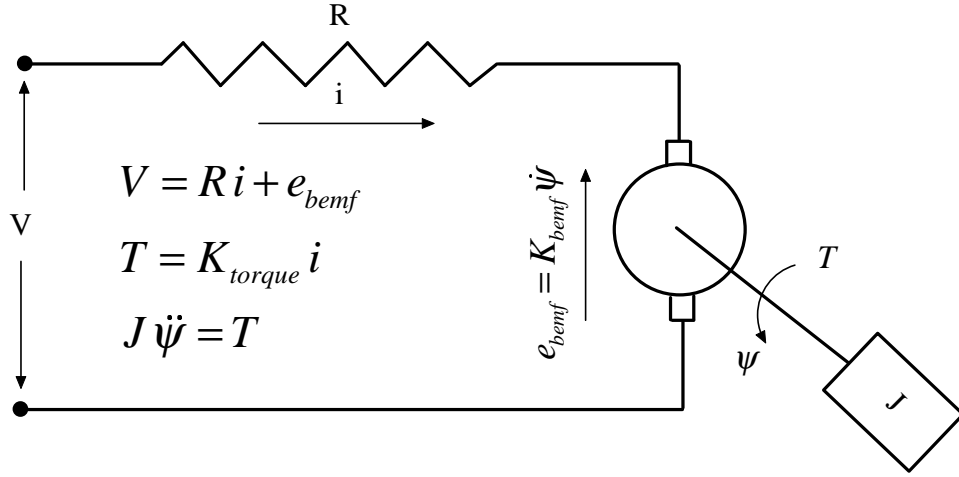


Figure 4.4: DC motor diagram.

where e is the leadscrew efficiency, which has a value of approximately 0.5. The translation variable x is related to the motor rotation angle ψ by the screw pitch p . The screw pitch is equal to $0.5 \text{ in/rev} = 0.00202 \text{ m/rad}$. The relation is $x = p \psi$. Inserting this relation into equation (4.1) and neglecting the viscous term, we obtain

$$M\ddot{x} = \frac{K_{torque}}{Rp} V \quad \rightarrow \quad \ddot{x} = K_{mx} V_x \quad (4.2)$$

where M is the equivalent mass, which is determined from

$$M = \frac{J_{eqe}}{p^2} \approx 22.46 \quad (4.3)$$

and

$$K_{mx} = \frac{K_{torque}}{pRM} \approx 2.0 \quad (4.4)$$

For the rotational motion, the motor rotates the jib assembly through a rotating table, which has a gear reduction ratio of $n = 45$. The total equivalent moment of inertia of the jib assembly is determined to be $J_{jip} = 4.4/n^2$. Because the trolley moves along the jib, its contribution to the moment of inertia varies. Hence, the trolley is not included in J_{jip} , but rather in the crane modeling in Chapter 2. The total of the moments is $J_{eq} = J_{jip} + J_{motor} = 0.00354$. The rotation of the tower is related to the motor rotation angle by

$\gamma = \psi/n$. Inserting this relation into equation (4.1), we find that the final moment of inertia is $J_o = J_{eq}n \approx 0.16$. Hence, the motor gain is

$$K_{m\gamma} = \frac{K_{torque}}{RJ_o} \approx 1.14 \quad (4.5)$$

According to our model derived in Chapter 2,

$$M_r = \frac{M_{trolley}}{J_o n} \approx 0.27 \quad (4.6)$$

Knowing the load mass m , we have

$$m_t = \frac{m}{M} \quad \text{and} \quad m_r = \frac{m}{J_o n} \quad (4.7)$$

This gives us all of the information needed to implement our controllers.

4.3 Differentiation and Filtering

In order to implement the designed controllers, we need the trolley velocity, the tower angular rotation, and the swing rates. Because we do not have sensors to measure these quantities, we calculate them by differentiation. The differentiator should be as close as possible to the ideal one to decrease its deteriorative effect. For this purpose, a comparison between three differentiators is conducted. The first one is the well-known first-order backward differentiator. The output y from this filter at instant k for an input x is determined from

$$y(k) = f_s [x(k) - x(k-1)] \quad (4.8)$$

The second filter is also a first-order one obtained by taking the inverse of the transfer function of a first-order integrator (Al-Alaoui, 1993). The difference equation of this filter is

$$y(k) = -\frac{1}{7}y(k-1) + \frac{8f_s}{7} [x(k) - x(k-1)] \quad (4.9)$$

The third filter is based on the previous idea, but the Simpson integration rule is used for the integrator (Al-Alaoui, 1994). Thus, the filter is second order and is given by

$$y(k) = -0.5358y(k-1) - 0.0718y(k-2) + \frac{3f_s}{3.7321} [x(k) - x(k-1)] \quad (4.10)$$

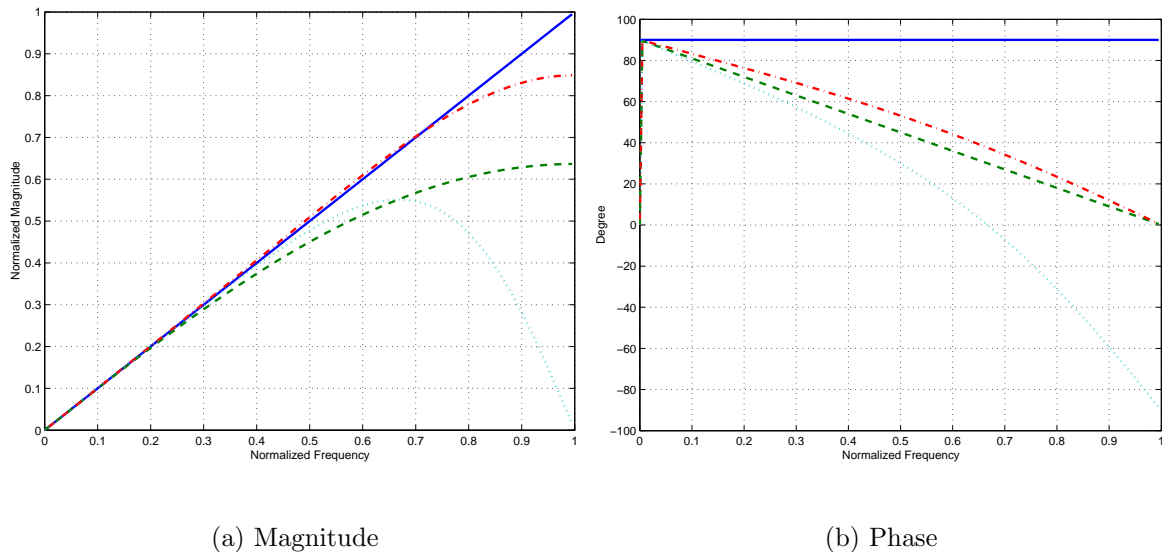


Figure 4.5: Comparison among three differentiators: — ideal, - - - backward, -.-.-.- first-order differentiator proposed by Al-Alaoui (1993), and second-order differentiator proposed by Al-Alaoui (1994).

Figure 4.5 shows the magnitude and phase of these differentiators compared with the ideal one. We note that all of them have a good magnitude response in the low-frequency range of interest. The Al-Alaoui first-order differentiator gives less phase lag, which is required in real-time control. However, the phase lag for all differentiators is almost the same in the low-frequency range. The Al-Alaoui second-order differentiator does not magnify the high frequencies as much the other differentiators; therefore, we choose this numerical differentiator.

The measured signals are usually contaminated with noise. This noise should be removed before differentiation. A low-pass filter is used to accomplish this task. In choosing the filter, we have to keep in mind that, besides the high-frequencies attenuation, the filter should not introduce high-phase distortion to the signal. The ideal filter should have zero-phase, which can not be obtained in real-time control. So, to achieve good noise reduction and to minimize the phase distortion, we choose a second-order Butterworth filter with a

cut-off frequency of $0.05 f_s$.

For the sampling frequency, it is well-known that, as the sampling frequency increases, the discretization effect on the system performance decreases. However, we are limited by the computer speed and word length and the encoder resolution. Otherwise, the quantization error will dominate. Middleton and Goodwin (1990) suggested that using a sampling frequency 50 times the highest frequency in the system is adequate to make the performance of the discretized system the same as the analog one. In our experiment, we use $f_s = 100$ Hz because our frequency range does not exceed 2 Hz.

4.4 Friction Coefficients Estimation

4.4.1 Translational Motion

First, we mention some observations about the trolley motion, which is driven by a leadscrew-nut mechanism.

- The performance of the trolley depends on the motion direction.
- When a filtered velocity is used in the control-action calculation, the motion in the positive direction becomes oscillatory with high magnitude. However, when unfiltered data is used, the motion becomes smoother, even with the noise introduced by the numerical differentiation!!. This behavior may be a result of the interaction between friction and the delay introduced by the filter. For this reason, the unfiltered velocity is used to determine the control action sent to the trolley motor.

To estimate the friction coefficients of the translational motion, we command the trolley to follow the reference signal

$$x_{ref} = 0.6 \left[-0.4 \sin \left(\frac{2\pi}{3} t \right) + 0.3 \sin \left(\frac{2\pi}{4} t \right) \right] \quad (4.11)$$

Table 4.1: Estimated friction coefficients for the translational motion.

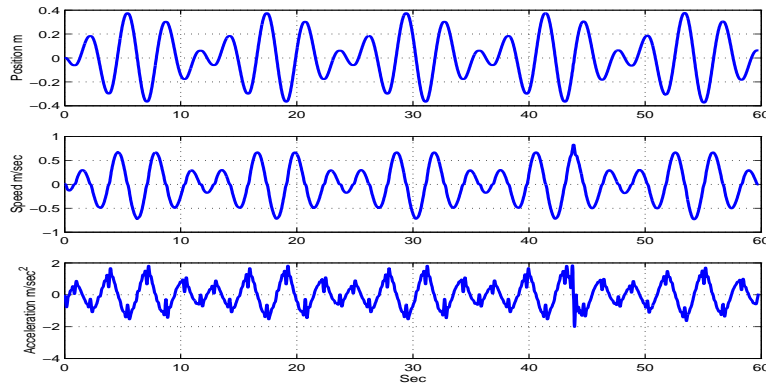
K_p	K_d	b_+/K_m	b_-/K_m	c_+/K_m	c_-/K_m
100	0.2	1.434	6.409	1.261	0.867
10	0.5	1.578	6.872	1.371	0.914
10	0	1.491	6.004	1.207	0.926

To stabilize the system, we use a PD controller. When we conducted the experiment using the tracking gains $K_p = 100$ and $K_d = 0.2$, we obtained two estimates for the friction coefficients. Comparing the outputs from several runs, we noted that the position and velocity differences are small. However, there is a large difference in the control actions. This is attributed to the magnification of the error caused by the high value of the controller gain K_p . To avoid this problem, we need to reduce K_p . A new set of gains is used: $K_p = 10$ and $K_d = 0.5$. Moreover, to avoid the problem arising from the velocity filtering, we use another set of gains: $K_d = 0$ and $K_p = 10$. The results of the estimation for different sets of gains are shown in Table 4.1. The system outputs are shown in Figure 4.6. The cut-off frequency used is $\omega_c = 5$ Hz, whereas $d_s = 0.1$.

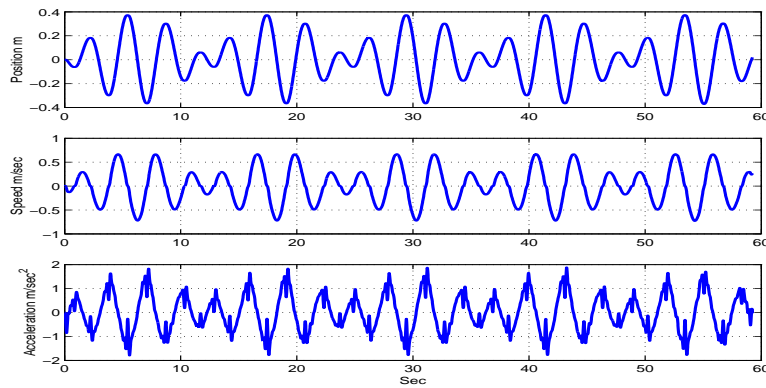
Examining these results, we note that the friction coefficients are nearly the same. These values are used as a starting guess for friction compensation. The final values obtained by fine-tuning are

$$\frac{b_+}{K_m} = 1.5, \quad \frac{b_-}{K_m} = 6, \quad \frac{c_+}{K_m} = 0.9, \quad \frac{c_-}{K_m} = 1.2 \quad (4.12)$$

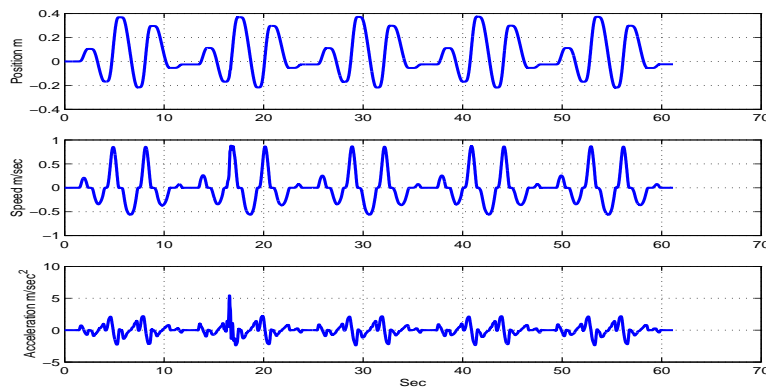
To validate these results, we applied a step input to the trolley and the friction was compensated using the tuned coefficients. The response is compared with that of a linear frictionless model, equation (3.4). The controller gains are chosen to be $K_p = 6$ and $K_d = 1.33$. This comparison is displayed in Figure 4.7, which shows that the friction compensation is acceptable. To complete the friction estimation, we determine the static



(a) $K_p = 100, K_d = 0.2$



(b) $K_p = 10, K_d = 0.5$



(c) $K_p = 10, K_d = 0$

Figure 4.6: The translational motion response for $x_{ref} = 0.6 \left[0.3 \sin \left(\frac{2\pi}{4} t \right) - 0.4 \sin \left(\frac{2\pi}{3} t \right) \right]$.

friction be

$$\frac{f s_+}{K_m} \approx 1.0, \quad \frac{f s_-}{K_m} \approx 1.2 \quad (4.13)$$

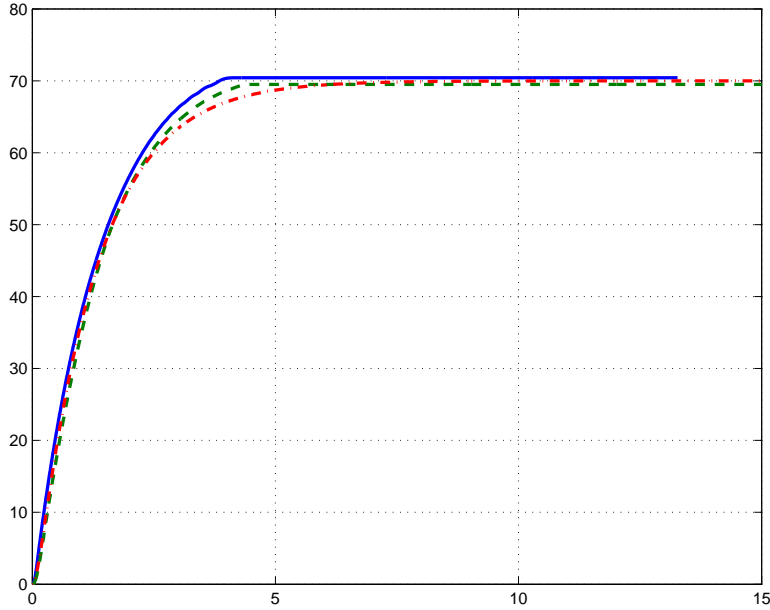


Figure 4.7: The translational motion response to a step input with friction compensation: — positive direction, - - - negative direction, -.-.- linear system.

4.4.2 Rotational Motion

To reduce the effect of the trolley on the rotational motion, we placed it near the rotation axis of the crane. Then, the crane was commanded to rotate and follow a trajectory given by

$$\gamma_{ref} = 2 \left[-0.4 \sin \left(\frac{2\pi}{3} t \right) + 0.3 \sin \left(\frac{2\pi}{4} t \right) \right] \quad (4.14)$$

Following a procedure similar to that used with the translational motion, we stabilized the system by a PD controller. We note that the rotational motion is smoother than the translational one. Also, we had to use the filtered velocity in the feedback because the measured

Table 4.2: Estimated friction coefficients for the rotational motion.

A	K_p	K_d	b_+/K_m	b_-/K_m	c_+/K_m	c_-/K_m
2.5	7.5	1.33	0.101	0.114	0.926	0.891
1.5	10	0.5	0.180	0.194	0.919	0.908

rotational angle is contaminated with high-frequency noise. The estimated parameters with different sets of controller gains are listed in Table 4.2, while the response is shown in Figure 4.8. We note that the estimated Coulomb friction is higher than the static friction. The calculated static frictions are

$$\frac{fs_+}{K_m} \approx 0.7, \quad \frac{fs_-}{K_m} \approx 0.6 \quad (4.15)$$

After some tuning, we chose the friction coefficients to be

$$\frac{b_+}{K_m} = 1.5, \quad \frac{b_-}{K_m} = 0.05, \quad \frac{c_+}{K_m} = 0.7, \quad \frac{c_-}{K_m} = 0.6 \quad (4.16)$$

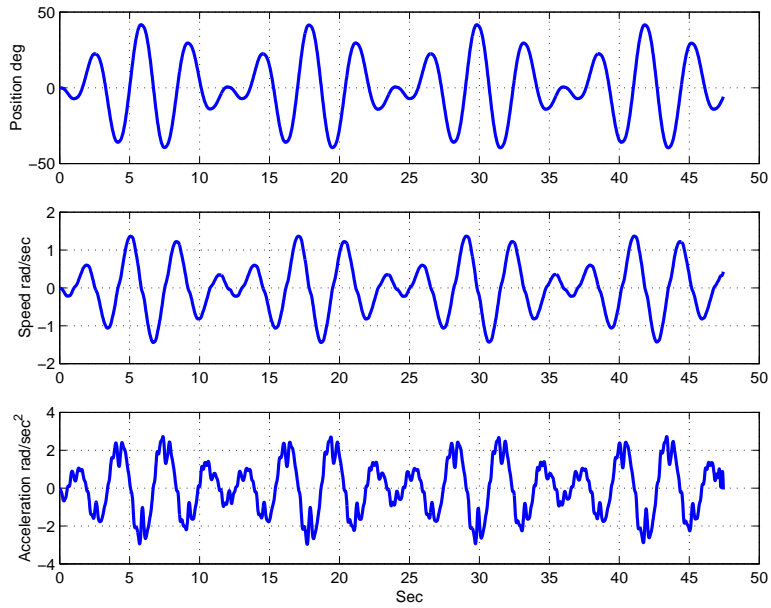
To validate these results, we applied a step input to the crane rotational motion and the friction was compensated using the tuned coefficients. The response was compared with that of a linear frictionless model, equation (3.4). The controller gains were chosen to be $K_p = 7.5$ and $K_d = 1.33$. This comparison is displayed in Figure 4.9, which shows that the friction compensation is also acceptable.

4.5 Gain-Scheduling Feedback Controller

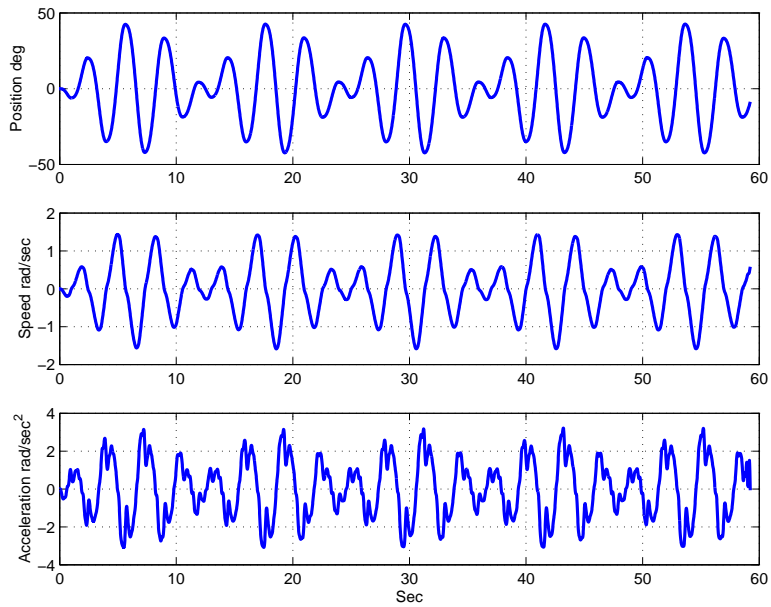
The load mass m used in the experiment is 2.0 Kg . Using equation (4.7) yields

$$m_t = 0.09, \quad m_r = 0.28 \quad (4.17)$$

The cable length used is 1 m . Now, we have all the information to determine the control gains. First, we ran the experiment using the partial-feedback controller and then the full-



(a) $K_p = 7.5, K_d = 1.33$



(b) $K_p = 10, K_d = 0.5$

Figure 4.8: The rotational motion response for $\gamma_{ref} = 2 \left[-0.4 \sin \left(\frac{2\pi}{3}t \right) + 0.3 \sin \left(\frac{2\pi}{4}t \right) \right]$.

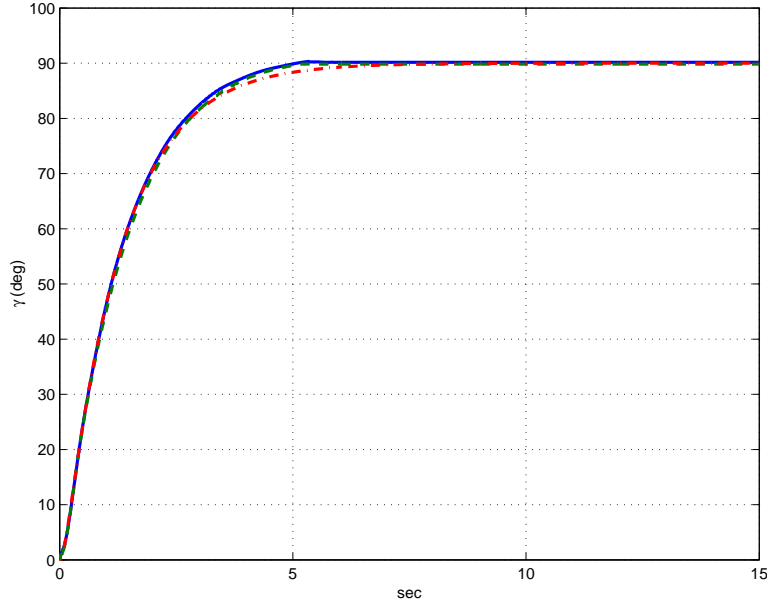


Figure 4.9: The rotational motion response to a step input with friction compensation: — positive direction, - - - negative direction, and -.-.- linear system.

state feedback controller. We note that the experimental results shown here are obtained using filtered data.

4.5.1 Partial-State Feedback Controller

For $K_{mx} = 2.0$, the feedback gains for the translational motion obtained from solving equations (3.22)-(3.25) are

$$K = \frac{3.8}{L}, \quad K_{\dot{x}} = 1.33\sqrt{L}, \quad K_{\phi} = L(3.9122 - 1.28925m_t) \quad (4.18)$$

The corresponding gains for the rotational motion with $K_{m\gamma} = 1.14$ and $M_r = 0.28$ were obtained as functions of m_r , L , and x by curve fitting. Because L and m_r are considered constants, we can determine the gains as functions of the trolley position only. The Mathematica software was used to solve for the gains and a series expansion is performed to

simplify the results; the results are

$$K = 6.66 + 1.8x^2, \quad K_{\dot{x}} = 1.33, \quad K_{\theta} = \frac{3.9122}{x} - 0.360989x \quad (4.19)$$

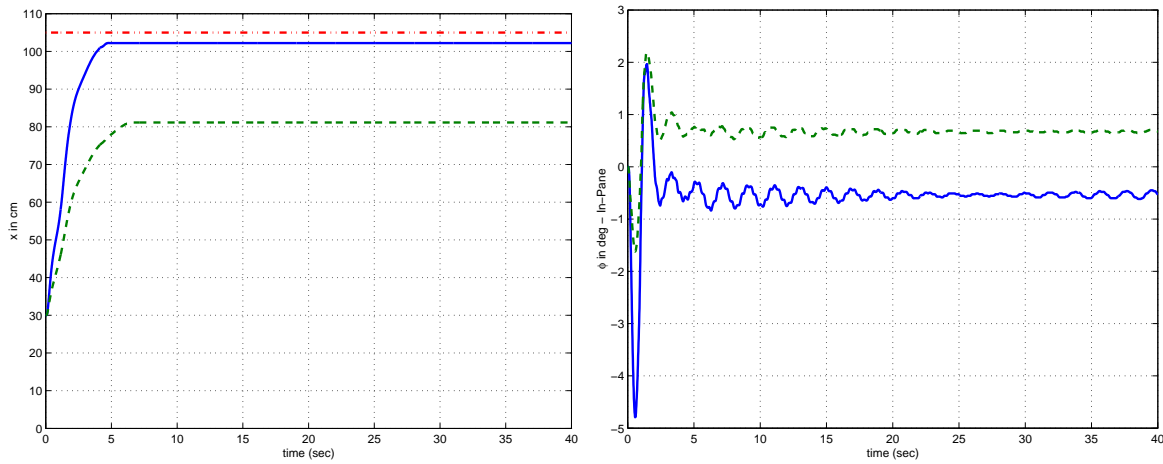
Three maneuvers were used to examine the control algorithm. First, a gantry crane was considered, where the trolley was commanded to transfer a load to a certain position without rotating the jib. In the second maneuver, the trolley was placed at a certain position, while the crane was commanded to rotate to a certain angle. The third maneuver combined both of the translational and rotational motions.

In the first maneuver, the trolley was placed at $x = 0.3 \text{ m}$, and then it was commanded to move to $x = 0.75 \text{ m}$ without rotating the jib; that is, γ is set equal to zero. Figure 4.10 shows the experimentally obtained response with and without friction compensation. Without friction compensation, the trolley position has a high steady-state error. Also, the swing is small and damped because of the slowness of the response, which results from the high frictional forces opposing the motion. With friction compensation, we note that the swing is suppressed; however, there is a steady-state error in the swing angle. This error results from an initial oscillation of the load. This error could be completely avoided if we use an absolute encoder rather than an incremental encoder. This error modifies the load destination point according to equation (4.20); that is,

$$X_{ref} = X_{ref} + K_{\phi}\phi_{ss} \quad (4.20)$$

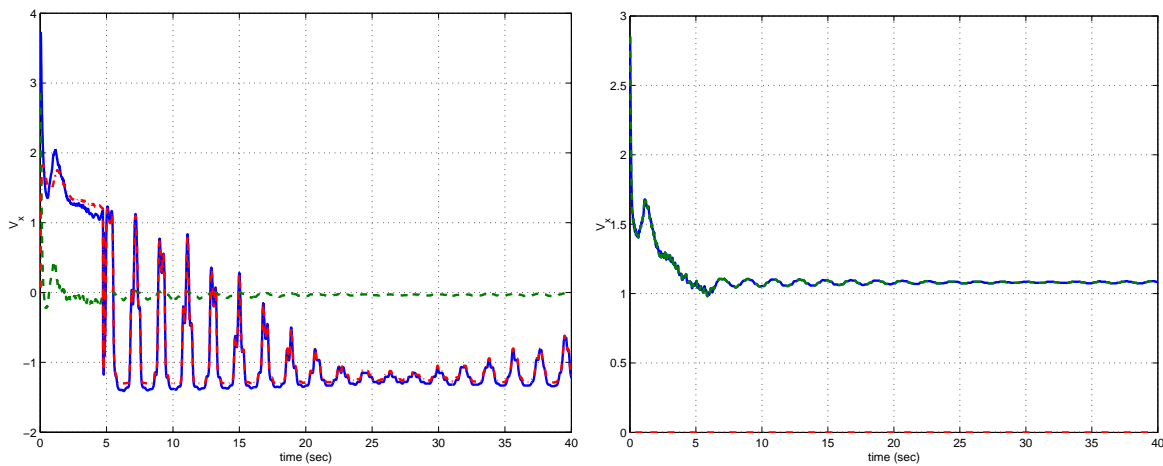
From the response in Figure 4.10, $\phi_{ss} \approx -0.52 \text{ deg} = 0.00907 \text{ rad}$, resulting in an actual set point of $X_{ref} = 1.014 \text{ m}$ instead of $X_{ref} = 1.05$. From this analysis, we conclude that the actual steady-state error of the trolley is 0.5 cm . This error is mainly due to friction, which could not be removed completely by friction compensation. The rotational motion is not excited by the translational motion. Therefore, we do not show the rotational motion response.

In the second maneuver, the crane was rotated by an angle $\gamma = 90 \text{ deg}$, while the trolley was located at $x = 0.9 \text{ m}$. The responses shown in Figures 4.11 and 4.12 indicate



(a) Trolley position: — with friction compensation, - - - without friction compensation, and -.-.- set point X_{ref}

(b) In-plane load swing: — with friction compensation and - - - without friction compensation



(c) Control action using friction compensation: -.-.- linear system, - - - - friction compensation, and — total

(d) Control action without friction compensation

Figure 4.10: Time histories of the translational motion when the trolley moves 0.75 m with and without friction compensation.

the effectiveness of the controller in transferring the load to its destination without swing. We note that the translational motion was excited by rotation. This is due to the coupling between the translational and rotational motions. The simplified equations used in the controller design do not include this coupling. However, due to the joint working of the translational and rotational controllers, the performance was not affected by this simplification. It is also shown that the response is totally unacceptable when friction compensation is turned-off. In this case, the in-plane swing and the trolley steady-state error are high because the generated action from the controller to correct these errors can not overcome friction. The rotational motion is smoother; hence, it is less deteriorated.

Finally, in the third maneuver, we started with the trolley at $x = 0.30$ and commanded it to move along the jib to $x = 1.05$ m. At the same time, the crane was rotated by $\gamma = 90$ deg. The response is shown in Figures 4.13 and 4.14, which demonstrate the effectiveness of the controller and the friction compensation.

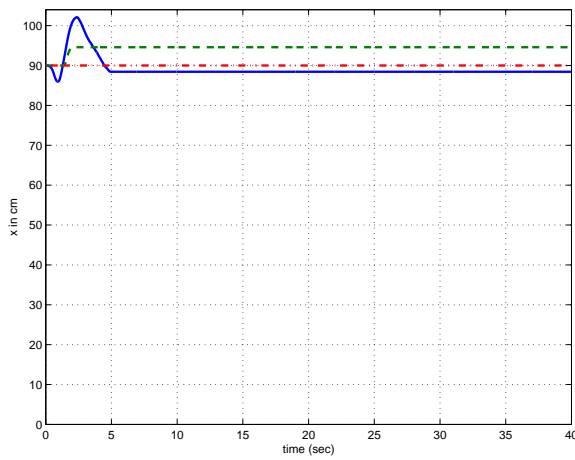
4.5.2 Full-State Feedback Controller

For the full-state feedback controller, we first chose the gain K . Then, we solved for the other feedback gains as functions of the load weight, cable length, and K . Similar to the partial-state feedback, the gains for the translational motion for $K = 2.0$ and $m_t = 0.09$ were obtained from solving equations (3.22)-(3.25). The result is

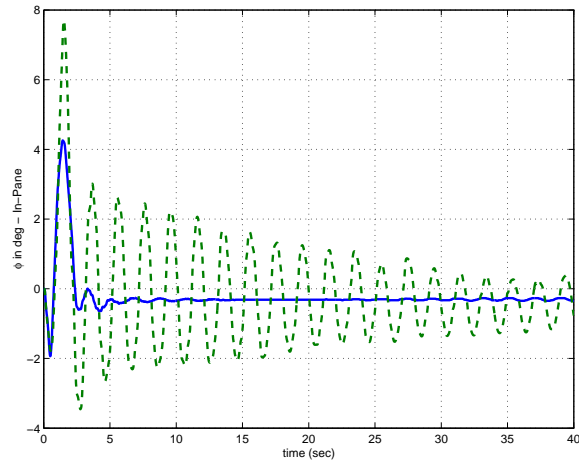
$$\begin{aligned} K_{\dot{x}} &= 1.00354 + \frac{0.63662}{\sqrt{K}} \\ K_{\phi} &= 1.4674 - \frac{-3.3551}{K} + \frac{6.261}{\sqrt{K}} \\ K_{\dot{\phi}} &= -1.00354 + \frac{1.9929}{\sqrt{K}} + \frac{0.93417}{\sqrt{K}} \end{aligned} \quad (4.21)$$

The corresponding gains for the rotational motion with $K_{m\gamma} = 1.14$, $M_r = 0.28$, and $m_r = 0.27$ are shown in Table 4.3.

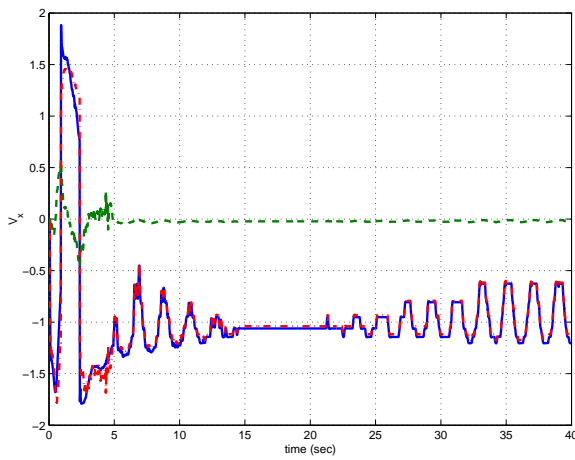
To examine the effect of changing the gain K on the system response, we performed



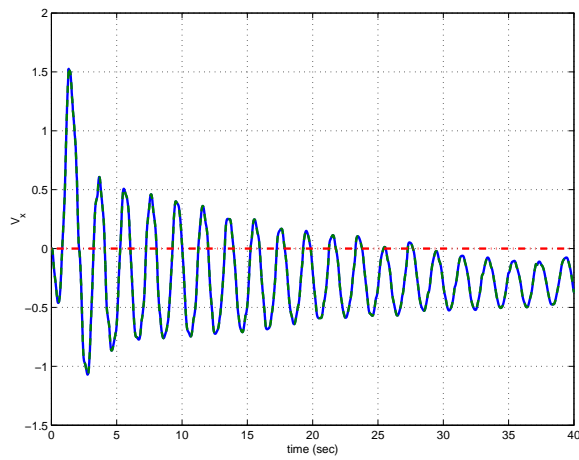
(a) Trolley position: — with friction compensation, - - - without friction compensation, and -.-.- set point X_{ref}



(b) In-plane load-swing angle — with friction compensation and - - - without friction compensation

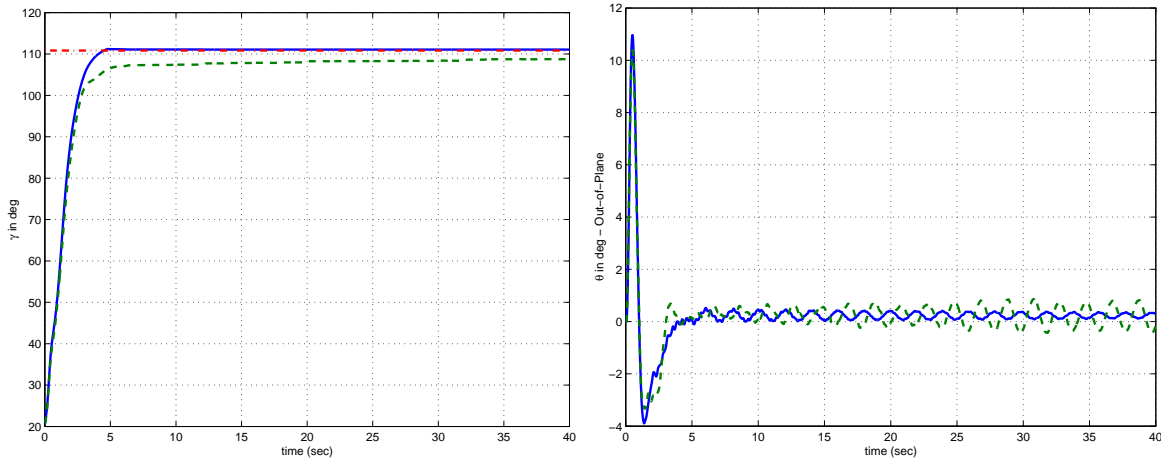


(c) Control action using friction compensation: -.-.-. linear system, - - - - friction compensation, and — total



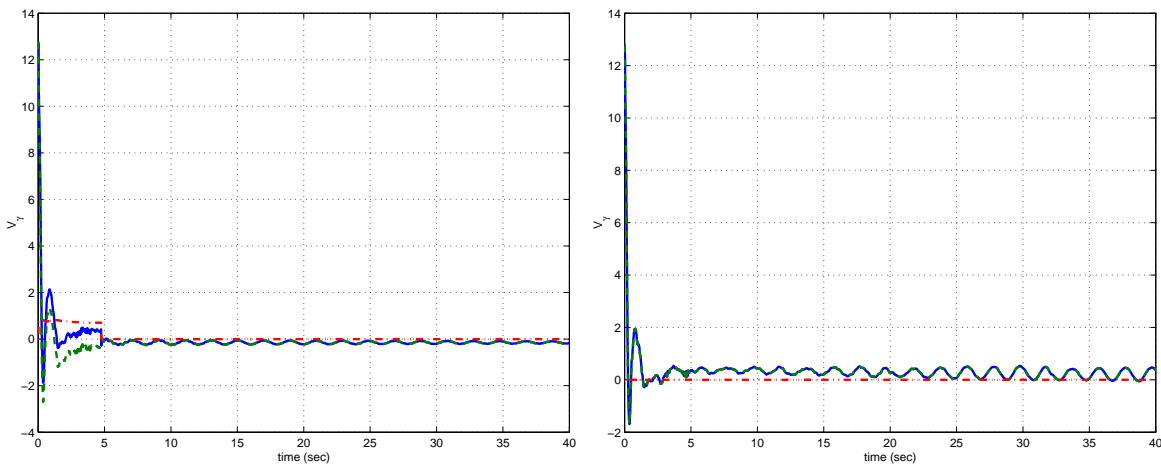
(d) Control action without friction compensation

Figure 4.11: Time histories of the translational motion when the crane rotates 90 deg and the trolley is positioned at $x = 0.9\text{ m}$ with and without friction compensation.



(a) Rotation angle; — with friction compensation, - - - without friction compensation, -.-.- set point γ_{ref}

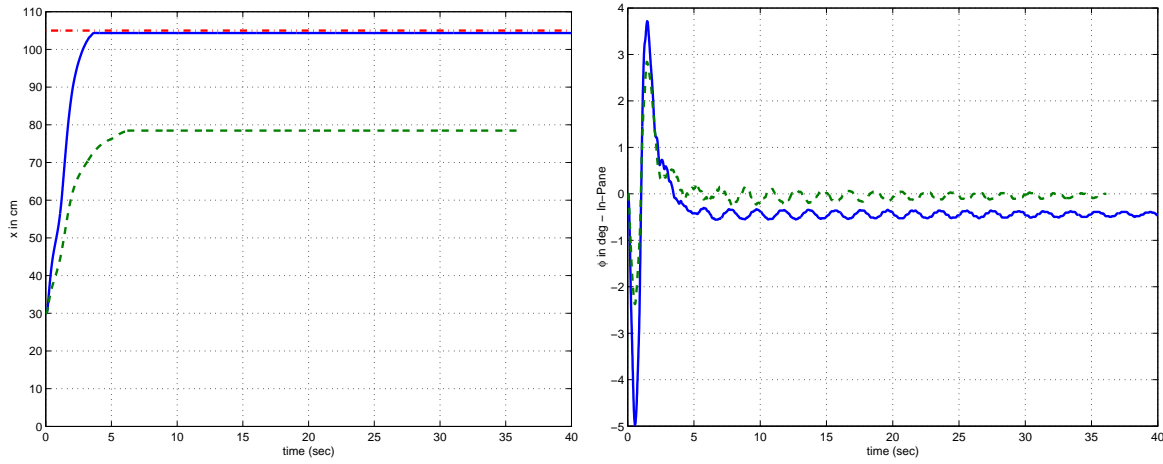
(b) Out-of-plane load-swing angle: — with friction compensation and - - - without friction compensation



(c) Control action using friction compensation: -.-.- linear system, - - - friction compensation, and — total

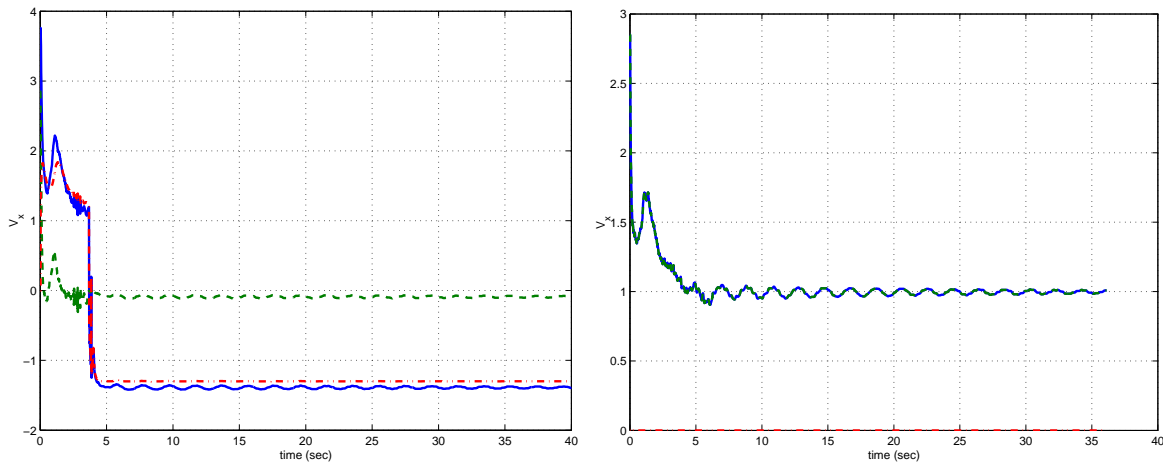
(d) Control action without friction compensation

Figure 4.12: Time histories of the rotational motion when the crane rotates 90 deg and the trolley positioned at $x = 0.9m$ with and without friction compensation.



(a) Trolley position: — with friction compensation, - - - without friction compensation, and -.-.- set point X_{ref}

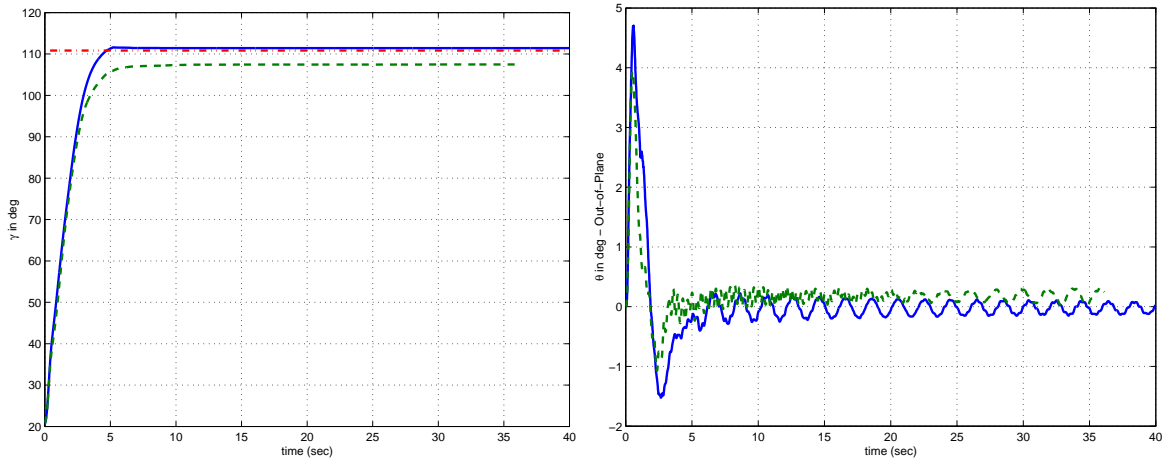
(b) In-Plane load-swing angle: — with friction compensation and - - - without friction compensation



(c) Control action using friction compensation: -.-.-. linear system, - - - - friction compensation, and — total

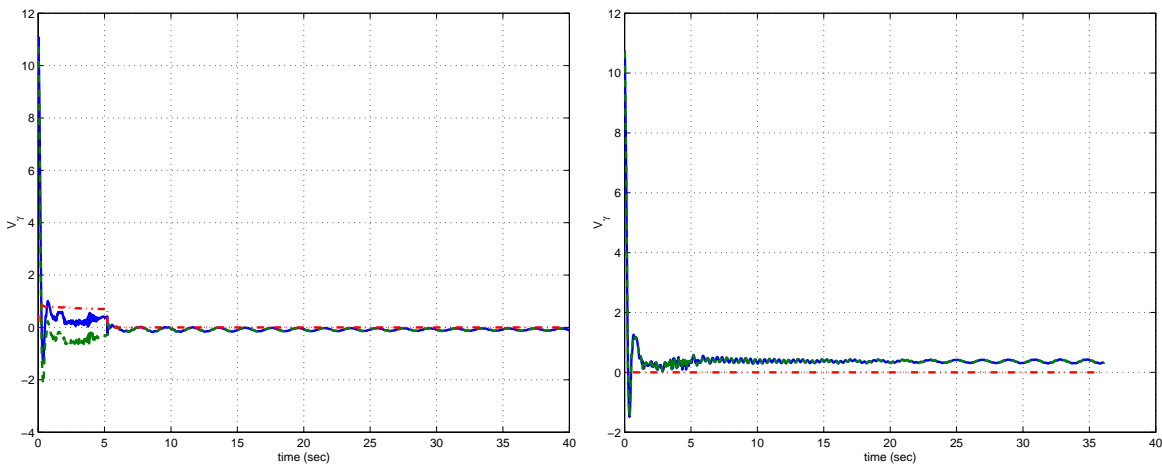
(d) Control action without friction compensation

Figure 4.13: Time histories of the translational motion when the crane rotates 90 deg and the trolley is moved $x = 0.75\text{ m}$ with and without friction compensation.



(a) Rotation angle: — with friction compensation, - - - without friction compensation, and -.-.- set point X_{ref}

(b) Out-of-plane load-swing angle: — with friction compensation and - - - without friction compensation



(c) Control action using friction compensation: -.-.- linear system, - - - friction compensation, and — total

(d) Control action without friction compensation

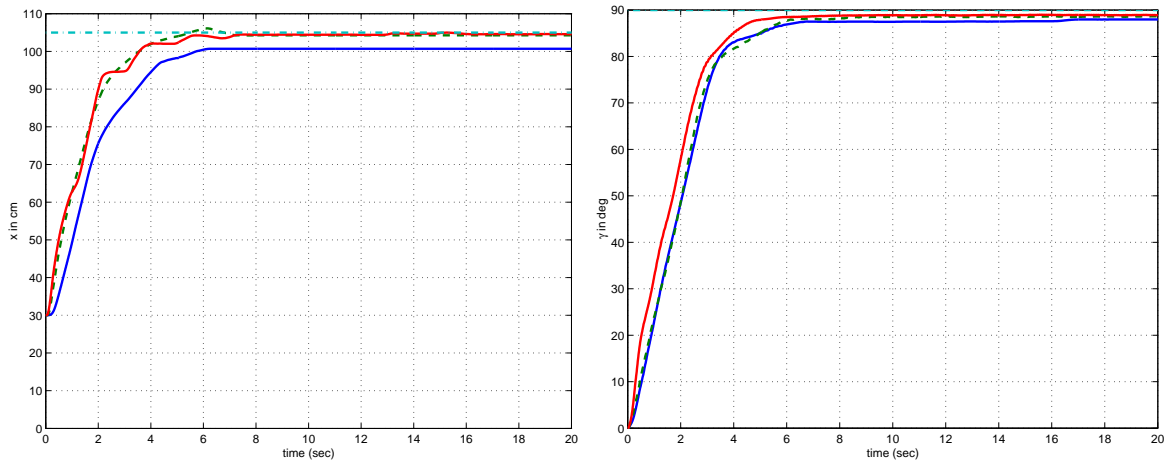
Figure 4.14: Time histories of the rotational motion when the crane rotates 90 deg and the trolley is moved $x = 0.75\text{ m}$ with and without friction compensation.

Table 4.3: The feedback gains of the rotational motion using full-state feedback

	$K = 2$	$K = 4$	$K = 8$
$K_{\dot{x}}$	$1.5416 + 0.075326x^2$	$1.384 + 0.05326x^2$	$1.27257 + 0.037663x^2$
K_{ϕ}	$\frac{4.6674}{x} - 0.787x$	$\frac{4.1683}{x} + (0.2324 - 1.75m_r)x$	$\frac{3.59278}{x} + (0.0.2247 - 0.875m_r)x$
$K_{\dot{\phi}}$	$\frac{01.2095}{x} + 0.5091x$	$\frac{0.2665}{x} + (0.157989 - 3.5m_r)x$	$\frac{-0.2529}{x} + 0.1549x$

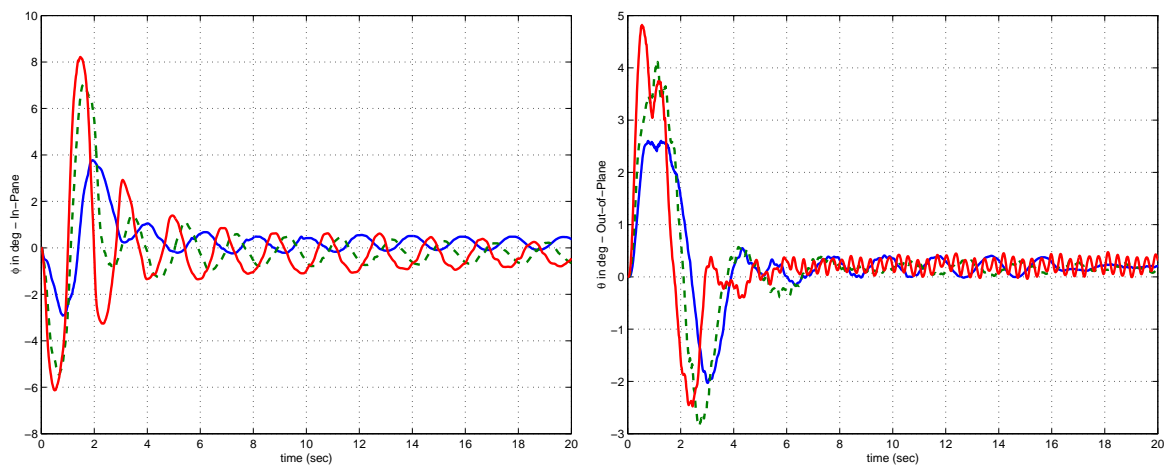
the third maneuver. We started with the trolley at $x = 0.30$ and commanded it to move along the jib to $x = 1.05$ m. At the same time, the crane was rotated by $\gamma = 90$ deg. During this maneuver, the friction compensation was turned on. Figure 4.15 shows the time response. The system slows down and the swing angle decreases with decreasing K . Because friction may change due to the environmental effects, we need to repeat the estimation process. We note also that when K is very small, the trolley position has a large steady-state error due to the error in the friction values. Therefore, we have to increase K as much as possible to reduce this deterioration effect.

To investigate the effect of disturbances, we started the crane from rest and then manually gave it a disturbance. Figure 4.16 shows the response of the system due to this disturbance with and without friction compensations. We note that the controller damped the load swing effectively and returned the crane to its rest position when friction compensation was used.



(a) Trolley position

(b) Rotation angle:



(c) In-Plane load-swing angle

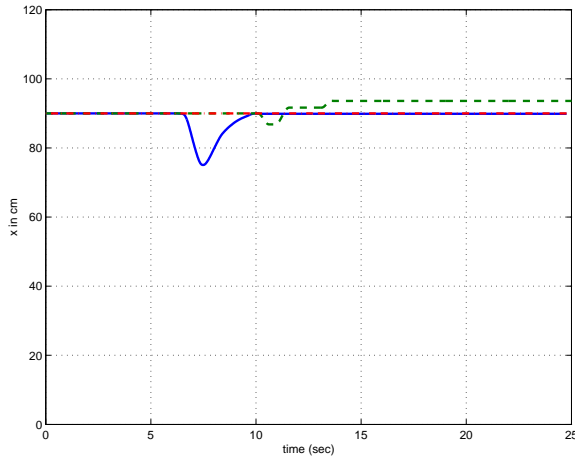
(d) Out-of-plane load-swing angle

Figure 4.15: Time histories of the combined motion with different values of the gain K : — $K = 2$, - - - $K = 4$, and -.-.- $K = 8$.

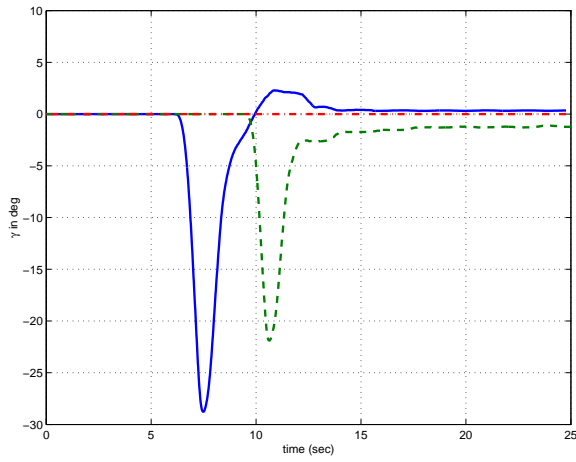
4.6 The Anti-Swing-Tracking Controllers

4.6.1 Delayed-feedback controller

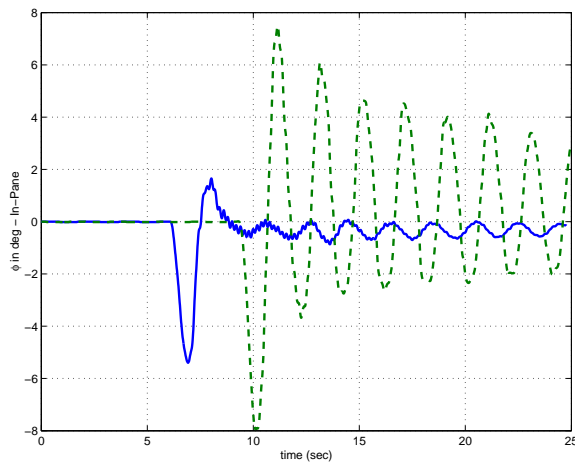
First, we ran a case in which the delayed-feedback gain K_{del} was set equal to zero to demonstrate the effectiveness of the anti-swing controllers. Figure 4.17 shows the response of the



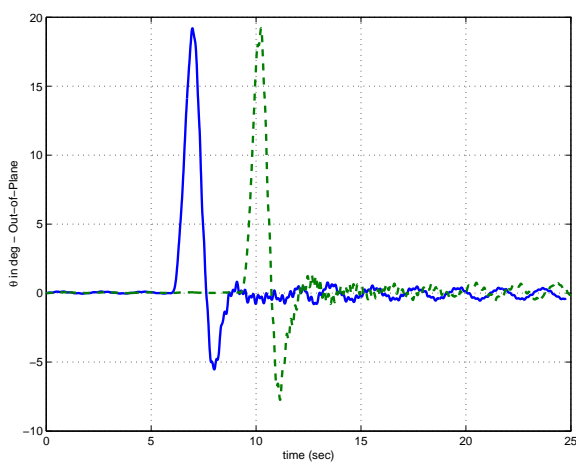
(a) Trolley position



(b) Rotation angle



(c) In-Plane load-swing angle



(d) Out-of-plane load-swing angle

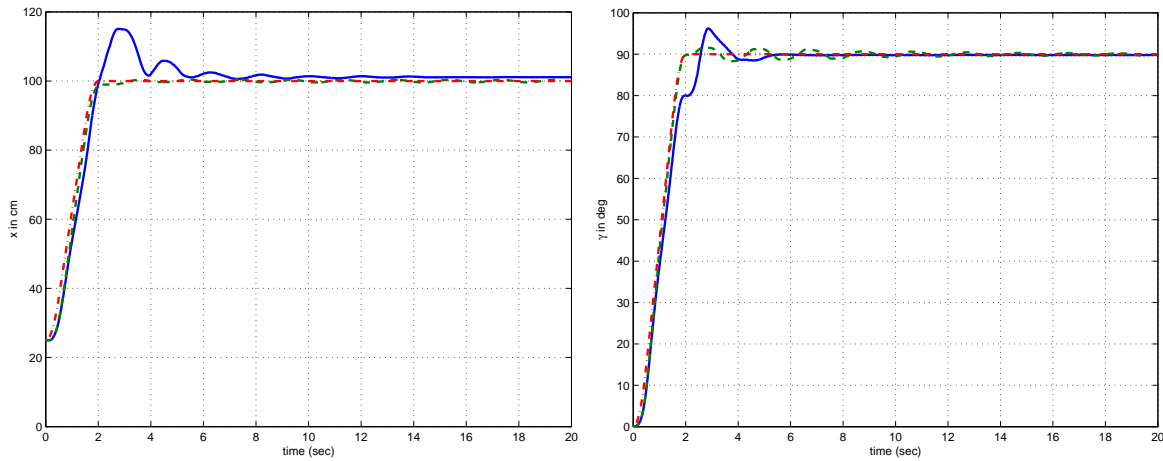
Figure 4.16: Time histories of the translational motion when the trolley is subjected to a disturbance: — with friction compensation, - - - without friction compensation, and -.-.- set point.

system for the third maneuver, which combines the translational and rotational motions. The trajectories used were obtained from equations (3.54) and (3.55). When the swing angle feedback was removed from the control loop, the system followed the trajectory without suppressing the swing. In the swing-controlled case, the system reached its destination without load swing. However, the system did not follow the prescribed trajectory and an overshoot was introduced. This overshoot increased with an increase in the maximum acceleration used to generate the motion trajectories.

Figure 4.18 shows the time response when the crane was rotated by 90 *deg* using two different trajectories. The final transfer time of the first trajectory had only one time period as in equation (3.55). On the other hand, the final time of second trajectory was chosen to be equal to two time periods as in equation (4.22). The corresponding acceleration of this trajectory was one-fourth that of the first trajectory. Although the designed final times were different, the real transfer times were nearly the same. The case with high acceleration resulted in a large position overshoot and a large swing angle during the transfer process. The second trajectory, which gave a low overshoot and a small swing angle, was actually the optimal trajectory for transferring a load using the gantry crane. This comparison gives us a guide for choosing the transfer trajectory parameters. They should be near the optimal parameters, as given by equation (4.22) to yield a good response:

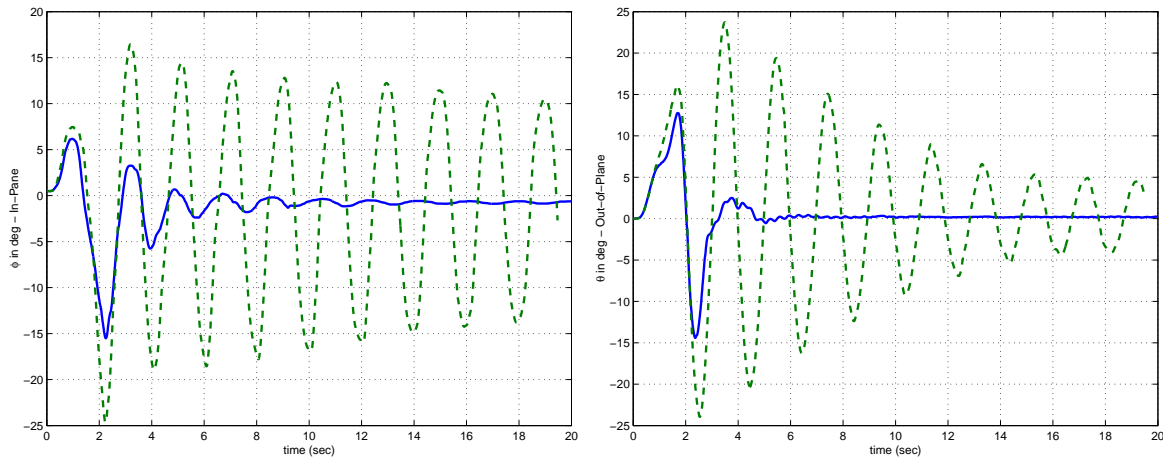
$$Z_\gamma = 90 \text{ deg}, \quad \Delta t_\gamma = \frac{T}{2}, \quad t_{f\gamma} = 2T \quad \Rightarrow \quad V_{max\gamma} = 1.0435/2, \quad a_{max\gamma} = 2.0796/4 \quad (4.22)$$

To validate the anti-swing controllers, we used the aforementioned three maneuvers. The response in the case of only the translational motion and using the trajectory given by equation (3.54) with and without friction compensation is shown in Figure 4.19. Without friction compensation, the steady-state error was large and the load swing was large, which took long time to damp. When friction compensation was turned on, the system reached its destination nearly without steady-state error and the load swing was suppressed successfully. The oscillations in the control action were mainly due to friction compensation in the



(a) Trolley position

(b) Rotation angle

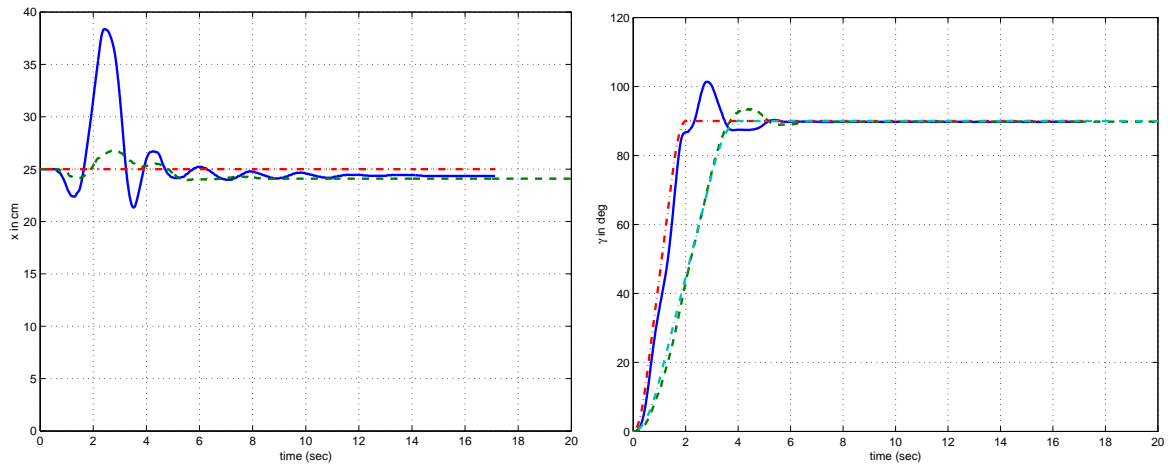


(c) In-plane load-swing angle

(d) Out-of-plane load-swing angle

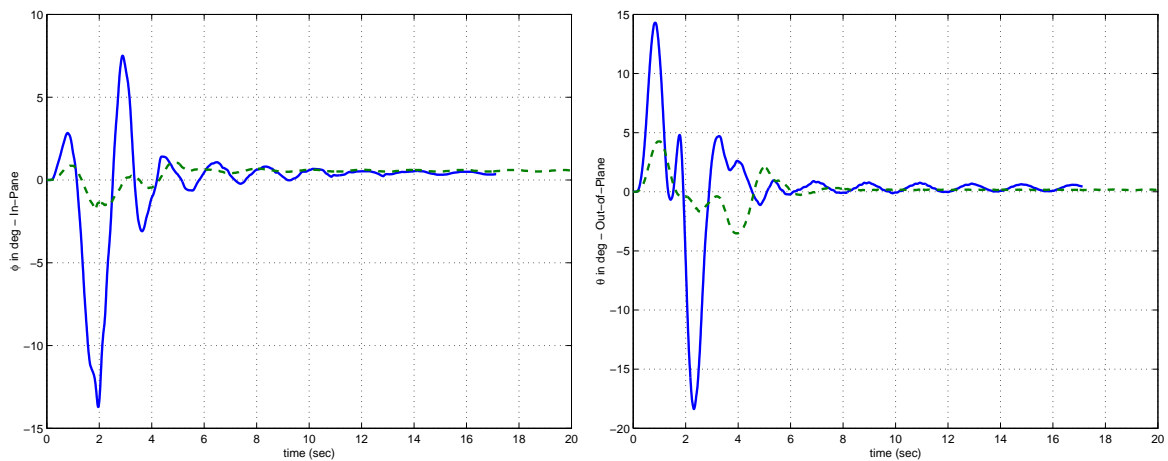
Figure 4.17: Time histories of the anti-swing delayed-feedback controller for the combined motion: -.-.- with anti-swing controller, - - - - without anti-swing controller $K_{del} = 0$, and -.-.- reference trajectory.

zero-speed range. These oscillations may introduce limit cycles, which make the response unacceptable. They could be eliminated by a proper choice of the static-friction values and the zero-speed range. We note that the static-friction and the zero-range parameters were



(a) Trolley position

(b) Rotation angle

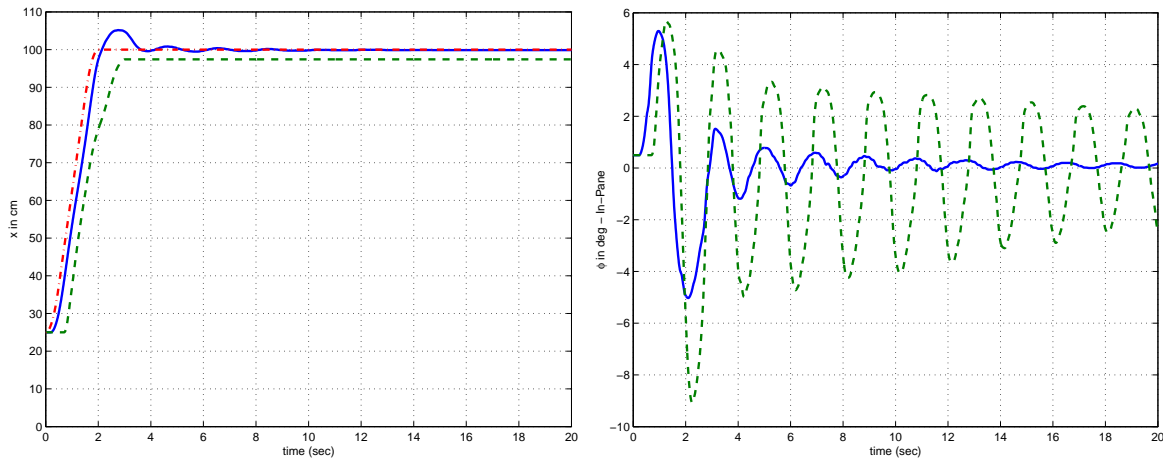


(c) In-plane load-swing angle

(d) Out-of-plane load-swing angle

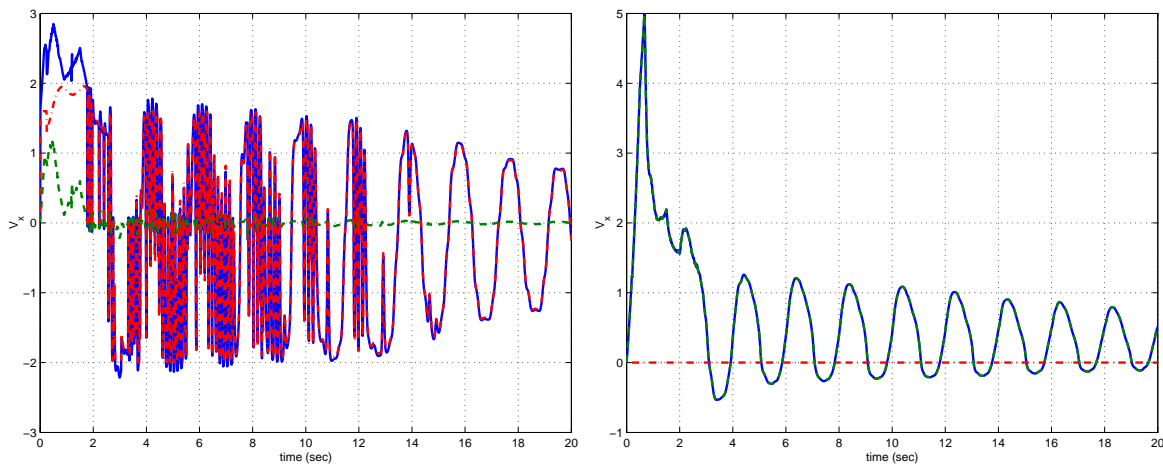
Figure 4.18: Time histories of the anti-swing delayed-feedback controller for the rotational motion: $-\cdot-\cdot-$ $t_f = T$, $-\cdot-\cdot-\cdot-$ $t_f = 2T$, and $-\cdot-\cdot-$ reference trajectory.

not included in the estimation process. We calculated these parameters by trial. These calculations need to be repeated to cope with the change in friction due to environmental effects and mechanical wear.



(a) Trolley position: — with friction compensation, - - - without friction compensation, and -.-.- reference trajectory X_{ref}

(b) In-plane load swing: — with friction compensation and - - - without friction compensation



(c) Control action using friction compensation: -.-.- linear system, - - - friction compensation, and — total

(d) Control action without friction compensation

Figure 4.19: Time histories of the translational motion using the delay controller with and without friction compensation.

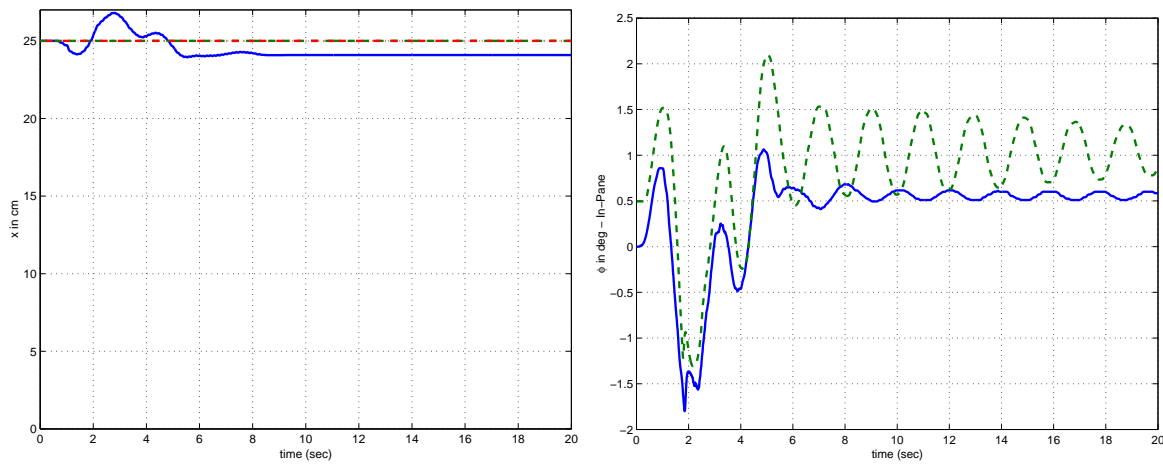
The response of the system for the second maneuver for a trajectory given by equation (4.22) is shown in Figures 4.20 and 4.21. The deterioration effect of friction was larger in the translational motion than in the rotational motion. Oscillations in the control action existed in both motions. However, friction compensation allowed the system to reach its final destination accurately without load swing.

The response of the system using the third maneuver and trajectories given by equations (3.54) and (4.22) is shown in Figure 4.22. The delay controller with friction compensation successfully transferred the load to its final destination, while the swing was completely suppressed.

To investigate the effect of disturbances on the system, we started the crane from rest and then manually gave the load a kick. Figure 4.23 shows the response with and without friction compensation. We note that the controller damped the load swing effectively when friction compensation was used. Without friction compensation, the trolley had large steady-state error and the load swing was very large, especially the in-plane swing angle.

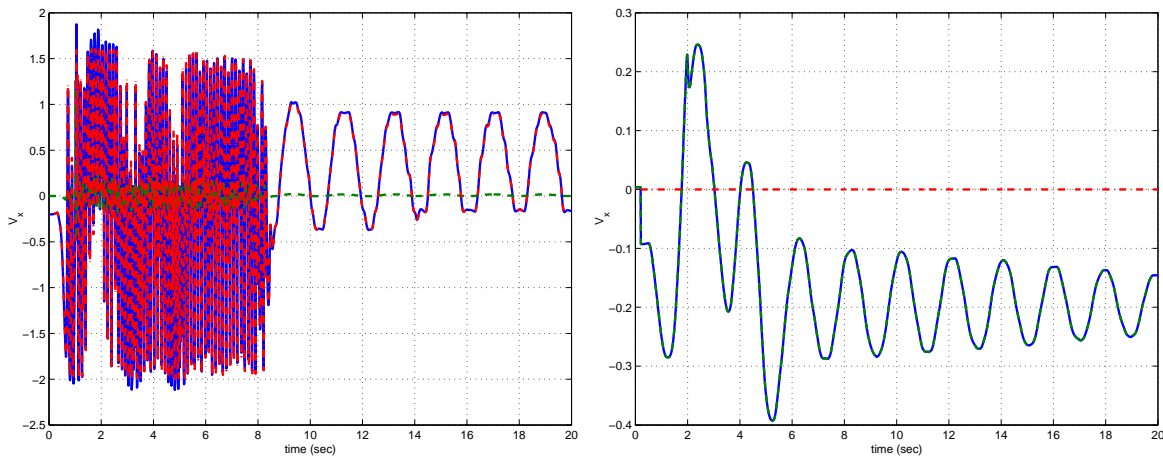
4.6.2 Fuzzy controller

The effect of friction compensation on the performance of the fuzzy controller is nearly the same as its effect on the delay controller. Therefore, we only show here a comparison between the fuzzy and delay controllers using the previous maneuvers. The system response for the first maneuver is shown in Figure 4.24, while the responses for the second and third maneuvers are shown in Figures 4.25 and 4.26, respectively. The responses using the fuzzy controller are nearly identical to those obtained with the delay controller except for small residual oscillations in the load swing angles. These oscillations may have resulted from the use of the swing-angle rate in determining the fuzzy control action. The swing-angle rate was obtained by differentiating the swing angle, which was contaminated with noise. The numerical differentiation made the signal noisy. These residual oscillations might be



(a) Trolley position: — with friction compensation, - - - without friction compensation, and -.-.- reference trajectory X_{ref}

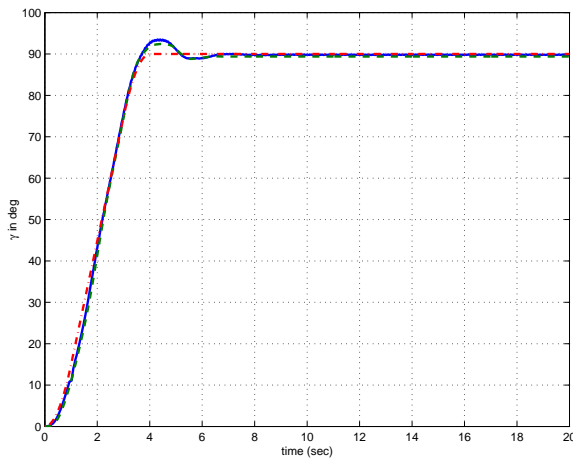
(b) Trolley position: — with friction compensation, - - - without friction compensation, and -.-.- reference trajectory γ_{ref}



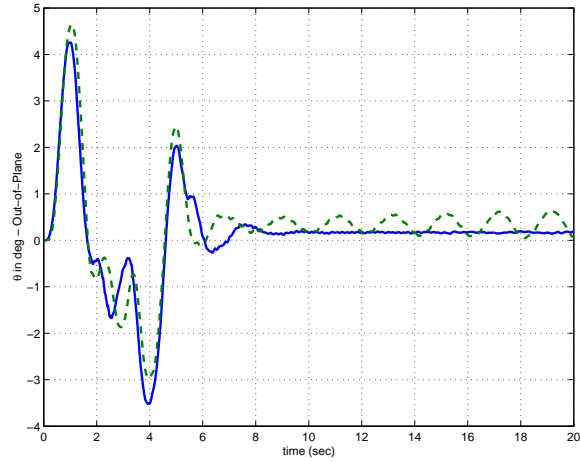
(c) In-plane load-swing angle — with friction compensation and - - - without friction compensation

(d) In-plane load-swing angle — with friction compensation and - - - without friction compensation

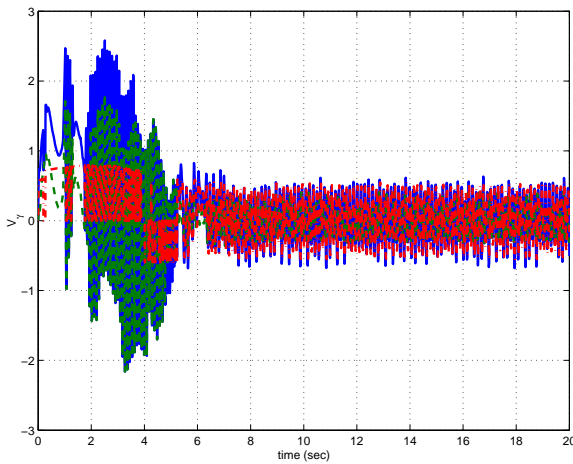
Figure 4.20: Time histories of the rotational motion using delayed-feedback controller with and without friction compensation.



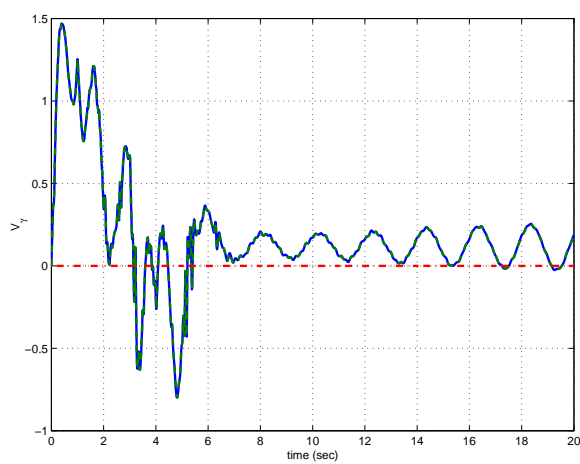
(a) Trolley position: — with friction compensation, - - - without friction compensation, and -.-.- reference trajectory X_{ref}



(b) Trolley position: — with friction compensation, - - - without friction compensation, and -.-.- reference trajectory γ_{ref}

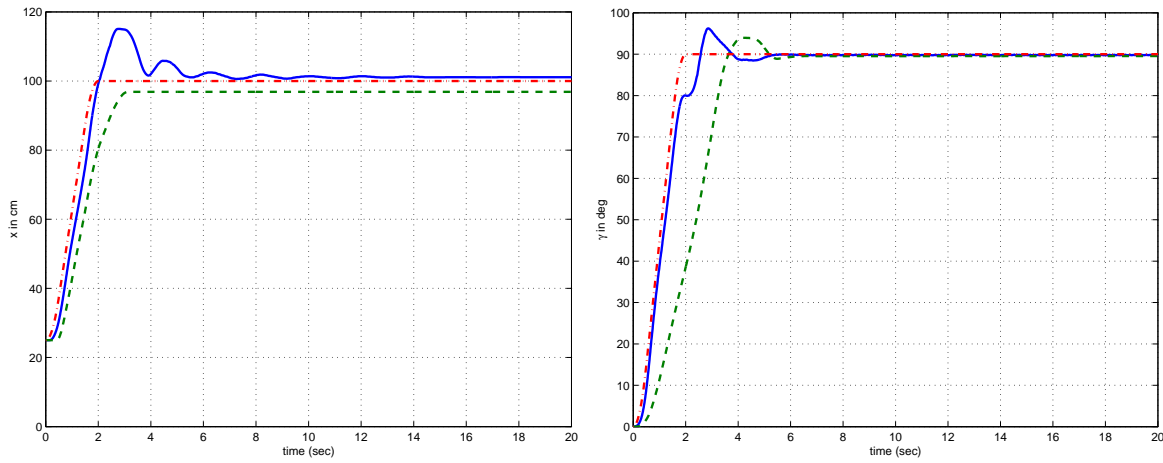


(c) In-plane load-swing angle — with friction compensation and - - - without friction compensation



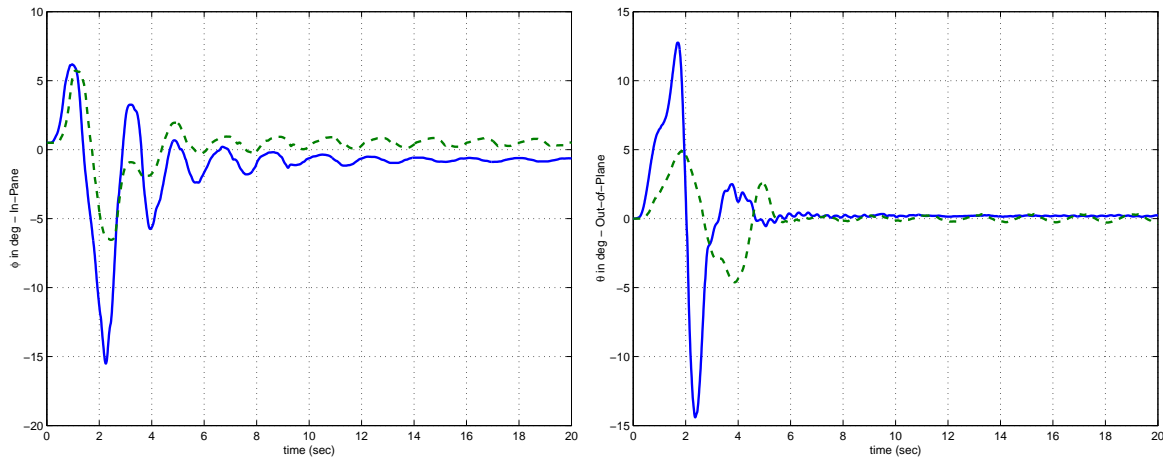
(d) In-plane load-swing angle — with friction compensation and - - - without friction compensation

Figure 4.21: Time histories of the rotational motion using delay controller with and without friction compensation.



(a) Trolley position

(b) Trolley position



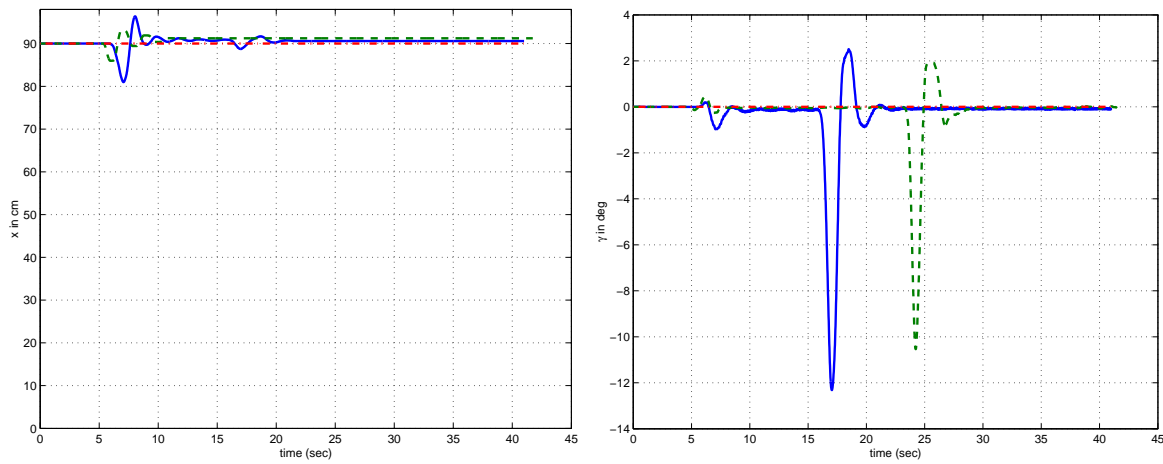
(c)

(d) In-plane load-swing angle

Figure 4.22: Time histories of the combined motion using delayed-feedback controller: — with friction compensation, - - - without friction compensation, and -.-.- reference trajectory.

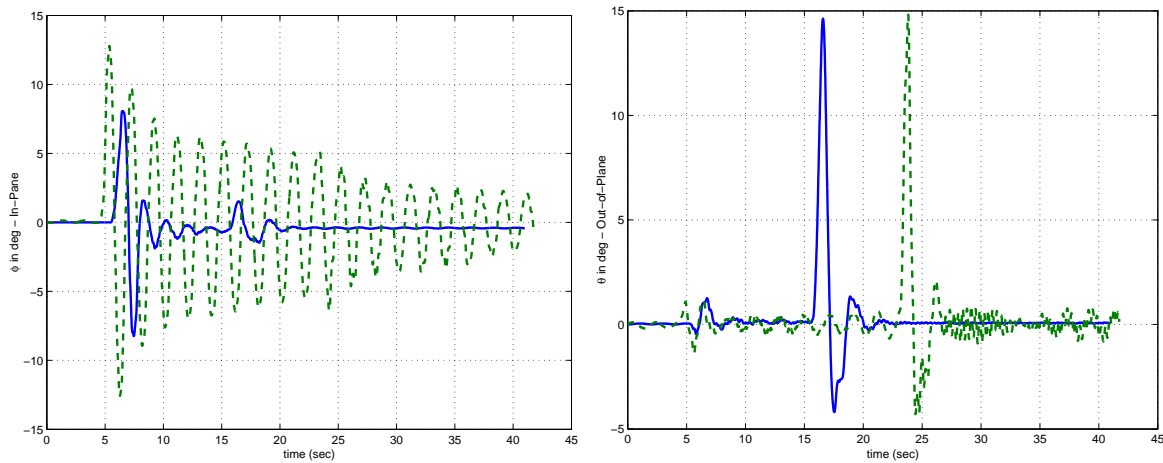
eliminated by using a sensor to measure the swing-angle rate rather than calculating it.

Comparison between the delay and fuzzy controllers due to external disturbances is



(a) Trolley position

(b) Rotation angle

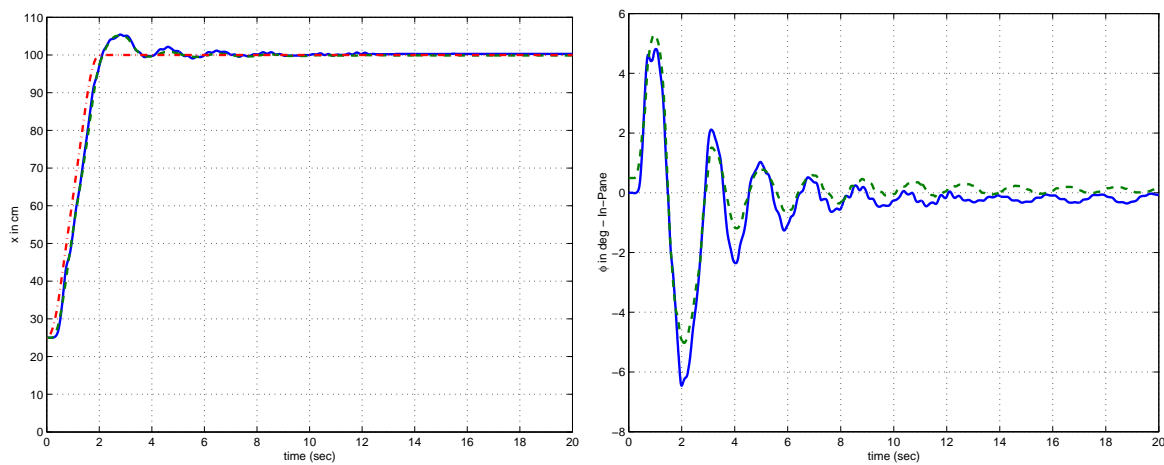


(c) In-plane load-swing angle

(d) Out-of-plane load-swing angle

Figure 4.23: Time histories due to external disturbance using delay controller:— with friction compensation, - - - without friction compensation, and -.-.- reference trajectory.

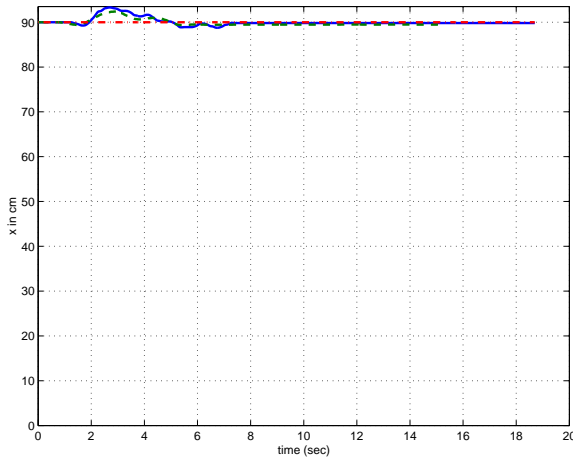
shown in Figure 4.27. Both controllers effectively damp the load swing and bring the system back to its rest position.



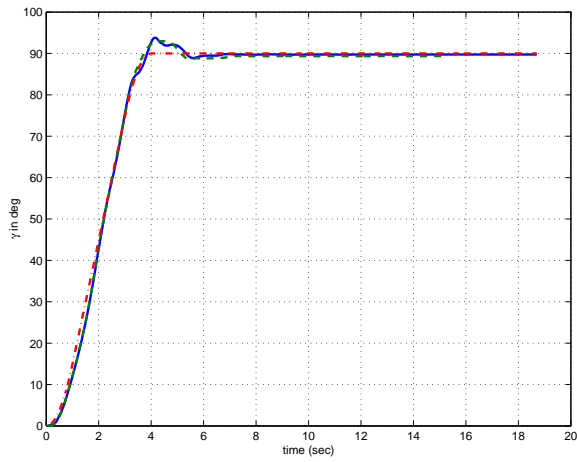
(a) Trolley position

(b) In-plane load-swing angle

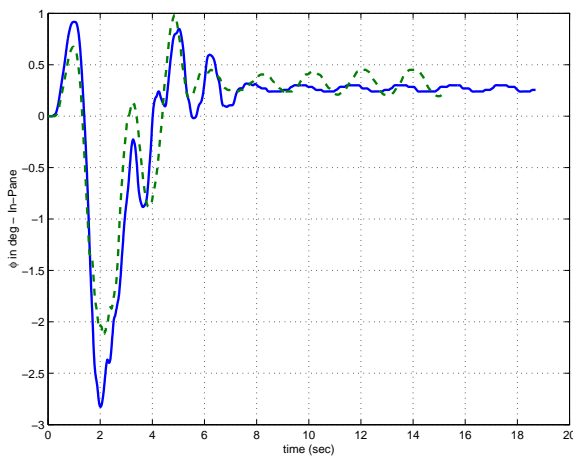
Figure 4.24: Time histories of the anti-swing controllers for the translational motion only:
— fuzzy, - - - delay, and -.-.- reference trajectory.



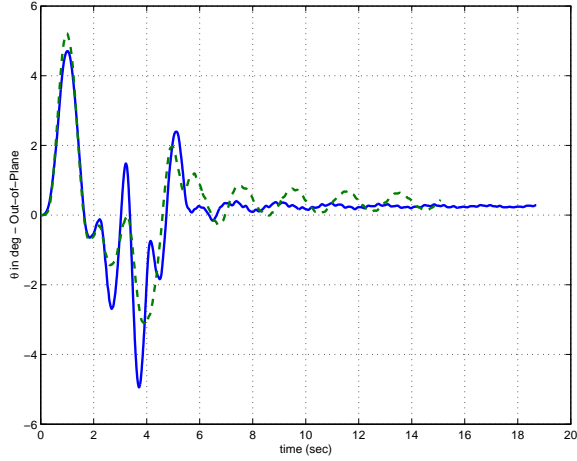
(a) Trolley position



(b) Rotation angle

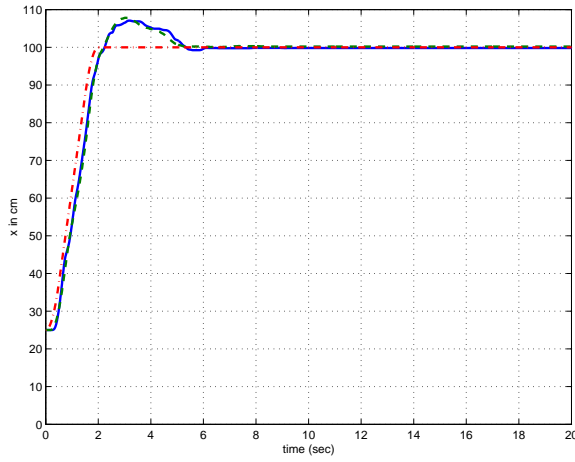


(c) In-plane load-swing angle

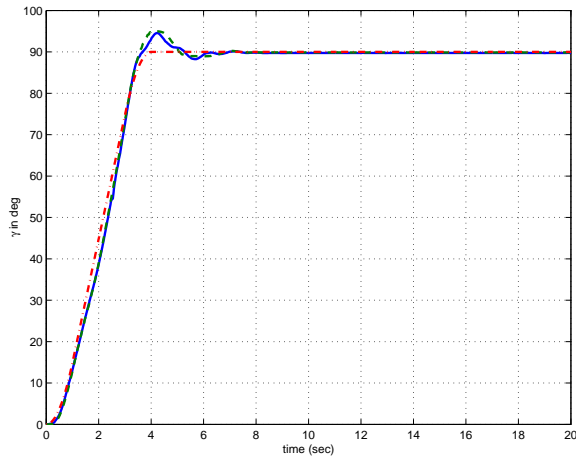


(d) Out-of-plane load-swing angle

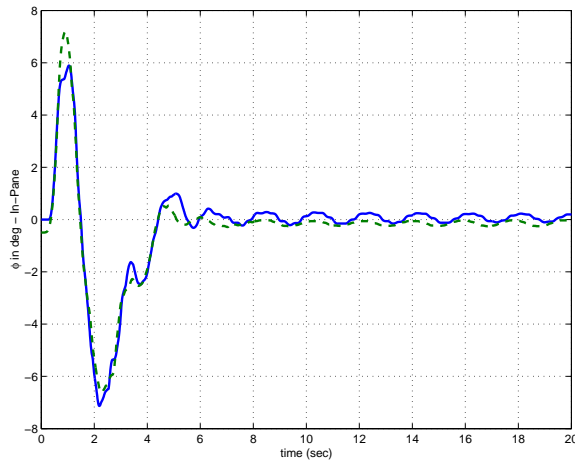
Figure 4.25: Time histories of the anti-swing controllers for the rotational motion only: — fuzzy, - - - - delay, and -.-.-.- reference trajectory.



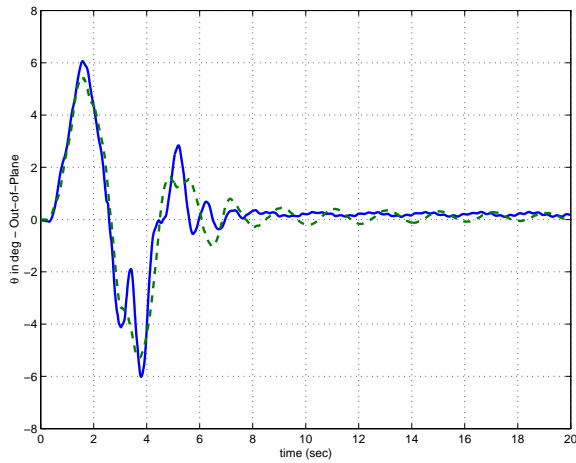
(a) Trolley position



(b) Rotation angle

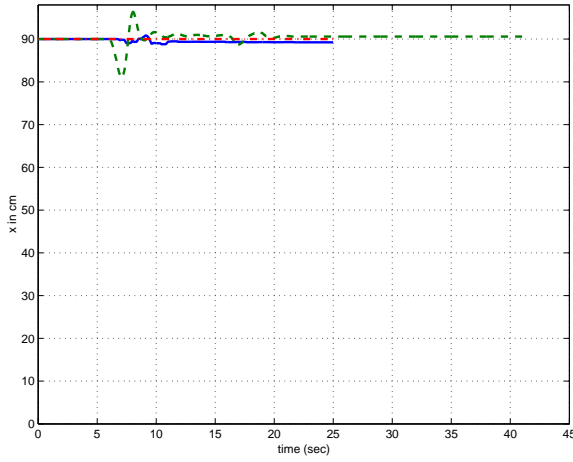


(c) In-plane load-swing angle

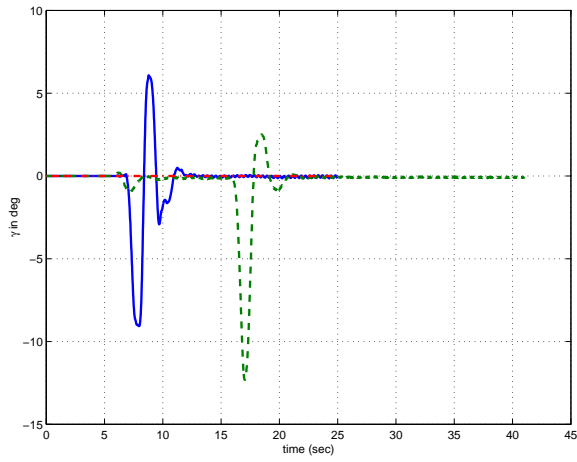


(d) Out-of-plane load-swing angle

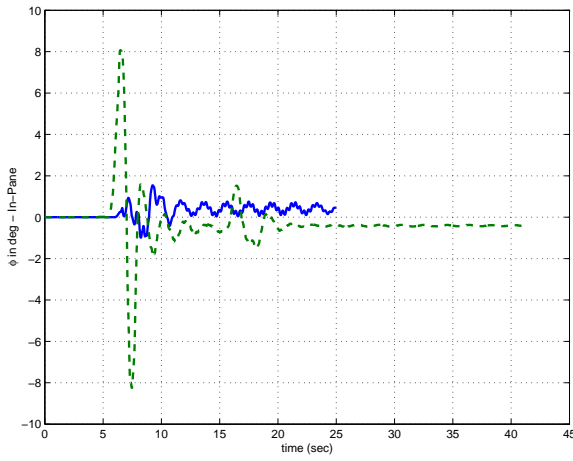
Figure 4.26: Time histories of the anti-swing controllers for the combined motion: — fuzzy, - - - delay, and -.-.- reference trajectory.



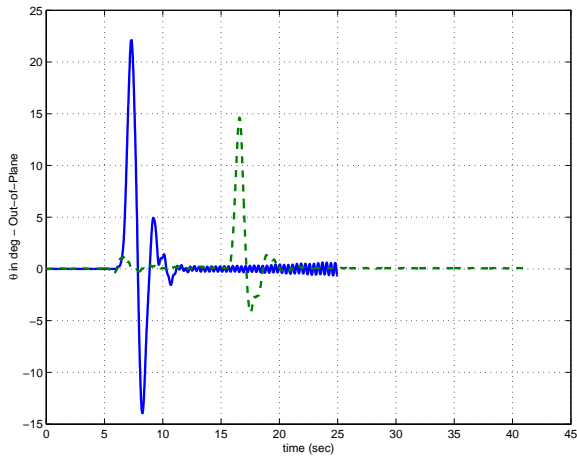
(a) Trolley position



(b) Rotation angle



(c) In-plane load-swing angle



(d) Out-of-plane load-swing angle

Figure 4.27: Time histories of the anti-swing controllers due to disturbance: — fuzzy, - - delay, and -.-.- reference trajectory.

Chapter 5

Conclusions and Future Work

The main objective of this work is to design robust, fast, and practical controllers for gantry and tower cranes. The controllers are designed to transfer the load from point to point as fast as possible and, at the same time, the load swing is kept small during the transfer process and completely vanishes at the load destination. Moreover, variations of the system parameters, such as the cable length and the load weight, are also included. Practical considerations, such as the control action power, and the maximum acceleration and velocity, are taken into account. In addition, friction effects are included in the design using a friction-compensation technique.

To accomplish this objective, we have developed full nonlinear mathematical models of gantry and tower cranes. The full nonlinear equations are used in the computer simulations. Then, we simplified these equations for control and analysis. Throughout this work, we designed our controllers based on the linear model of the gantry crane. Next, these controllers were modified to handle tower cranes by considering the coupling between the rotational and translational motions.

The designed controllers are based on two approaches. In the first approach, a gain-scheduling feedback controller is designed to move the load from point to point within one

oscillation cycle without inducing large swings. The settling time of the system is taken to be equal to the period of oscillation of the load. This criterion enables calculation of the controller feedback gains for varying load weight and cable length. The position references for this controller are step functions. Moreover, the position and swing controllers are treated in a unified way. In the second approach, the transfer process and the swing control are separated in the controller design. This approach requires designing two controllers independently: an anti-swing controller and a tracking controller. The objective of the anti-swing controller is to reduce the load swing. The tracking controller is responsible for making the trolley follow a reference position trajectory. We use a PD-controller for tracking, while the anti-swing controller is designed using three different methods: (a) a classical PD controller, (b) two controllers based on a delayed-feedback technique, and (c) a fuzzy logic controller that maps the delayed-feedback controller performance.

The computer simulations show that the controllers designed using both approaches successfully transfer the load to its final destination without residual oscillations. The gain-scheduling controllers transfer the load smoothly without inducing an overshoot in the trolley position. Moreover, the load can be transferred in a time near to the optimal time with small swing angles during the transfer process. With full-state feedback, the crane can reach any position in the working environment without exceeding the system power capability by controlling the forward gain K in the feedback loop. For large distances, we have to decrease this gain, which in turn slows the transfer process. Therefore, this approach is more suitable for short distances. Another concern about this controller is the large control action at the beginning of the motion, which may excite the rigid-body motion of the load. The tracking-anti-swing control approach is usually associated with overshoots in the translational and rotational motions. These overshoots increase with an increase in the maximum acceleration of the trajectories. The transfer time is longer than that obtained with the first approach. However, the crane can follow any trajectory, which makes the controller cope with obstacles in the working environment. Also, we do not need to recalculate the feedback gains for each transfer distance as in the gain-scheduling feedback controller.

To validate the designed controllers, an experimental setup was built. Although the designed controllers work perfectly in the computer simulations, the experimental results are unacceptable due to the high friction in the system. This friction deteriorates the system response by introducing time delay, high steady-state error in the trolley and tower positions, and high residual load swings. To overcome friction in the tower-crane model, we estimate the friction, then we apply an opposite control action to cancel it. To estimate the friction force, we assume a mathematical model and estimate the model coefficients using an off-line identification technique using the method of least squares (LS). First, the process of identification is applied to a theoretical model of a DC motor with known friction coefficients. From this example, some guidelines and rules are deduced for the choice of the *LS* parameters. Then, the friction coefficients of the crane model are estimated and validated. Unfortunately, the estimation process needs to be repeated from time to time to cope with changes in friction due to environmental effects and mechanical wear. Improper estimation, especially in the static-friction parameters, may result in limit cycles.

With friction compensation, the experimental results are in good agreement with the computer simulations. The same behaviors are observed. The gain-scheduling controllers transfer the load smoothly without inducing overshoots in the trolley position. The transfer time is near to the optimal time and the load-swing angles are small during the transfer process. For long distances, the required control action at the beginning of the motion is very high and it may exceed the available voltage limit. The full-state feedback overcomes this problem, but it needs the swing-angle rate for implementation. This signal is not measured but obtained by differentiating the swing angle. Differentiation introduces noise, especially in the steady-state swing angle even after its filtering. The resulting noisy signal interferes with friction compensation. This interference may deteriorate the response of the system by introducing limit cycles in the trolley motion, which in turn excite the load swing. The tracking-anti-swing control approach is usually associated with overshoots in the translational and rotational motions. These overshoots can be minimized by a proper choice of the trajectory parameters. The delay controller feeds back only the swing angles, while the

fuzzy controller needs both swing angles and their rates. Due to the use of the load-swing angle rate, the fuzzy controller performance may deteriorate if the friction-compensation parameters are not chosen correctly. The fuzzy controller has a smaller transfer time and an overshoot and higher swing angles. This response can be improved by a proper tuning of the parameters of the membership functions.

5.1 Future Work

We designed our control algorithms to work with any cable length. Most likely, they will perform properly if load hoisting is included in the transfer maneuvers. However, further simulations and experimental tests are needed to investigate the effect of the rate of change of the cable length on the controller performance.

The swing angle is first filtered and then used in implementing the control algorithms. The filtering process is associated with time delay. A sensitivity analysis is needed to investigate the effect of the filter delay on the performance of the anti-swing delayed-feedback controller.

The anti-swing fuzzy controller performance can be improved by a proper tuning of the parameters of the membership functions (i.e., a and b). Optimization techniques can be used to determine the optimum values for these parameters.

The friction estimation can be improved by using a more complicated model. This model should include the static friction. Moreover, the friction estimation needs to be done on-line to cope with changes in friction due to environmental changes and mechanical wear. Beside the friction estimation, the load mass is difficult to measure and it should be included in the estimation process.

Bibliography

- [1] Abdel-Rahman, E. M., Nayfeh, A. H., and Masoud, Z. N., 2002, “Dynamics and control of cranes: A Review,” to appear in *Journal of Vibration and Control* **9**.
- [2] Al-Alaoui, M. A., 1993, “Novel digital integrator and differentiator,” *Electronic Letters* **29**(4), 376-378.
- [3] Al-Alaoui, M. A., 1994, “Novel IIR differentiator from the Simpson integration rule,” *IEEE Transactions on Circuits and Systems-1: Fundamental Theory and Applications* **41**(2), 186–187.
- [4] Al-Moussa, A., Nayfeh, A., and Kachroo, P., 2001, “Control of rotary cranes using fuzzy logic,” in *ASME 2001 Design Engineering Technical Conference and Computers and Information in Engineering Conference*, Pittsburgh, PA, September 9-12, DETC2001/VIB-21598.
- [5] Armstrong B., Dupont, P., and Canudas, C., 1994, “A survey of models, analysis tools, and compensation methods for the control of the machines with friction,” *Automatica* **30**(70), 1083–1138.
- [6] Astrom, K. J. and Wittenmark, B., 1994, *Adaptive Control*, Addison-Wesley, CA.
- [7] Auernig, J. W. and Troger, H., 1987, “Time optimal control of overhead cranes with hoisting of the load,” *Automatica* **23**(4), 437–447.

- [8] Balachandran, B., Lee, Y. Y., and Fang, C. C., 1999, "A mechanical filter concept for control of non-linear crane-load oscillation," *Journal of Sound and Vibration* **228**(3), 651–682.
- [9] Beeston, J. W., 1983, "Closed-loop time optimal control of a suspended load," in *Proceedings of the 4th IFAC World Congress*, Warsaw, Poland, pp. 39–50.
- [10] Canudas, C., Astrom, K. J., and Braun, K., 1986, "Adaptive friction compensation in DC motor drives," in *IEEE Conference on Decision and Control*, Piscataway, NJ, pp. 1556-1561.
- [11] Canudas, C., 1988, *Adaptive Control for Partially Known Systems: Theory and Applications*, Elsevier, Amsterdam, Netherlands.
- [12] Canudas, C., Olsson, H., and Astrom, K. J., 1995, "A new model for control of systems with friction," *IEEE Transactions on Automatic Control* **40**(3), 419-425.
- [13] Golashani, A. R. and Aplevich, D., 1995, "Computation of time-optimal trajectories for tower crane," in *Proceedings of the IEEE Conference on Control Applications*, Albany, NY, pp. 1134–11139.
- [14] Hazlerigg, A. D. G., 1972, "Automatic control of crane operations," in *Proceedings of the 5th IFAC World Congress*, Paris, France, pp. 11–13.
- [15] Henry, R. J., 1999, "Cargo pendulation reduction on ship-mounted cranes," M.S. Thesis, Virginia Tech., Blacksburg, VA.
- [16] Henry, R. J., Masoud, Z. N., Nayfeh, A. H., and Mook, D. T., 2001, "Cargo pendulation reduction on ship-mounted cranes via boom-luff angle actuation," *Journal of Vibration and Control* **7**, 1253–1264.
- [17] Hurteau, R. and Desantis, R. 1983, "Microprocessor-based adaptive control of a crane system," in *Proceedings of the IEEE Conference on Decision and Control Including The Symposium on Adaptive Processes*, New York, NY, Vol. **2**, pp. 944-947.

- [18] Itho, O., Migita, H., Irie, Y., and Itaho, J., 1994, "Application of fuzzy control to automatic crane operation," *Japanese Journal of Fuzzy Theory and Systems* **6**(2), 283–296.
- [19] Jamshidi, M., Vadiiee, N., and Rose, T. J., 1998, *Fuzzy Logic and Control: Software and Hardware applications*, Prentice Hall , Englewood Cliffs, NJ.
- [20] Karihaloo, B. L. and Parbery, R. D., 1982, "Optimal control of dynamical system representing a gantry crane," *Journal of Optimization Theory and Applications* **36**(3), 409–417.
- [21] Karnopp B. H., Fisher, F. F., and Yoon, B. O., 1992, "A strategy for moving a mass from one point to another," *Journal of the Franklin Institute* **329**(5), 881–892.
- [22] Lee, H-H., 1998, "Modelling and control of a three-dimensional overhead crane," *Journal of Dynamic Systems, Measurement, and Control* **120**, 471–476.
- [23] Lee, H-H., Cho, S-K., and Cho, J-S., 1997, "A new anti-swing control of overhead cranes," in *IFAC Automation in the Industry*, Korea, pp. 115–120.
- [24] Li, W. and Cheng, X., 1994, "Adaptive high-precision control of positioning tables - Theory and experiments," *IEEE Transactions on Control Systems Technology* **2**(3), 265–270.
- [25] Manson, G. A., 1982, "Time-optimal control of an overhead crane model," *Optimal Control Applications and Methods* **3**, 115–120.
- [26] Masoud, Z., 2000, "A control system for the reduction of cargo pendulation of ship-mounted cranes," Ph.D. Dissertation, Virginia Tech, Blacksburg, VA.
- [27] Masoud, Z. N., Nayfeh, A. H., Henry, R. J., and Mook D. T., 2002, "Sway reduction on container cranes using delayed feedback controller," in *Proceedings of the 43rd AIAA/ASME/ASCE/AHS/ASC Structures, Structural Dynamics, and Materials Conference*, Denver, CO, AIAA-2002-1279.

- [28] Middleton, R. H. and Goodwin, G. C., 1990, *Digital Control and Estimation: A Unified Approach*, Prentice Hall, Englewood Cliffs, NJ.
- [29] Nalley, M. J. and Trabia, M. B., 1994, "Design of a fuzzy logic controller for swing-damped transport of an overhead crane payload," *Dynamic System and Control* **1**, 389–398.
- [30] Ohnishi, E., Tsuboi, I., Egusa, T., and Uesugi, M., 1981, "Automatic control of overhead crane," in *IFAC 8th Triennial World Congress*, Kyoto, Japan, pp. 1885–1890.
- [31] Omar, H. M. and Nayfeh, A. H., 2001, "A simple adaptive feedback controller for tower cranes," in *ASME 2001 Design Engineering Technical Conference and Computers and Information in Engineering Conference*, Pittsburgh, PA, September 9-12, DETC2001/VIB-21606.
- [32] Oppenheim, A. V., Schafer, R. W., and Buck, J. R., 1999, *Discrete-Time Signal Processing*, Prentice Hall, Englewood Cliffs, NJ.
- [33] Ridout, A. J., 1989a, "Anti-swing control of the overhead crane using linear feedback," *Journal of Electrical and Electronics Engineering* **9**(1/2), 17–26.
- [34] Ridout, A. J., 1989b, "Variable damped control of the overhead crane," in *IECON Proceedings, IEEE*, Los Alamitos, CA, Vol. **2**, pp. 263–269.
- [35] Robinett, R. D., Parker, G. G., Feddema, J., Dohrmann, C. R., and Petterson, J., 1999, "Sway control method and system for rotary crane," USA Patent No. 5908122, June.
- [36] Sakaw, Y. and Shindo, Y., 1981, "Optimal control of container cranes," in *Proceedings of the 8th IFAC Triennial World Congress on Control Science and Technology*, Kyoto, Japan, pp. 257–265.
- [37] Salminen, R., Marttinen, A., and Virkkunen, J., 1990, "Adaptive pole placement control of a piloted crane," in *Proceedings of the IFAC 11th Triennial World Congress*, Tallinn Estonia, USSR, pp. 313–318.

- [38] Servo To Go, Inc., 1999, *ISA Bus Servo I/O Card, Model 2 Hardware Manual*, Revision 2.0.
- [39] Singhose, W. E., Porter, L. J., and Seering, W., 1997, "Input shaped of a planar gantry crane with hoisting," in *Proceedings of the American Control Conference*, Albuquerque, NM, pp. 97–100.
- [40] Teo, C. L., Ong, C. J., and Xu, M., 1998, "Pulse input sequences for residual vibration reduction," *Journal of Sound and Vibration* **211**(2), 157–177.
- [41] Vaha, P., Pieska, A., and Timonen, E., 1988, "Robotization of an offshore crane," in *Robots: Coming of Age, Proceedings of the 19th ISIR International Symposium*, pp. 637–648.
- [42] Wang, L. and Mendel, J., 1992, "Generating fuzzy rules by learning from examples," *IEEE Transaction on Systems, Man, and Cybernetics* **22**(6), 1414-1427.
- [43] Yang, H., Kinouch, Y., and Sugio, N., 1996, "Anti-swing fuzzy control of overhead cranes referring a velocity pattern," *Control and Cybernetics* **25**(2), 209-281.
- [44] Zinober, A. S. I., 1979, "Automatic control crane operations," in *Proceedings of the 5th IFAC Symposium, Identification and System Parameter Estimation*, Darmstadt, Germany, pp. 1161–1167.

Vita

Hanafy M. Omar was born on August 23, 1971 in El-Wady El-Jadeed, Egypt. He joined the Aerospace Department, Cairo University in 1990, where he earned his Bachelor's Degree with distinction in 1994. After graduation, he was appointed to the Aerospace Engineering Department, Cairo University, as an assistant lecturer. He worked in the Flight Mechanics and Control Group with his advisor Prof. Sayed D. Hassan. He received his Master's Degree from the same department in 1997. He earned a research assistantship at Virginia Tech to continue his Ph.D in Junly 1999. Under the supervision of Prof. Ali Nayfeh, he started his Ph.D program in the Nonlinear Dynamics and Control Group, Engineering Science and Mechanics Department. Currently, he occupies an assistant professor position at the Aerospace Engineering Department, Cairo University.